

Spring 5-2023

Nanosecond Pulsed Electric Field Modulates Electron Transport and Mitochondrial Structure and Function

Lucas Nelson Potter
Old Dominion University, lucas.potter.eng.3@gmail.com

Follow this and additional works at: https://digitalcommons.odu.edu/biomedengineering_etds



Part of the [Biochemistry Commons](#), [Biology Commons](#), and the [Biomedical Engineering and Bioengineering Commons](#)

Recommended Citation

Potter, Lucas N.. "Nanosecond Pulsed Electric Field Modulates Electron Transport and Mitochondrial Structure and Function" (2023). Doctor of Philosophy (PhD), Dissertation, Electrical & Computer Engineering, Old Dominion University, DOI: 10.25777/jmn3-r324
https://digitalcommons.odu.edu/biomedengineering_etds/23

This Dissertation is brought to you for free and open access by the Biomedical Engineering at ODU Digital Commons. It has been accepted for inclusion in Biomedical Engineering Theses & Dissertations by an authorized administrator of ODU Digital Commons. For more information, please contact digitalcommons@odu.edu.

**NANOSECOND PULSED ELECTRIC FIELD MODULATES ELECTRON
TRANSPORT AND MITOCHONDRIAL STRUCTURE AND FUNCTION**

by

Lucas Nelson Potter
B.S. May 2015, Virginia Commonwealth University

A Dissertation Submitted to the Faculty of
Old Dominion University in Partial Fulfillment of the
Requirements for the Degree of

DOCTOR OF PHILOSOPHY

BIOMEDICAL ENGINEERING

OLD DOMINION UNIVERSITY
May 2023

Approved by:

Shu Xiao (Director)

Stephen J. Beebe (Member)

Barbara Hargrave (Member)

Nicola Lai (Member)

ABSTRACT

NANOSECOND PULSED ELECTRIC FIELD MODULATES ELECTRON TRANSPORT AND MITOCHONDRIAL STRUCTURE AND FUNCTION

Lucas Nelson Potter
Old Dominion University, 2023
Director: Dr. Shu Xiao

Pulsed power treatment has been used to induce regulated cell death (RCD) in cells or ablate tumors in animals. A subset of pulsed power as electroporation with high voltage and pulse duration of milliseconds is used for biomedical treatment to induce pores in the plasma membrane of cells. Nanosecond Pulsed Electric Fields (nsPEFs)— an extension of electroporation, uses waveforms with pulse durations on the order of 10-900 nanoseconds. nsPEF treatment has demonstrated intracellular effects for potential biomedical applications. In this work, nsPEF treatment is used to demonstrate changes that affect viability, plasma membrane permeability ROS (Reactive Oxygen Species) in the cytosol and mitochondria, and Electron Transport Chain (ETC) in cell cultures. The preferential effectiveness of nsPEF on cultured cancerous versus non-cancerous breast epithelial cells is shown. The nsPEF treatment compromised the integrity of the plasma membrane and outer mitochondrial membrane (OMM), without affecting the integrity of the inner mitochondrial membrane (IMM). Also, nsPEF - changes in redox proteins such as NADH dehydrogenase both in the plasma membrane and in Complex I. A reduced cellular oxygen consumption after nsPEFs treatment indicates an alteration of the ETC at Complex I in intact and permeabilized cells as well as in isolated hepatocyte mitochondria This evidence suggests a new paradigm for considering nsPEF effects on cell function. The combination of nsPEF and rotenone synergistically enhanced ROS production in intact cells suggesting that nsPEF and rotenone act at different Complex I sites. These studies establish how nsPEF impacts several intracellular mechanisms that disrupt mitochondrial function directly on Complex I and IV and indirectly by

Ca²⁺- and ROS-mediated mechanisms that cooperate to collapse the mitochondrial membrane potential and cause cell death. Together, these observations provide new evidence for mechanisms triggered by nsPEF treatment for inducing cancer cell death and changing cellular metabolism in ways useful for treating cancer and other diseases in clinical settings.

Copyright, 2023, by Lucas Nelson Potter, All Rights Reserved.

I stand on the shoulder of giants only because of the helping hands of everyone that has ever offered me kindness.

ACKNOWLEDGMENTS

Funding was generously provided by the ODU Department of Electrical and Computer Engineering, especially via Dr. Oscar Gonzalez. Additionally, funding was in part provided by Air Force grants through Dr. Shu Xiao. Funding was also provided from the laboratories of Drs. Nicola Lai and Stephen J Beebe. I would like to thank Brittney Ruedlinger, Anthony Nanijian, Bhabuk Koriala, James Hornef, Xavier-Lewis Palmer, and everyone in the SAMPE and Beebe Labs for their support.

NOMENCLATURE

ADP: Adenosine DiPhosphate

ATP: Adenosine TriPhosphate

C1: Complex I (NADH ubiquinone oxireductase)

C2: Complex II (Succinate Dehydrogenase or succinate-Co. reductase)

C3: Complex III (Cytochrome bc1 complex or CoQH₂-cytochrome c reductase)

C4: Complex IV (Cytochrome C Oxidase)

C5: Complex V (ATP Synthase)

cAMP: Cyclic adenosine monophosphate

CCK-8: Cell Counting Kit 8

C-H₂DCFDA: Carboxy-H₂DCFDA [5-Carboxy-2',7'-dichlorodihydrofluorescein diacetate].

Excitation = ~492–495, Emission = 517–527 nm

CCCP: [(3-chlorophenyl)hydrazono]malononitrile

cROS: Cytosolic ROS

CytC: Cytochrome C

DOC: De-Oxy Cholate

EC₅₀: Half maximal effective concentration

ECAR: Extracellular Acidification Rate

ER: Endoplasmic Reticulum

ETC: Electron Transport Chain

FCCP: Carbonyl cyanide-p-trifluoromethoxyphenylhydrazone

IC₅₀: half maximal inhibitory concentration

IEA: intermediate electron acceptor

kV: KiloVolt

M: Molar (Solution)

mPTP: mitochondrial Permeability Transition Pore

MitoSOX: Excitation = 510nm, Emission = 580nm

mROS: Mitochondrial ROS

NAO: Nonyl Acridine Orange (Excitation = 495nm, Emission = 522nm)

ns: Nanosecond

nsPEF: Nanosecond Pulsed Electric Field

OCAR: Oxygen Consumption Rate

RCD: Regulated Cell Death

RCF: Relative Centrifugal Force

RHOD-2: Excitation = 552, Emission = 581 nm

ROS: Reactive Oxygen Species

RNS: Reactive Nitrogen Species

SIP: Standard Incubation Protocol

TMRE: Tetramethylrhodamine (Excitation = 549nm, Emission = 575 nm)

TNBC: Triple Negative Breast Cancer

TMPD: N,N,N',N'-Tetramethyl-p-phenylenediamine dihydrochloride

tPMRT: trans-Plasma Membrane Redox Transport

VDAC: Voltage Dependent Anion Channel

YO-PRO-1: Excitation = 491nm, Emission = 509nm

$\Delta\Psi$: Mitochondrial Membrane Potential

TABLE OF CONTENTS

	Page
LIST OF TABLES	xi
LIST OF FIGURES	xii
LIST OF GRAPHS	xiii
LIST OF EQUATIONS	xvi
Chapter	
CHAPTER 1: INTRODUCTION	0
General Effect of nsPEF Treatment on Cells	0
Effect of nsPEF Treatment on the Plasma Membrane	1
Effect of nsPEF Treatment on the Mitochondrial Membrane	4
Effect of nsPEF Treatment on Enzymes	6
Effect of nsPEF Treatment on ROS Generation	8
CHAPTER 2: METHODS	12
Cell Lines	12
Cell Culture	13
nsPEF Generation Methods	13
Plasma Membrane	15
Mitochondrial Membrane Integrity Methods	19
Bioenergetic Assay	21
ROS Detection Methods	25
Isolated Mitochondrial Methods	26
Statistical Methods	27
CHAPTER 3: RESULTS	28
Plasma Membrane	28
Mitochondrial Membrane	41
Mitochondrial ETC Complex Changes	49
Mitochondrial ROS ETC Effects	60

	Page
Isolated Mitochondria	66
CHAPTER 4: ANALYSIS OF THE CHARGING EFFECT	67
Effect of nsPEF Treatment on H9C2 Cells	67
CHAPTER 5: DISCUSSION.....	77
nsPEF Treatment Effect on Cell Viability, Plasma, and Mitochondrial Membranes	77
Changes in Mitochondrial ETC Protein Behavior Due to nsPEF Treatment.....	79
Changes in Mitochondrial ROS Production Due to nsPEF Treatment	80
Changes in Mitochondrial ETC Protein Behavior Due to nsPEF Treatment on Isolated Mitochondria	82
CHAPTER 6: PILOT STUDIES AND SUGGESTED EXPERIMENTS	83
Effect of Picosecond Pulsed Electric Fields (psPEF) on Viability	83
Effect of Picosecond Pulsed Electric Fields (psPEF) on Complex I Activity	89
Rhod-2 for Ca in Mitochondria.....	91
Cell Susceptibility to nsPEF Treatment	94
Modeling nsPEF Effects on Mitochondrial Membranes.....	94
CHAPTER 7: CONCLUSION	100
REFERENCES	101
APPENDICES	122
Appendix A: Cell Growth / Culture media	122
Appendix B: Electrode Media.....	124
Appendix C: Substrate Permeabilization	125
Appendix D: Full Permeabilized Protocol	127
Appendix E: Intact Oxygen Flux (O2K) Residual Oxygen Flux Correction.....	129
Appendix F: Liver Mitochondria Extraction.....	131
Appendix G: Common Pulse number to Charging Effect Conversions.....	135
VITA.....	136

LIST OF TABLES

Table	Page
1: Summary of the enzymes in the Electron Transport Chain Complex (ETC)	7
2: IC 50 values for viability determined by the WST-8 viability assay.....	31
3: EC50 for YO-PRO in the presence (Ca+) and absence (Ca-) of 2mM of Ca2+.....	40
4: EC50 for dissipation of the mitochondrial membrane potential with and without Ca2+.....	44

LIST OF FIGURES

Figure	Page
1: Summary of mitochondrial ROS formation.....	10
2: nsPEF Pulse waveform with oscilloscope reading inset. Inset shows an oscilloscope reading of a single 60ns, 15ns (fast) rise time, 40kV/cm pulse.	14
3: WST-8 assay mechanism.....	17
4: Effect of nsPEF on general mitochondrial morphology.	48
5: Effect of nsPEF on mitochondrial cardiolipin staining.....	49
6: A schematic representation of the geometry of cellular membranes for the Electrical Model of these membranes.....	95
7: Effect of a monopolar, 70kv/cm, 60ns, fast rise/fall time pulse on individual mitochondrial cristae.....	96

LIST OF GRAPHS

Graph	Page
1: nsPEF treatment differently decreases cell viability in a dose dependent manner in four cell lines.	29
2: Viability decrease due to nsPEF treatment has linear behavior when using the charging effect as a dependent variable.....	30
3: PMRS activity significantly decreases 20 minutes after nsPEF treatment as measured by the WST-8 kinetics assay.....	33
4: Example PMRS kinetics assay with H9C2 cells (see Graph 3).....	34
5: nsPEFs induce a dose-dependent increase in plasma membrane permeability to propidium iodide (PI)	35
6: Charging increases the plasma membrane permeabilization in H9C2 cells.	36
7: Exogenous calcium has a cell type-dependent effect on plasma membrane permeabilization quantified by cellular YO-PRO fluorescence uptake.	38
8: Calcium modulates YO-PRO fluorescence differently in cancerous and non-cancerous cell lines.	39
9: Mitochondrial membrane potential (MMP) drop is dependent on calcium at low levels of nsPEF treatment.....	42
10: Effect of nsPEFs (charging effect) on the mitochondrial membrane potential with and without Ca ²⁺ in cancerous and non-cancerous cell lines.....	43
11: nsPEF treatment can effectively disrupt OMM integrity without compromising the IMM of H9C2 and 4T1 cells.	46
12: Inhibition of Complex V by Oligomycin provides indirect evidence of IMM integrity.....	47
13: nsPEFs attenuate oxygen flux in 4 different cell lines with intact plasma membranes	50
14: nsPEF treatment shows a dose-dependent decrease in ETC complex I activity for H9C2 cells.	52
15: The temporal profile of Oxygen Consumption Rate (OCAR) for H9C2 cells.	53
16: The temporal profile of Extracellular Acidification Rate (ECAR) for H9C2 cells.	54

17: OCAR and ECAR rates of nsPEF treated cells show significant changes.	55
18: OCAR from Seahorse XF significantly drops in 3 cell lines.	56
19: ECAR from Seahorse XF significantly drops in 2 human-based cell lines	57
20: Three cell lines suspended with exogenous mitochondrial substrates and treated with nsPEF show significant change to complex I activity.....	58
21: Three cell lines suspended with exogenous mitochondrial substrates and treated with nsPEF show significant change to complex IV activity.....	60
22: nsPEF treatment leads to elevated cellular ROS. Type of ROS is dependent on cell line.....	61
23: nsPEF treatment and ETC complex inhibitors demonstrate compounding effects on mROS in H9C2 cells.....	63
24: nsPEF treatment and Rotenone (Complex I inhibitor) demonstrate rotenone dose-dependent effects on mROS for rotenone concentration above 15 μ M in H9C2 cells.....	64
25: Effect of time after nsPEF treatment on mitochondrial ROS production.	65
26: nsPEF treatment has an effect on the ETC complex activity of isolated mitochondria.....	66
27: H9C2 cells show non-simultaneous effects of nsPEF treatment on the plasma membrane (PI) and the OMM without an effect on the IMM.....	68
28: H9C2 cells show significant decrease in function around 10 40kV/cm, 60ns monopolar pulses (7.6 10 ⁻³ Volt*sec/cm).....	69
31: Charging effect levels for several intracellular effects	71
32: Comparison of the Complex I function and PMRS activity for 4 cell lines.	72
33: The decrease of OMM integrity and membrane potential occurs at similar pulse conditions as the increase of the plasma membrane permeability.	73
34: nsPEF treatment across H9C2 and 4T1 cells shows that Mitochondrial Membrane Potential drop precedes OMM permeabilization - and CI function decreases with similar sensitivity.	74
35: The decrease of the mitochondrial membrane potential ($\Delta\Psi$) and the increase of the Plasma Membrane permeability tends to occur almost for the same charging effect for all cell lines.	75

36: Calcium has an effect on both $\Delta\Psi$ and Plasma Membrane Permeability.	76
37: psPEF treatment affects cell viability via the Charging effect.....	84
38: Temperature change in cell growth media when treated with psPEF shows less than 5 degrees Celsius of variability over 40 minutes.....	87
39: Temperature change in cell growth suspension shows less than 3 degrees Celsius of variability.....	88
40: psPEFs do not affect the oxygen consumption rate in all intact cell lines.....	89
41: psPEF treatment do not affect the Complex I function in all cell lines.	90
42: Calcium release into the mitochondria occurs at high doses of psPEF treatment, even when exogenous calcium is chelated.	92
43: Calcium effects the mobilization of Rhod-2 into the mitochondria.....	93
44: After nsPEF treatment, succinate may infiltrate past the plasma membrane.....	125
45: Example of Permeabilized analysis - CI and indirect CIII - unprocessed data.....	127
46: Example of Permeabilized analysis - CIV - unprocessed data	128
47: Subtraction of residual oxygen flux does not change any significant analysis	129
48: CI activity with AA correction shows no changes in statistical significance	130

LIST OF EQUATIONS

Equation	Page
1: Relationship among electric field, nsPEF pulse number and duration and charging effect.....	30
2: psPEF pulse frequency Charging effect equation	93

CHAPTER 1: INTRODUCTION

General Effect of nsPEF Treatment on Cells

Electroporation is a biological mechanism by which cell membranes are either permeabilized or destroyed via the high voltage signals (Chang, 2006) with a pulse duration in the order of milliseconds. An extension of the electroporation is nanosecond Pulsed Electric Field (nsPEF) therapy, where this high voltage signal has a duration in the time domain on the order of nanoseconds. For an exploration on the generation of short-duration electrical pulses, a seminal contribution to the field was authored in 2003 (Behrend et al., 2003; Schoenbach et al., 2009). This led to a design for delivering these pulses to biological samples in early 2000 (Beebe et al., 2003a; Beebe et al., 2003b; Schoenbach et al., 2001; Vernier et al., 2003) and later Sanders et al (2009). The effects of nsPEF treatment on cells has been investigated for both time and electric field domains. These investigations showed a calcium release from the Endoplasmic Reticulum (ER) (White et al., 2004) and Cytochrome C (CtyC) release from the mitochondria (Beebe et al., 2003b) after nsPEF treatment (Weaver et al., 2012).

One of the first large *in vivo* studies to use nsPEF treatment to ablate tumors and to show that thermal effects were not a major consideration for the mechanism of nsPEF treatment was in 2006 – nsPEF treatment was lauded as a potential drug-free therapy to destroy melanoma tumors (Nuccitelli et al., 2006). Additionally, it has also been reported that the angiogenesis of the tumor was inhibited in a skin tumor model treated with nsPEF (Nuccitelli et al., 2009).

These seminal works were followed by other studies focusing on identifying the more sensitive cell lines to the nsPEF treatment and understanding the mechanisms of nsPEF treatment. MG-63 Osteocarcinoma cells, when treated 40 kilovolts/centimeter (kV/cm), 100 nanoseconds (ns) showed a dose-dependent decrease in viability (as assayed by CCK-8) and significant increase

in apoptosis via flow cytometry (Miao et al., 2014). Under the same conditions in another study, Human Hepatocellular Carcinoma (HCC) cell line SMMC7721 showed signs of apoptosis via Transmission Electron Microscopy (TEM) and a significant drop in viability as demonstrated by CCK-8 (Yin et al., 2014). Caspase-activated apoptosis was induced in both Human Jurkat T lymphoblasts (TIB-152) and Rat glioma 36 (CCL-107) (Vernier et al., 2003) when using fields of 40kV/cm.

nsPEF treatment has been used to study the specific effects to induce cancer cell death and prevention of tumor growth (Chen et al., 2012; Chen, et al., 2013; Hornef, et al., 2020; Rossi et al., 2019). The application of nsPEF to treat oncological conditions has been well-studied. Several cell models have been utilized to study cancer cell viability and apoptosis (Beebe, 2016) in cells treated with nsPEF.

Jurkat Cells (Ren et al., 2012) were the first cell type used to demonstrate apoptosis due to nsPEF treatment (Beebe et al., 2003). HeLa S3 cells (Morotomi-Yano et al., 2014), E4 squamous cell carcinoma (Ren & Beebe, 2011), Murine lymphoma/colorectal cancers (Rossi et al., 2019), N1-S1 (Beebe et al., 2013), Human Histiocytic Lymphoma (U937) (Pakhomova et al., 2013) (Pakhomova et al., 2014), CHO and BPAE cells (Pakhomova et al., 2014).

Effect of nsPEF Treatment on the Plasma Membrane

Although nsPEFs uniquely (but not solely) affect intracellular membranes, the nsPEF treatment effects on the plasma membrane continue to be investigated. It has been shown that nsPEF treatment can create pores in the plasma membrane that are significantly different in structure (Pakhomov et al., 2007) than those obtained with irreversible electroporation (Rosenheck & Neumann, 1973; Weaver, 1990) This permeabilization was initially (Pakhomov et al., 2007) attributed to the absorbed dose. A follow up study indicated that the nsPEF pores changed with

absorbed energy and rise-fall times (Ibey et al., 2009). Furthermore, the size of the pores does not change due to nsPEF treatment when the amplitude of the field is held constant, but the number of the formed pores are a function of the number of pulses delivered (Pakhomov et al., 2015). Pore size is sensitive to the electric field changes of the nsPEF treatment (Fernandez et al., 2012).

Several aspects of pore formation have been quantified with computational modeling including the field to generate the pores in the lipid bilayer that surrounds the cell (Ziegler & Vernier, 2008) and the interaction of water dipoles on the lipid bilayer of the plasma membrane (Vernier et al., 2006). Furthermore, another computational study has shown that pulse exposure time plays a key role in determining how plasma membrane is charged (White et al., 2011). Fast rise-time pulses on the nanosecond scale exposes the cell to a uniform electric field – in essence the pulse goes “through” the cell and not “around” the plasma membrane of the cell as is the case of electroporation (Gowrishankar et al., 2006). The response to the nsPEF treatment depended on the cholesterol composition of the plasma membrane. Cholesterol depletion increased the permeability of cells and decreased the “dose” of nsPEFs for lethality (Cantu et al., 2016).

Some past work used observations in the amount of cell swelling to indicate plasma membrane electroporation (Romeo et al., 2013). Both Propidium Iodide (PI) and YO-PRO-1 (YO-PRO) have been used to assay the permeability of the plasma membrane previously using microscopy (Vernier, 2011) (Deng et al., 2003), and Ethidium homodimer has been used with flow cytometry (Beebe et al., 2013; Beebe, 2015a) as has YO-PRO (Beebe et al., 2009; Carr et al., 2017). Plasma membrane permeability has even been linked to elevated cytotoxicity that arises with the nsPEF treatment at high electric fields (Yin et al., 2016). Cell death was shown to require a loss in the mitochondrial potential (abbreviated as $\Delta\Psi_m$) in the presence of increases in

intracellular calcium due to plasma membrane permeabilization, but cell death did not occur in the presence of increases in intracellular calcium without a loss of $\Delta\Psi_m$ (Beebe et al., 2012).

PI is approximately 668 Daltons (Nexcelom Bioscience, 2021), whereas YO-PRO is slightly smaller (“629 Daltons for the di-iodide salt; 375 Daltons for free base”) (Virginio et al., 1997). Thus, PI has been used to study permeabilization where the pores are larger than those obtained with nsPEF whereas YO-PRO may be more sensitive than PI in showing the nanopores induced by the nsPEF treatment. This was proven in an earlier work using Jurkat T lymphoblasts (Vernier et al., 2006).

The effects of nsPEF treatment on lipid bilayer which constitutes the cell membranes can be explained by an electrical circuit representation. Assuming the lipid bilayer as capacitive surfaces, the delivery of a pulse builds charge on this surface. The charge build-up on the surface causes damage to these membranes (Weaver, 1995) inducing mobilization of intra-cellular granules containing calcium (Schoenbach et al., 2001). Theoretically, the shorter the pulse rise time, the more effective these pulses will be in charging the intracellular membranous structures (Beebe et al., 2012). In addition, due to the smaller capacitance of the internal cellular membranes, the electric pulse travels less well through the intracellular components (Gowrishankar et al., 2006) – this is of importance to the effects of nsPEF treatment on the mitochondrial membrane.

Effect of nsPEF treatment on the Plasma Membrane Repair Mechanisms

The above-mentioned electrical models obviously do not do justice to the dynamic nature of the plasma membrane of the mammalian cell. The effects of nsPEF on the plasma membrane are noted not only in the formation of pores but also on the protein’s mobilization through the pores. Specifically, the presence of the protein like phosphatidylserine on the exterior leaflet of the lipid bilayer of the cell plasma membrane, is interpreted as a marker of a cellular trauma. This

protein which is typically present on the inner leaflet of the plasma membrane acts as a signal for apoptosis as it migrates to the outer leaflet of the plasma membrane (Nagata et al., 2016). Interestingly, by using nsPEF, no direct physical interaction with the cell is needed against an external agent for this externalization of Phosphatidylserine (Vernier et al., 2004) and this externalization process has been modeled *in silico* (Vernier et al., 2006).

Plasma membranes have their own repair mechanisms. The common injury of membrane disruption (Cooper & McNeil, 2015) are thought to be regulated by calcium (Cheng et al., 2015) with cellular signaling mechanisms for autophagy (Ullery et al., 2015). There are approximately 6 conceptual mechanisms of plasma membrane repair (Moe et al., 2015), and the study of these in the context of the damage done by nsPEF to the plasma membrane of the cell has not been a topic of intensive study. It has been reported that damage to the plasma membrane after 300ns pulses are able to be repaired on a time scale of minutes, and exogenous calcium facilitates this process (Muratori et al., 2021). The investigation of this phenomena is challenging because a nanoporated hole closure in the plasma membrane occurs on a timescale of around of 10 seconds (Klenow et al., 2021).

Effect of nsPEF Treatment on the Mitochondrial Membrane

The effect of nsPEF treatment on the mitochondrial membranes has been previously investigated. It has been shown that the nsPEF treatment decreased mitochondrial potential ($\Delta\Psi_m$) traced by JC-1 (Beebe et al., 2009; He et al., 2017), Rhodamine 123, TMRE (tetramethyl rhodamine ethyl ester) (Beebe et al., 2009; Beebe, 2015b; Vernier, 2011). Additionally, the tracking of Cytochrome C (CytC) release has been a popular topic in the domain of studying types of cell death in the field of nsPEF treatment. Usually, CytC release is indicated as a means of

indicating apoptosis, (Beebe et al., 2003; Beebe et al., 2009; Beebe et al., 2013; Cosentino & García-Sáez, 2014; Love et al., 2017; Ren & Beebe, 2011).

It is expected that the nsPEF treatment affects the IMM and OMM differently because of their composition is not the same. Particularly, in the outer membrane, the protein-lipid ratio is about 50:50 (1-part protein per every 1-part lipid), like the plasma membrane lipid: protein ratio. In the IMM, this ratio increases dramatically to 80:20 (Stefan, 2001; Shaikh & Brown, 2013). This has been previously studied and cardiolipin may be a factor in this heterogeneity (Aryaman et al., 2019). As noted later, there are age-related changes in IMM integrity (Liu et al., 2020). Membrane composition and its relationship with mitochondrial function is important. Mitochondrial dysfunction has been related to phospholipid dependent mechanisms (Leskova, 2017). Among the phospholipids, Cardiolipin that resides within the IMM (Horvath & Daum, 2013) has been related to mitochondrial function. When Cardiolipin is reduced in the IMM, Complexes I and IV become destabilized (Pfeiffer et al., 2003; Claypool et al., 2008), and contribute to other cases of mitochondrial dysfunction (Chicco, 2007). Cardiolipin amounts vary in different subpopulations of mitochondria (Stefanyk et al., 2010). While lipids regularly permeabilize the OMM (Rostovtseva et al., 2017), the IMM is not usually biologically permeable except to solutes with specific transporters (Lemasters, 2007)

The role of calcium in the process of apoptosis has also been an intense topic of study. (White et al., 2004; Zharkova et al., 2018). Ca^{2+} has broad applications as a second messenger in intra/extra-cellular signaling, in large part in the mitochondria it works in conjunction with ROS (Görlach et al., 2015). Ca^{2+} has been studied in the amounts located in cellular microdomains in the para-mitochondrial components of the cell (Drago et al., 2010), in the specific transporters of calcium into the cellular environments (Beebe, et al., 2012; Williams et al., 2013), and as a link to

cardiac cell excitation (Wang et al., 2009). In addition, the effect of calcium on ROS generation (and the link to ATP (Brookes et al., 2004)) in the cellular environment is also important (See Introduction - Effect of nsPEF treatment on ROS Generation).

Effect of nsPEF Treatment on Enzymes

Previous studies focused on the direct nsPEF effects on apoptosis or cellular differentiation (Zhang et al., 2014), and on the effects of the pulse time treatment on reversible or irreversible Electroporation (IRE) pulsing parameters (Goswami et al., 2018). nsPEF treatment has been reported to indirectly affect calcium ion channels by allowing sodium ion entry to depolarize the cell (Craviso et al., 2010). Only one study focused on the effects of nsPEF treatment on cellular energy metabolism (Estlack et al., 2014) whereas glycolytic energy metabolism of cancerous cell lines has been compared to resting non-dividing non-cancerous cells using oxphos metabolism, where cancerous cell lines utilize both glycolytic and oxphos metabolism (Jose et al., 2011; Solaini et al., 2011)

Because nsPEF treatment affects the mitochondrial membranes it is also possible that other enzymes of the Electron Transport Chain (ETC) could be affected. The alteration of activities of the enzymes that compose the ETC are particularly important for the metabolic function of the mitochondria. A summary of the Complexes of the ETC can be found in Table 1.

Complex Designation	Full name	Primary Function	Secondary Function
I (1)	NADH:ubiquinone oxidoreductase, NADH-CoQ reductase, NADH dehydrogenase;	Reduces NADH and Quinol	Proton Pump
II (2)	succinate dehydrogenase or succinate-CoQ reductase	Reduces succinate	None
III (3)	Cytochrome bc1 complex or CoQH2-cytochrome c reductase	Reduces Ubiquinol and oxidises Cytochrome C	Proton Pump
IV (4)	Cytochrome c oxidase, cytochrome AA3	Reduces Cytochrome C	Proton Pump
IV (5)	ATP Synthase	Phosphorylate ADP, form ATP	None

Table 1: Summary of the enzymes in the Electron Transport Chain Complex (ETC). Each of the first four complexes has a primary function which is carried out in the process of transporting protons. Complex II has a secondary function as an enzyme in the Krebs cycle and operates as an intermediate between Complex I and III. Complex V uses the proton gradient that is established by Complexes I, II, and IV to phosphorylate ADP into ATP, to be used by other energy systems in the cell.

Complex I (CI) is an ETC protein with two domains. The 7 integral, membrane-bound, hydrophobic subunits (encoded by the mitochondrial genome) are attached to an additional 7, extramembranous, hydrophilic subunits. The main function of this extramembranous domain is to utilize NADH (produced from the tricarboxylic acid cycle (Berg, 2002) at the Flavin Mononucleotide at the edge of the extramembranous domain and transfer the resulting electron through a series of Iron-Sulphur (Fe-S) centers towards the membrane-bound domain, through the quinone-binding site (which is notably "...long, narrow, and enclosed" (Baradaran, et al., 2013)) and to the IMM (Hirst, 2013; Wikstrom, et al., 2015). This quinone binding site has a major role in the Complex I inhibition by Rotenone (Heinz et al., 2017; Palmer, et al., 1968) which is typically used in protocols to assess mitochondrial function. Importantly, dysfunction of Complex I has been shown to cause the release of Reactive Oxygen Species (ROS), also known as Oxygen Radicals (Wirth, et al., 2016). Deficiency of Complex I is one of the most common respiratory chain defects leading to mitochondrial dysfunction in humans (Kirby et al., 1999; Skladal et al., 2003; Triepels, et al., 2001).

Complex III has a dimeric construction, despite having a monomeric mechanism (Crofts et al., 2008). It directly transports 1 electron through an FE-S pathway (similarly to Complex I). The inhibitory agent for this complex is antimycin A, which prevents the oxidation of the bh heme, though Myxothiazol and Stigmatellin could also be used (Crofts et al., 2008).

Complex IV, consisting of three primary subunits, interacts with 4 CytC molecules at a time, in order to oxidize a dioxygen molecule to water and thereby translocates a proton to the OMM in exchange (Wikstrom et al., 2015). It is inhibited by sodium azide.

The effect of nsPEF treatment on cellular membranes has been largely investigated, but the effect of nsPEF treatment on protein activity were not sufficiently established. A single study showed that nsPEF treatment can deactivate the phosphotransferase activity of the catalytic subunit of the cAMP-dependent protein kinase (Beebe, 2015). Beside the nsPEF effects on enzyme activities, another important aspect related to the impact of nsPEF treatment on cellular metabolic function is how nsPEF exposure affect redox proteins and whether this change allow the cell to remain viable.

Effect of nsPEF Treatment on ROS Generation

In a cell culture study has been reported that nsPEF treatment induces ROS generation (Pakhomova et al., 2012), and that production of ROS contributes to redox-based signaling (Trewin et al., 2019). ROS and Ca^{2+} are considered to be part of a “cross-talk” that enables cellular regulation between the mitochondria and the endoplasmic reticulum (Görlach et al., 2015). Under typical physiological conditions, 0.2-2% of electrons in the ETC contribute to ROS production) (Cadenas & Davies, 2000; Turrens, 2003). This is also occurring to greater extents in pathological conditions (Feno et al., 2019), and aging (Scialò et al., 2016). This is on top of Ca^{2+} serving to

excite the dehydrogenases in the Krebs cycle (Balaban, 2002) through regulation of substrate oxidation (Hansford & Zorov, 1998).

ROS is also hinted at having an effect in the innate immune response (West et al., 2011) and recruitment of inflammatory cells (Li et al., 2017)– this could augment the effectiveness that nsPEF has in oncological treatment, since some variants of cancer have been linked to mitochondrially produced ROS (Sabharwal & Schumacker, 2014; Sosa et al., 2013). ROS may also be a signaling mechanism in the case of aging (Velarde et al., 2012) It has been shown that mitochondrial ROS can be produced in the IMM via Complex I and III, and released into inner-membrane space and the cytoplasm from Complex III (Li et al., 2013). This is summarized in figure 2, through the action of SOD 1 (superoxide dismutase 1), SOD2 (superoxide dismutase 2), and GPX (glutathione peroxidase). The exact sites of this ROS production are still a matter for debate (Goncalves et al., 2015).

While healthy mitochondria can release ROS by oxidative phosphorylation, the upregulation of mitochondrial activity or deactivation of complexes causes a backflow of electrons that induces a condition known as reverse electron transport (Selivanov et al., 2011). This is especially noted in the deactivation of CI (Hernansanz-Agustín et al., 2017). In fact, there is a growing body of evidence that suggest CI may influence the reverse electron transport in the mitochondria as governed by $\Delta\Psi$, pH, a reduced amount of CoQ (ubiquinone) and high ATP/ADP levels (Robb et al., 2018; Scialò, et al., 2017).

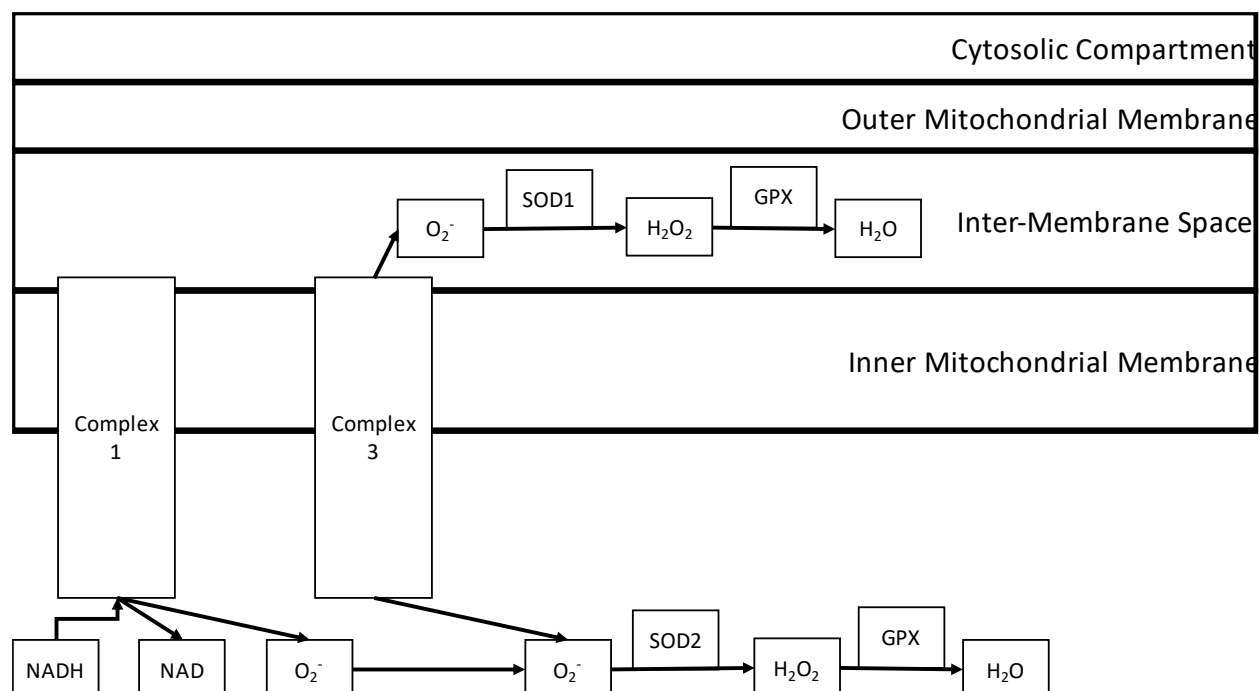


Figure 1: Summary of mitochondrial ROS formation. Note that both ETC Complex I and III contribute to mitochondrial ROS inside of the mitochondrial matrix, but only Complex III contributes to ROS in the inter-membrane space of the mitochondria. ROS production of Complex I is stored in the mitochondrial matrix. Both ETC complexes can produce O₂⁻ ions, and SOD1 (Superoxide Dismutase 1, in the Inter-membrane space) and SOD2 (Superoxide Dismutase 2 in the mitochondrial matrix), reacts with O₂⁻ ions to produce H₂O₂. GPX (Glutathione Peroxidase) continues this reaction by reacting with Hydrogen Peroxide to form water. The sites of interest to ROS formation in Complex I is the FMN (Flavin Mononucleotide) (where the electrons are transferred from the extra-membranous section to the integral portion of the protein) site and the CoQ (Coenzyme Q or ubiquinone) binding site (which is located within the IMM (Lenaz et al., 2006)) (Zhou et al., 2019). Complex III, while it creates less ROS compares to the production of C1 (Brand, 2010) still can produce ROS through the COQH2 binding site (sometimes referred to as the Q_o site) (Turrens et al., 1985) (Richter et al., 1995). For more about how disintegrate the IMM specifically via the use of GPX, refer to the future experiments section.

It is not completely understood the relationship between mitochondrial ETC protein function (measured via oxygen flux) and ROS production. It has been suggested that the lowered oxygen flux in a nsPEF treated cell might be related to a higher production of ROS (Zhang et al., 2018) whereas the increase in ROS production is calcium dependent (Nuccitelli et al., 2013). ROS is directly detectable by several methods – namely mass spectrometry probes, fluorescent probes, genetically encoded sensors, and redox signaling GFP (Collins et al., 2012). Also, flow cytometry

could be used to verify the presence of ROS in the cells after nsPEF treatment. One challenge is represented by the fact that ROS production cannot be easily related to the to the ETC protein activities measured by oxygen flux measurements (Djafarzadeh & Jakob, 2017).

Fluorescent dyes that can be used for microscopy or flow cytometry include MitoSOX, (ThermoFisher, 2021) which is a superoxide indicator that sequesters in the mitochondria and fluoresces red or green in the presence of superoxide (diatomic oxygen). It has previously been used in live cells (Mukhopadhyay et al., 2007) and to assay mitochondrial ROS via flow cytometry (Puleston, 2015). Additionally, indirect evidence ascribes superoxide production to multiple sites of the mitochondria (Drose & Brandt, 2008; Goncalves et al., 2015; St-Pierre et al., 2002; Wong et al., 2017), whereas a direct analysis points to Complex I as a major contributor to mitochondrial superoxide production rate (Murphy, 2008; Robb, et al., 2018). Another fluorescent dye, Carboxy-H₂DCFDA, (ThermoFisher, 2021) is a general oxidative stress indicator, used to detect ROS within the cell without localizing ROS production from mitochondria (Albano, et al., 2015; Guo, et al., 2010).

CHAPTER 2: METHODS

Cell Lines

Four different cell lines were used. H9C2, MCF10A, 4T1 and HCC-1937.

H9C2 cells are murine cardiomyocytes from *Rattus Norvegicus* (ATCC, 2021). They were chosen due to their high density of mitochondria, which is ideal for bioenergetics studies: H9C2 cells expressed nearly twice the mitochondrial mass as assayed via citrate synthase as a comparable cardiac line (Aminzadeh & Mehrizadi, 2018). Previous works on these cells include studies on mitochondrial ETC complexes (Mohsin et al., 2020), metabolism (Zordoky & El-Kadi, 2007), and viability (Bouitbir et al., 2019). It tends to differentiate with passage number (Witek, 2016); thus all the experiments were conducted with cells below 20 passages. Cells were typically passaged at least once a week, media changed every 3-4 days, and used at 80-90% confluence.

Mouse 4T1 cells (ATCC, 2021) have a relatively fast doubling time of 14 hours (Schrörs, et al., 2020) (DuPre, et al., 2007). They have undergone multi-omic analysis that shows a lack of Estrogen, Progesterone, and Epidermal growth factor receptors, similar to human Triple Negative Breast Cancer (TNBC) cells. Notably, the 4T1 line has been shown to be a particularly heterogeneous line (Wagenblast, et al., 2015).

HCC 1937 is another breast cancer cell line. It was selected with another cell line without cancerous characteristics (human MCF10A line) as a control. These breast epithelial cells can be easily cultured under normal conditions (ATCC, 2021). HCC-1937 cells (ATCC, 2021) are human basal TNBC type, and can be compared to the 4T1 line, to study potential differences between the murine human cell models (Dong, et al., 2019).

Cell Culture

All cell lines were kept in a 37 °Celsius, humidified, 5% CO₂ incubator when not in use. This was considered the standard incubation protocol (SIP) which was used for most of the experiments. Specific media compositions can be found in appendix 1. The base media for the cells lines is as follows: H9C2- Corning DMEM with 4500 mg glucose. 4T1- Corning RPMI-1640. MCF10A- Corning DMEM. HCC1937 – ATCC RPMI-1640. 0.4% Trypan blue mixture and a hemocytometer was used for basic estimates of cell concentration.

Generally, to test the cells after nano-second pulse treatment, cells were cultured (5% CO₂ at 37 °Celsius) in complete growth media (with serum added). At 80 to 90% confluence, they were treated with Corning 0.25% Trypsin, 2.21mM EDTA solution (Corning, 2021) for 5 minutes (except for MCF10A cells, which required 15-20 minutes incubation with Trypsin solution). Trypsin was neutralized with an equivalent volume of serum-containing growth media. Cells were centrifuged in a Hermle Benchmark Z 446 K centrifuge for 5 minutes at 300 rcf and then resuspended in 500uL of growth media. The cell solution was split in 100uL cuvettes for nsPEF treatment. The nsPEF conditions were 60 nanosecond pulses at 40 kilovolts/cm field strength with pulses of 10-15 ns rise times.

nsPEF Generation Methods

Much of the research presented in this work was carried out by using a single nsPEF generation unit (Xiao, 2021). This generator, a pulse-forming line, delivered pulses of 60ns duration with 15 ns rise and fall times- as defined by the time it takes a single pulse to change from 10% of its maximum voltage to 90% of its maximum voltage (IEEE, 2011). Most of the experiments were obtained with 40 kilovolts/cm for different numbers of pulses administered at approximately 1 Hertz (Hz). The ideal waveform of a single nsPEF pulse is seen in Figure 2.

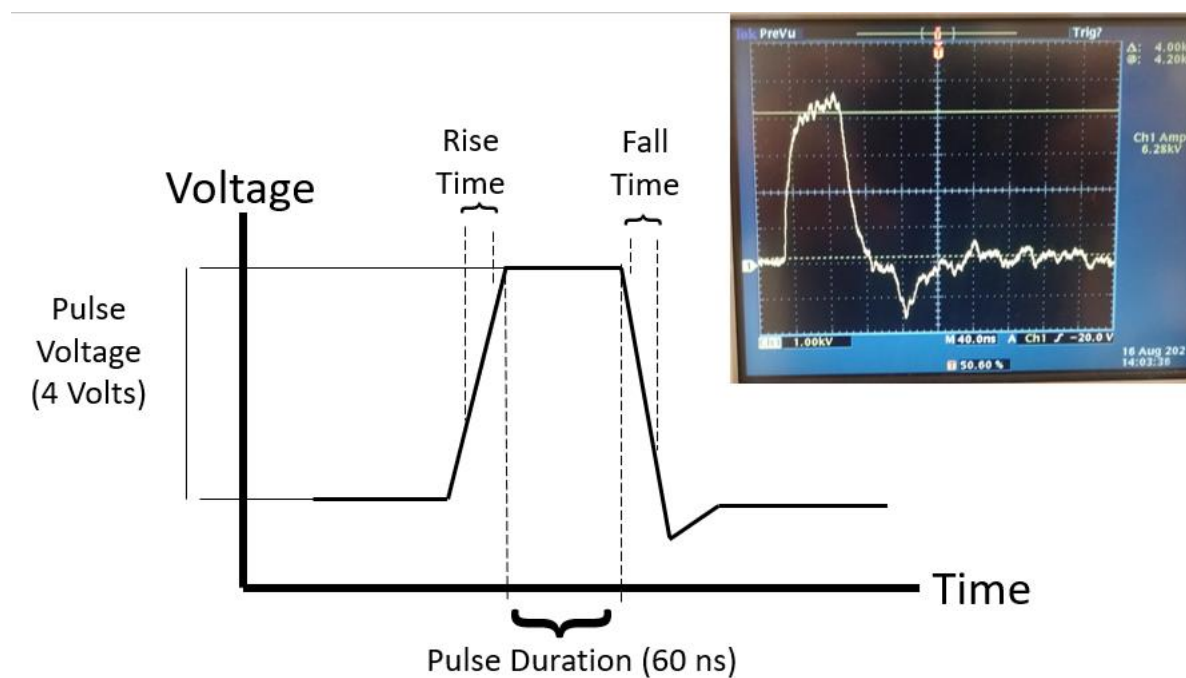


Figure 2: nsPEF Pulse waveform with oscilloscope reading inset. Inset shows an oscilloscope reading of a single 60ns, 15ns (fast) rise time, 40kV/cm pulse. Note that for the ideal waveform, the voltage as displayed by the vertical axis is only 4 volts. This translates to a 40kV/cm field as the cuvettes used in this study have 1 mm (0.1cm) gap for the nsPEF treatment. Additionally, the rise/fall times are similar, though the fall time has a discernable amount of overshoot before the voltage returns to ground level. The “fast” rise and fall times (Determined via the length of time required to reach the maximum voltage, in turn demonstrated by the oscilloscope) are important for intracellular effects (*Schoenbach, et al., 2001*) of the nsPEF treatment. Note on the inset that the vertical scale where a single vertical tic mark is equivalent to 1 volt- (Note that the voltage reading is only 4 volts instead of 4kV because of the attenuator deployed. Since the cuvette is 0.1cm, this corresponds to a 40kV/1cm field) and the horizontal tic mark is 40ns, thus the entire pulse is approximately 60 ns in duration).

To deliver picosecond Pulsed Electric Field Treatment a different unit was used (See Chapter 6: Pilot Studies and Suggested Experiments).

A typical signal waveform is shown in Figure 2. The amplitude of the electric field was measured; additionally the rise/fall times and pulse duration were confirmed via a Tektronix 3052B 2 channel color digital phosphor oscilloscope (Tektronix, 2006).

Most experiments below are shown as bar graphs with the different pulsing amounts or numbers separated by discrete intervals. In some cases, to compare the results obtained with

different parameters of the nsPEF treatment, the delivery of nsPEFs based on their Charging Effect was used and computed as follows (Eqn. 1):

$$\text{Charging Effect} = E_{\text{Field}} \left(\frac{V}{\text{cm}} \right) * \text{Pulse Duration (ns)} * \sqrt{\text{Pulse Number}} \rightarrow \frac{\text{Volt} * \text{Sec}}{\text{cm}}$$

Equation 1: Relationship among electric field, nsPEF pulse number and duration and charging effect

This relationship accounts for the electric field, pulse duration, and pulse number used for the nsPEF treatment (Schoenbach et al. 2009). The electric field (40 kV/cm) and pulse duration (60 ns) was held constant, and the pulse number was varied. The square root is used only for cells in suspension that receive pulses from different orientations to the anode and cathode as they move in solution in the cuvette as a mimic of the random walk hypothesis (Schoenbach et al., 2009). Appendix 7 demonstrates some commonly used pulse number to charging effect conversions.

The equation provides the full charging effects applied and can be used to normalize pulse treatments with different pulse durations and electric fields and thus allows to analyze the experiments with the charging effect as a variable in the continuous domain. The charging effect as a metric of nsPEF treatment presents a limitation with bipolar pulses (Sozer & Vernier, 2019). Bipolar nsPEF pulses has been reported to have less effect on plasma membrane permeability than that obtained with monopolar pulses. Nevertheless, in this work nsPEF included only treatments with monopolar pulses.

Plasma Membrane

Cell Viability

The preliminary set of experiments was used to determine the cell viability after pulsing, irrespective of the type or nature of this cell death and find the conditions under which the cell

remains predominantly viable. The viability was determined with the reagent generically known as CCK-8 and commercially available as the WST-8 reagent (Dojindo Molecular Technologies, 2021). WST-8 reagent and 1-methoxy PMS were administered to cells without cytotoxicity effects. This assay measures the plasma membrane redox system (PMRS) as trans plasma membrane electron transport (tPMET), which is directly proportional to cell number in an appropriated range of cell numbers, which must be pre-determined. To determine the viability of H9C2 and 4T1 cells were used 10 and 40 thousand cells, respectively.

This cell impermeable WST-8 reagent is a normally colorless tetrazolium salt named [2-(2-methoxy-4-nitrophenyl)-3-(4-nitrophenyl)-5-(2,4-disulfophenyl)-2H-tetrazolium, monosodium salt] and is typically used in conjunction with the 1-methoxy PMS (an intermediate electron acceptor, IEA) as a metric of viability by measuring the activity of what has been called the Plasma Membrane Redox (Reduction-Oxidation) System (PMRS). It measures the redox activity of NAD-NADH by the IEA or PMS (phenazine methosulfate) irreversibly reducing the WST-8 dye, which then generates an orange dye. The accumulation of dye by this irreversible reaction over 2-4 hours is directly proportional to cell number within a range of cell numbers and is a reliable indicator of cellular viability. It should be noted that the endogenous ascorbate affects the tPMET (trans-Plasma Membrane Redox Transport) activity measured by the combined WST-8 kit. Thus, the experimental protocol accounted for the background endogenous ascorbate. The tPMET is a NADH dehydrogenase protein that spans the plasma membrane and is mounted on the exterior of the cell. The function of the assay is summarized in Figure 3. If the rate of the reduction of WST-8 dye is measured, which is done in the presence of high cell numbers (4×10^5 cells) the kinetics of the active tPMET proteins in the plasma membrane redox system (PMRS) can be determined.

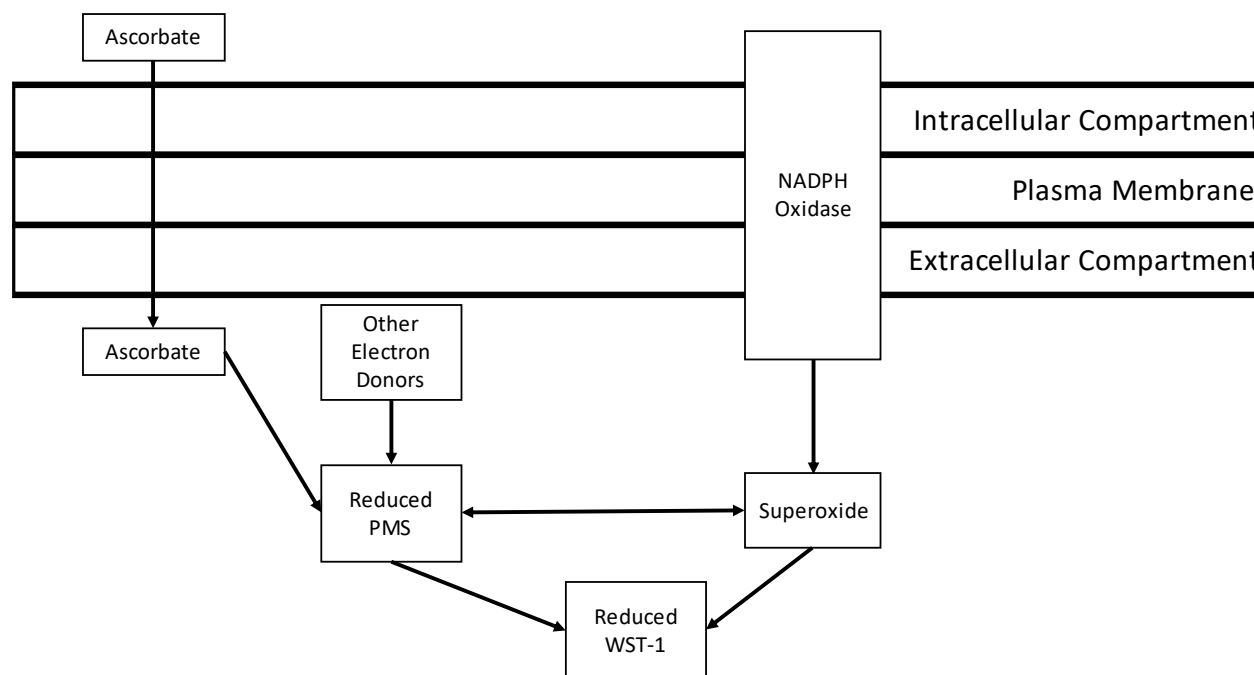


Figure 3: WST-8 assay mechanism. Note that both the reduced PMS (phenazine methosulfate) and plasma membrane produced superoxide can contribute to reducing the WST-1 molecule (Kelly et al., 2018), and this WST-1 molecule is the primary component of the WST-8 assay. The plasma-membrane mounted NADPH oxidase bears responsibility for NAD – and the electrons released by this reduce the WST-8 which in turn generates an orange dye.

After the treatment, the reaction shown in Figure 3 (where the WST-8 molecule is reduced) is run for several hours until completion while the reagent is added to the cell sample for more than 1 hour. The kinetics of the PMRS complex can be determined by using the method in the section below.

Cell Viability by WST-8

Cells were suspended in 96 well plates after nsPEF treatment and returned to SIP. 24 hours later, they were administered 10 μ L of WST-8 reagent the plate was returned to SIP for two hours. Then the plate was placed in a Molecular Devices, Spectra Max i3 plate reader (Molecular Devices, 2013). The absorbance of light at 450 nm was recorded. Resultant absorbance was analyzed with SoftMax Pro (Version 6.5.1). For this experiment, nsPEF treatment was given at increments of 0

(control), 1, 5, 10, 50, and 100 pulse groups. A blank group which contained only media and CCK-8 reagent was used to determine background absorbance, which was subtracted from all other data points. Light absorbance data was normalized to the control cell absorbance. The cell absorbance of control cells is assumed to correspond to a 100% viability. The absorbance difference between control and treated cells reflected the fraction of viable cells expressed as a percentage.

tPMET by the PMRS

The CCK-8 reagent was additionally used to determine the change in electron transport activity in the PMRS (Plasma Membrane Redox System) immediately after nsPEF treatment. All cell lines (H9C2, 4T1, MCF10A, and HCC-1937) were (similarly to the viability experiment described above) treated with different 40kV/cm fields at for 60ns duration (0.0024 V*s/cm/pulse) pulses. After treatment, cells were thoroughly mixed with WST-8 reagent in a 96 well plate. Then the absorbance of light at 450 nm was continuously measured every 10 min (for 60-90 minutes) using the same reader as the above viability experiment. The linear region of the sigmoid curve of the absorbance at 450 nm was recorded. And used to interpret the change in the kinetics of the PMRS after treatment as change in absorbance 450nm / min. For this experiment, nsPEF treatment was given at 0, 5, 10, 15, 25, 50, and 100 pulses. It was of special importance to assay this part of the cell as some cancer cell lines have been found to utilize significant levels of oxygen through the trans-Plasma Membrane Electron Transport system (as measured by a Clark Electrode) (Herst, 2007).

Plasma Membrane Permeability

To determine the plasma membrane permeability, 1×10^5 cells were pulsed in the presence of YO-PRO dye (ThermoFisher, 2021) and fluorescence was determined with a Miltenyl Biotec

MACS Quant Analyzer 10 Flow Cytometer (Miltenyl Biotec, 2021) were utilized. All flow cytometry experiments used this same system.

YO-PRO is a nucleic acid stain that is impermeant to samples that have intact plasma membranes. Only in the case the plasma membrane is porated or permeabilized YO-PRO becomes detectable. However, YO-PRO shows permeabilization with the active P2X7 receptor, which is present in all the cell lines tested.

Samples were suspended in DPBS (Ca⁺), or PBS with 2mM EGTA added (Ca⁻) to chelate calcium. Immediately after pulse treatment, 2 μ L of 200 μ M YO-PRO was added to 100 μ L of sample (4 μ M final concentration) and cells were incubated in darkness at room temperature for 20 minutes. The pulse conditions chosen for this experiment were 0 (control), 5, 10, 25, 50, 100, and 200 pulses. The PE-A channel (FL-2, or B-2) was used. This method provides the fraction of cells (in percent) permeable to the reagent as an index of plasma membrane permeability. Thus, the fraction of cell with YO-PRO, indicates the fraction of cells with plasma membrane permeable to that reagent.

Mitochondrial Membrane Integrity Methods

Mitochondrial Membrane Potential

TMRE (ThermoFisher, T669) (ThermoFisher, 2021) were administered to cells (1×10^5) immediately after pulsing. TMRE is a plasma membrane permeant dye sequestered in mitochondria that show high mitochondrial membrane potential. This potential is the magnitude of the separation of charge between the interior and exterior of the IMM. Samples were suspended in DPBS (Ca⁺), or PBS with 2mM EGTA added (Ca⁻) to chelate calcium. Immediately after pulse treatment, 2 μ L of TMRE was added to 100 μ L of sample (200nM final concentration), and the samples were incubated in darkness at room temperature for 20 minutes. The pulse conditions

chosen for this experiment were 0 (control), 5, 10, 25, 50, 100, and 200 pulses. After the initial gating for live cells and singlet gating, the PE-A channel (FL-2, or B-2) was used to determine which cells still retained high mitochondrial potential after treatment.

Mitochondrial Membrane Integrity

A polarographic assay was used to evaluate whether the functional integrity of the inner (IMM) and outer (OMM) mitochondrial membranes was preserved after nsPEF treatment. A protocol originally used to evaluate the inner and outer mitochondrial membrane integrity in isolated skeletal muscle mitochondria (Lai et al., 2018) was used with some modifications to quantify the effect of the nsPEF treatment on the integrity of the mitochondrial membranes. H9C2 cells were treated with 0, 25, 50 and 100 pulses, and for all other cell lines treated with 0, 50, 100, and 200 pulses. Cells were resuspended in Mir05 solution (See appendix 2 for buffer solution composition) in a high-resolution respirometer (Oroboros O2K). The oxygen consumption rate determined with the Datlab 7.1.0.121 software (Oroboros Ecosystem, 2021; Oroboros Ecosystem, 2020) was continuously monitored during the experiment. The cells were sequentially treated with Digitonin (203.4nM), ADP (2.5mM), NADH (14uM, prepared fresh each day and stored on ice), CytC (2uM), and DOC. After the injection of digitonin, the cells were allowed 15 minutes to fully permeabilize. The concentration values of these chemicals are referred to the concentration in the chamber. An increase of the oxygen consumption rate with the addition of exogenous NADH indicated an alteration of the IMM, whereas an increase of the oxygen consumption rate with the addition of CytC indicates an alteration of the OMM. Thus, when the integrity of the IMM and OMM is preserved, NADH and CytC are impermeable to the IMM and OMM (respectively). The detergent DOC was used to determine the condition representing the positive control at the end of

the experiment. The detergent was administered to chemically induce mitochondrial membrane disruption.

Mitochondrial Morphology with DAPI, Mitotracker-Green, and NAO

A pilot study was done to determine the state of the IMM and OMM with microscopy using H9C2 cells pulsed at 0, 50, 100, 150, and 200 pulses dyed with Mitotracker Green (ThermoFisher, 2021), used previously (Vernier, 2011) to look at the effect of nsPEF treatment on mitochondrial morphology. Mitotracker-Green attaches to “free thiol groups of cysteine residues” (Presley, et al., 2003). An Opkelco Microscope with Olympus DP80 camera system was used, with both x10 and x20 objective lenses. Similar study was done using DAPI (ThermoFisher, 2021) to stain for nuclear material, in conjunction with either Mitotracker green to stain overall mitochondrial membrane (ThermoFisher, 2021), or Nonyl Acridine Orange (NAO)) (Jacobson, 2002; Kaewsuya, et al., 2007; ThermoFisher, 2021) to stain for cardiolipin- a protein found only on the surface of the IMM (Mileykovskaya, et al., 2001) with a 60X objective lens. This series of experiments was subject to entirely qualitative analysis.

Once the morphology of the membranes was totally analyzed, the relative activities of the ETC complexes had to be delineated. To do this, polarographic methods were used.

Bioenergetic Assay

O₂ Consumption Rate in Intact Cells

Bioenergetics assays were performed in intact cells resuspended in Gemish solution (See appendix 2) using a high resolution respirometry (Oroboros Ecosystem, 2020). The oxygen kinetics were processed with Datlab 7.1.0.121 (Oroboros Ecosystem, 2021) to determine the oxygen consumption rate. The protocol consisted of a sequential injection of Oligomycin (0.632 uM), CCCP (0.075uM, Carbonyl cyanide m-chlorophenyl hydrazone), Rotenone (0.03 μM), and

Antimycin A (0.025uM). The concentrations values refer to the concentration of the chemicals within the metabolic chamber. This protocol allows for the Complex I activity of the mitochondria, without exogenous substrates, to be delineated and compared across cell lines and treatment types.

To calibrate the O2k system, the unit required 45-60 minutes to reach an equilibrium between air atmospheric conditions and the buffer solution in the chamber. After the solution with the cells were added to the chamber and it was sealed. 20 minutes were sufficient to determine the basal oxygen consumption rate. It required 5-10 minutes to observe a complete inhibition of ATP synthase (or Complex V) by Oligomycin. CCCP titrations were variable, depending on the cell type. A full inhibitory effect of Rotenone and Antimycin A on Complex I and III were observable after 10-20 minutes.

Both the bioenergetics and WST-8 assay were performed on intact cells.

The Seahorse XF analyzer mini was used to determine the glycolytic flux in the cell lines after nsPEF treatment. The Seahorse XF analyzer uses “optical fluorescent biosensors” to detect change in oxygen consumption and pH change (Agilent, 2020). Oxygen consumption and hydrogen ion production were measured simultaneously to evaluate oxidative phosphorylation and the extracellular acidification rate (ECAR) (Agilent, 2019). The measure of ECAR that can be used to quantify indirectly the cellular glycolytic flux rate, allows to evaluate whether the nsPEF treatment can switch cell metabolism from oxidative phosphorylation to glycolytic metabolism or vice versa, or if the two energy systems are affected differently. This test includes injections of Oligomycin, FCCP, Rotenone, and Antimycin A. The manufacturer supplied Mitochondrial Stress Test injects Rotenone and Antimycin A at the same time. The assay was modified to inject Rotenone and Antimycin A separately to determine the Complex I activity. To compare the oxygen consumption rate obtained with the O2K with that obtained with the seahorse, CCCP instead of

FCCP was used for the Seahorse XF protocol. The Seahorse XF protocol requires an intact monolayer of cells as opposed to using cells in suspension, as in the Oroboros O2k). The manufacturer's (Agilent) recommendations are to plate cells 24 hours in advance and then allow for cell growth to form a complete monolayer. Regarding this feature of the Seahorse XF, the O2K system is different because permits treated cells to be metabolically characterized nearly immediately after the pulse treatment is administered. However, since the effect of nsPEF treatment was expected to be transient, only 1 hour was permitted to elapse before the testing began, instead of the recommended 24 hours. So relatively high cell plating densities were used. H9C2 cells were used at a concentration of 50,000 cells per well, 4T1 at 300,000 cells/well, MCF-10A at 100,000 cells/well, and HCC-1937 at 50,000 cells/well. The number of cells was elevated in comparison to typical assays of this kind – meaning that since little time elapsed from the treatment to testing, cell division or growth was not expected to be a significant factor. Because cell growth was not a factor and in the case of H9C2 cells, not even enough time had elapsed for the cells to stretch to their typical, kite-shaped morphology, more cells were used to create a useable monolayer. To compensate for the absence of 24 hours of growth time of the cells, more cells were used to form the requisite monolayer. For this assay, cells were in DMEM, and the media was supplemented with pyruvate (1 mM), glutamine (2 mM), and glucose (10 mM). The assay required in-depth preparation and calibration procedures, though they have not been changed from the standard protocol, except for the reduction in cell incubation time and commensurate rise in cell number (Agilent, 2019).

A similar strategy was done previously with U937 and Jurkat cells but did not differentiate the Complex I respiration independently from the rest of the oxygen flux (primarily Complex III) (Estlack, et al., 2014).

O₂ Consumption Rate in Permeabilized Cells

With the protocol that used intact cells, it was not possible to determine whether the cellular oxygen consumption rate was not substrate limited. The bioenergetic assay in intact cells relies on the endogenous substrates present in the cell, whereas the bioenergetic assay in permeabilized cells allows the addition of a specific substrate for each complex of the ETC. This feature allows to maximize the stimulation of the ETC and obtain the maximal mitochondrial oxygen consumption rate and distinguish the effect of a specific condition or treatment on each complex of the electron transport chain. An existing protocol was adapted to evaluate mitochondrial function with Complex I, and IV substrates (Ye & Hoppel, 2013). After the cells were treated with nsEPF they were replaced in the incubator for 20 minutes and later put into the metabolic chamber with 2mL of MIR05 solution. The oxygen consumption rate of the cells was normalized to the concentration of the sample (millions of cells/volume). The protocol was performed according to the following sequence: Malate (0.4uM), pyruvate (0.5uM), digitonin (0.406uM), ADP (2.5mM), glutamate (10mM), succinate (10mM), CCCP - H9C2 cells used 0.1uM, MCF10A cells used 5uM, Rotenone (3.75uM), and Antimycin A (0.25uM). Ascorbate (2mM) and TMPD (N,N,N',N'-Tetramethyl-p-phenylenediamine dihydrochloride, 0.5mM) were added near-simultaneously and then Sodium Azide (Na-Az, 200M). The amount added to the chamber is referred to as the final concentration.

The mitochondrial respiration rates were corrected for oxygen flux to account for instrument background. The difference between the uncoupled mitochondrial respiration rate (ET) and that in the presence of rotenone (R), which quantifies mainly the contribution of C-II to uncoupled oxidation, was used to determine NADH-linked respiration rate (ET-R), while the azide sensitive respiration rate in the presence of ascorbate plus TMPD was used to determine Complex IV respiration rate (C-IV). Respiration flux was expressed in pmol of O₂ s⁻¹ 10⁶ cells⁻¹.

Both MIR05 and Gemish media contained EGTA to sequester the free calcium in intact or permeabilized oxygen flux assays. Ca^{2+} serves to excite the dehydrogenases in the Krebs cycle (Balaban, 2002) through regulation of substrate oxidation (Hansford & Zorov, 1998). Therefore, it would be difficult if not impossible to separate out the effects of nsPEF from the effects that calcium had on the Krebs cycle pathways.

ROS Detection Methods

Four assays were done to quantify the amount of ROS production. All the studies rely on the earlier cited MitoSOX dye (ThermoFisher, 2021).

The first study used MitoSOX Red (to measure ROS in the mitochondria) and C-H₂DCFDA (to measure ROS in the cytosol). All four cell lines were pulsed 0, 5, 10, and 25 times. (The positive control was represented by a cell sample suspended with excessive amounts of H₂O₂). The ROS content in each cell was related to the content of the positive control.

The second study used H9C2 cells treated with 0, 10, 20, and 40 pulses and then treated with inhibitors of ETC complexes. Rotenone was added to 100uL of cell suspension (0.015mM), Antimycin A (0.01mM), oligomycin (2.528nmol), and a final group that added both Rotenone and Antimycin A (the same amounts as above). This study helped to identify the rough ideal inhibitor type and pulse doses needed to determine maximum mROS production parameters.

A third pilot study was used to identify the appropriate concentration of rotenone and pulsing dose. This used H9C2 cells pulsed at 0, 15, 20, and 25 pulses, with rotenone in the following concentrations: 0mM, 0.75uM, 3.75uM, 7.5uM, 15uM, and 30uM. This is to effectively demonstrate the effect of Complex I on the production of ROS, and to delineate the effective kinetics of the rotenone-nsPEF effect on mitochondrial ROS production.

Another study was performed to detect ROS production over time from mitochondria after the pulse was administered and the MitoSOX was added. MitoSOX is typically used in the case of microscopy analysis, so it would be useful for future studies to know the most effective incubation time for MitoSOX when used with flow cytometry. Additionally, it was a final confirmation of the synergism of nsPEF and inhibition of rotenone.

Isolated Mitochondrial Methods

The effect of nsPEF treatment on mitochondrial function were determined not only in cultured cell samples but also in mitochondria isolated from murine liver samples (see appendix 6 for protocol). A previously reported process was used (Hoppel et al., 2002). The issues with utilizing isolated mitochondria for polarographic analysis are many – the extraction of the tissue itself is not terribly difficult. Once all four lobes of the liver are identified, retrieving the liver is possible with a scalpel or shears and a pair of fine tweezers. Yet one must be careful to not also obtain the gallbladder, as the stored biliary acids could have a deleterious effect on the mitochondria during the isolation process. Once the mass of liver was weighed, it was rinsed in MSM solution, blotted dry with filter paper, minced without additional liquid, resuspended in MSM-EDTA solution, then subjected to mechanical homogenization, then centrifuged to removed other cellular components. After the weight was found, the liver was kept on ice until tested (with the brief exception of being exposed to the nsPEF pulses). For the full list of instructions for isolating liver mitochondria, see appendix 6. Once the liver mitochondria were isolated, they were exposed to a series of substrates added in sequence: ADP (2.5mM), glutamate (10mM), succinate (10mM), and CytC (4mM). Finally, DOC (127.4mM) was added to completely disrupt the mitochondrial membranes.

Statistical Methods

The results are reported as means with error bars representing 1 standard deviation. The comparison between any two samples were analyzed with a two tailed Student's t Test and two-sample equal variance. A difference of $p < 0.05$ was considered for significance. Most experiments (unless otherwise noted) have an n of 3. Microsoft Office 365 with Excel version 2104 was used. For the YO-PRO, TMRE, RHOD-2, and MitoSOX flow cytometry testing, an alpha of 0.001 was used.

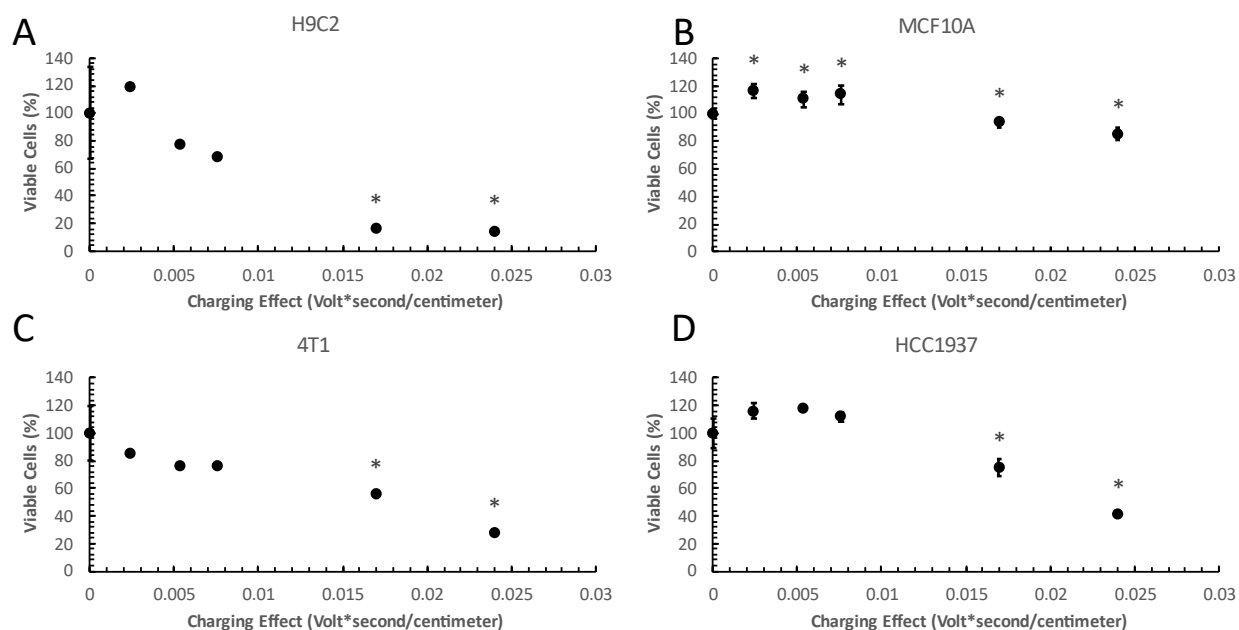
CHAPTER 3: RESULTS

The top left quadrant (A) for most figures, contains the results for H9C2 cells that tended to show the most significant results due to their sensitivity to the nsPEF treatment. The top right quadrant (B) for most figures, contains the results for MCF10A cells, the “nominal” line that exhibits indications of cancerous metabolism. In the lower left (C) and right quadrant (D) is reported for most figures, the 4T1 and HCC1937 cell results, respectively.

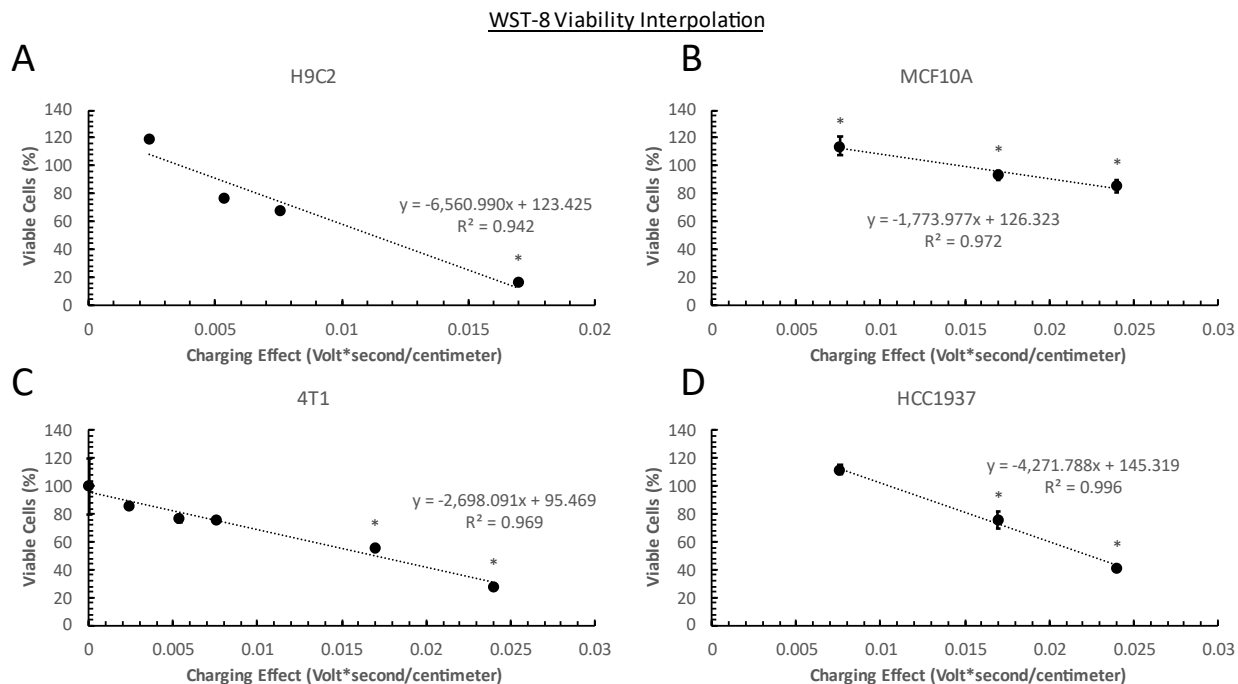
Plasma Membrane

The cell viability was measured after 24 hours the nsPEF treatment (Graph 1 and 2). Most of the cell lines showed a small increase in viability at low pulse doses (H9C2, MCF10A, and HCC-1937). Only for MCF10A cells there was a statistical increase with charging effect used as a continuous variable to standardize the nsPEF treatment parameters to a single metric. This increase could either be due to an increase in proliferation or an increase in the PMRS kinetics observed during the 24 hours post treatment (See Graph 3). Notably, the cell viability decreased to 20% or less of the original population in 3 of the cell lines, whereas only in the MCF10A line the viability decreased to approximately 70% of its original value. The robust nature of these cells will be a recurring theme in the experiments to come. The overall viability was also used as a metric to obtain an IC50 value for each of the cell lines (Table 2). IC50 values were calculated by taking a linear subsection of the above viability curve (Graph 1), linearly fitting the results, and solving for 50% viability. This was accomplished with the libraries available in Excel of Microsoft Office 365.

24 Hour Post-Treatment Viability (WST8)



Graph 1: nsPEF treatment differently decreases cell viability in a dose dependent manner in four cell lines. Four cell lines (H9C2, MCF10A, 4T1, and HCC1937) were suspended in growth media (See appendix 1), pulsed with a variable charging value of 60ns, 40kv/cm, 15ns rise-time pulses - 0, 1, 5, 10, 50, or 100, and then suspended in additional growth media in a 96 well plate. After 24 hours WST-8 (CCK-8) reagent was added, the cells were incubated for 1-2 hours, and absorption at 450 nm was recorded. The viability is plotted on the Y axis (normalized to control) as a percentage. The abscissa represents the Charging Effect (calculated as Volt*Sec/cm). Black filled circles denote the percentage of cells (normalized to the control) that remained viable 24 hours after treatment. Error bars represent 1 standard deviation. (*difference between treatment doses with $\alpha=0.05$, Student's T Test).



Graph 2: Viability decrease due to nsPEF treatment has linear behavior when using the charging effect as a dependent variable. Four cell lines (H9C2, MCF10A, 4T1, and HCC1937) were pulsed with a variable amount of 60ns, 40kv/cm, 15ns rise-time pulses - 0, 1, 5, 10, 50, or 100 – and then suspended in growth media. After 24 hours WST-8 (CCK-8) reagent was added, and fluorescence intensity was recorded. In the figure above, a subset of the overall viability (from Graph 1) is plotted on the Y axis and a linear interpolation is performed and reported as a percentage of the control (unpulsed/sham treatment) cells. The graph represents the effect of Charging Effect (Volt*Sec/cm) on cell percentage (normalized to the control) that remained viable 24 hours after treatment. Error bars represent 1 standard deviation. (with $\alpha = 0.05$, Student's T Test).

The regression lines of each cell line (Graph 2) were obtained using the following sets of data: H9C2 (1, 5, 10, and 50 pulses). MCF10A (10, 50, and 100 pulses). 4T1 (0, 1, 5, 10, 50, and 100 pulses). HCC-1937 (10, 50, and 100 pulses). IC50 value for each of the 4 cell lines were determined by the regression line. The primary purpose of the IC50 is to predict in later experiments the death susceptibility of the cell lines investigated. The threshold for significant effects on the PMRS activity of the cell are as follows: H9C2 – 0.009295 V*Sec/cm, MCF10A - 0.024 V*sec/cm, 4T1 – between 0.012 and 0.024 V*sec/cm, HCC-1937 – 0.012 V*Sec/cm.

Cell Line	IC50 Charging Effect (Volt*Sec/cm)	Pulse Number (#)	R ²
H9C2	0.011	22	0.942
MCF10A	0.043	321	0.972
4T1	0.017	49	0.969
HCC1937	0.022	86	0.996

Table 2: IC 50 values for viability determined by the WST-8 viability assay. The scaling effect of the linear interpolation is derived to have a continuous variable to standardize the nsPEF treatment parameters to a single metric. For given pulses (40kV/cm, 60ns), the charging effect and approximate pulses to obtain 50% viability were reported in the second and third columns. The final column contains the coefficient of determination for the linear regression.

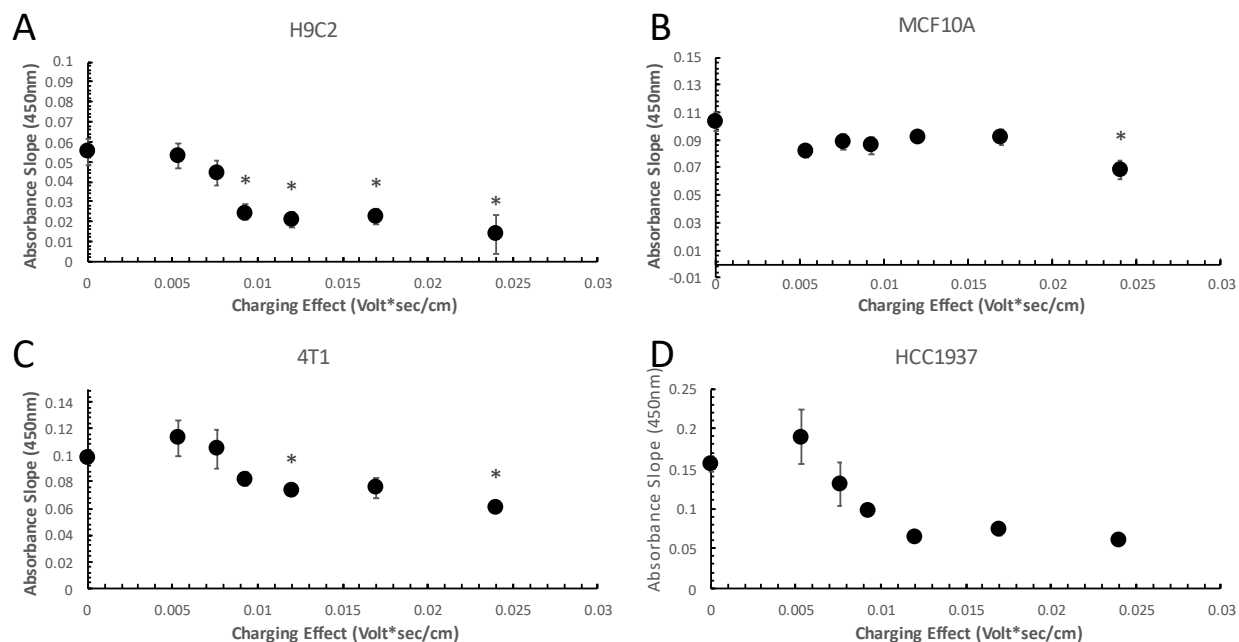
The non-cancerous MCF10A, which is derived from a non-malignant breast epithelial model, is by far the most robust cell type whereas the H9C2 cells appear to be the most sensitive cell type followed by the cancerous cell types.

The WST-8 assay has been a reliable assay. However, the fact that nsPEF treatment could change protein function brought some doubt upon whether the mechanism by which the WST-8 dye acted is valid for determination of nsPEF-mediated viability. However, any given effect of the activity of the oxidoreductases in the minutes after nsPEF treatment would have to impact the values 24 h after treatment. Nevertheless, the significant increase in viability of the MCF10A cells at low pulse numbers, requires further analysis to determine if this is due to a proliferation of cell numbers or some lasting effect of nsPEFs on the PMRS activity in MCF10A cells. The dehydrogenase activity was redox linked, and so in theory nsPEF treatment may affect this activity; however, there is no significant effect on activity for such a finding here. Later, it is shown that mitochondrial ETC is significantly affected, indicating that nsPEFs can affect electron transport. Thus, the kinetics of the WST-8 assay as a measure of electron transport activity were determined to know if nsPEF treatment influenced PMRS activity.

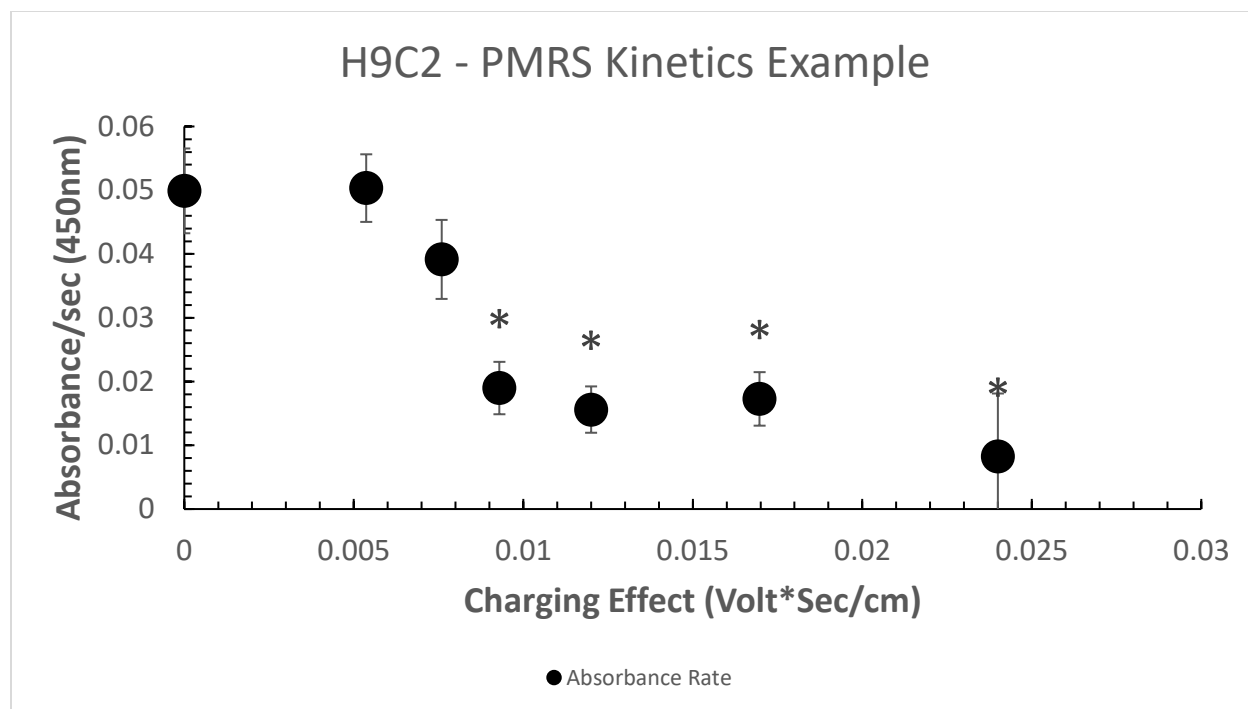
Once the viability was determined, the PMRS active post-pulsing was determined because the WST-8 assay that is used to indirectly assay viability, relies on trans-plasma membrane electron transport (tPMET) activity. For this reason, it was worthwhile to determine whether PMRS activity was significantly affected after the treatment. Thus, increased cell numbers were used to determine tPMET rates of the PMRS activity in real time immediately after nsPEF treatment, the rate of the light absorbance at 450nm was recorded at 1.5-minute intervals for 2 hours. The interval of data with a linear change of absorbance was used to calculate the slope in AU/second.

The charging effect on the PMRS activity varies with the cell line. This is not unreasonable given that the oxidoreductases that comprise the PMRS are different among cell types. Specifically, a significant drop on PMRS activity is observed at 0.009 V*Sec/cm in H9C2 cells, at 0.024 V*sec/cm in MCF10A cells, between 0.012 and 0.024 V*sec/cm in 4T1 cell, and at 0.012 V*Sec/cm in HCC-1937 cells. PMRS activity assayed by the WST-8 reagent varied greatly most likely due to the different oxidoreductases among cell types, especially in cancer cells. The PMRS activity of the HCC-1937 cells is, at control levels, nearly 3 times higher than that of the H9C2 cells. Also, the PMRS activity in 4T1 and MCF10A lines are higher than that of the H9C2 cells- by twofold. Importantly, H9C2, 4T1, and HCC-1937 cells show a pronounced decrease in PMRS activity at 25 pulses (0.012 V*sec/cm) whereas MCF10A cells show a significant decrease only at 100 pulses (0.024 V*sec/cm). The doubled dose of charging effect needed to achieve the same PMRS activity change demonstrates the robust characteristics of the MCF10A cell line to nsPEF treatment. In contrast, H9C2 and HCC1937 are more sensitive to the nsPEF treatment.

tPMET Activity Immediately Post nsPEF Treatment

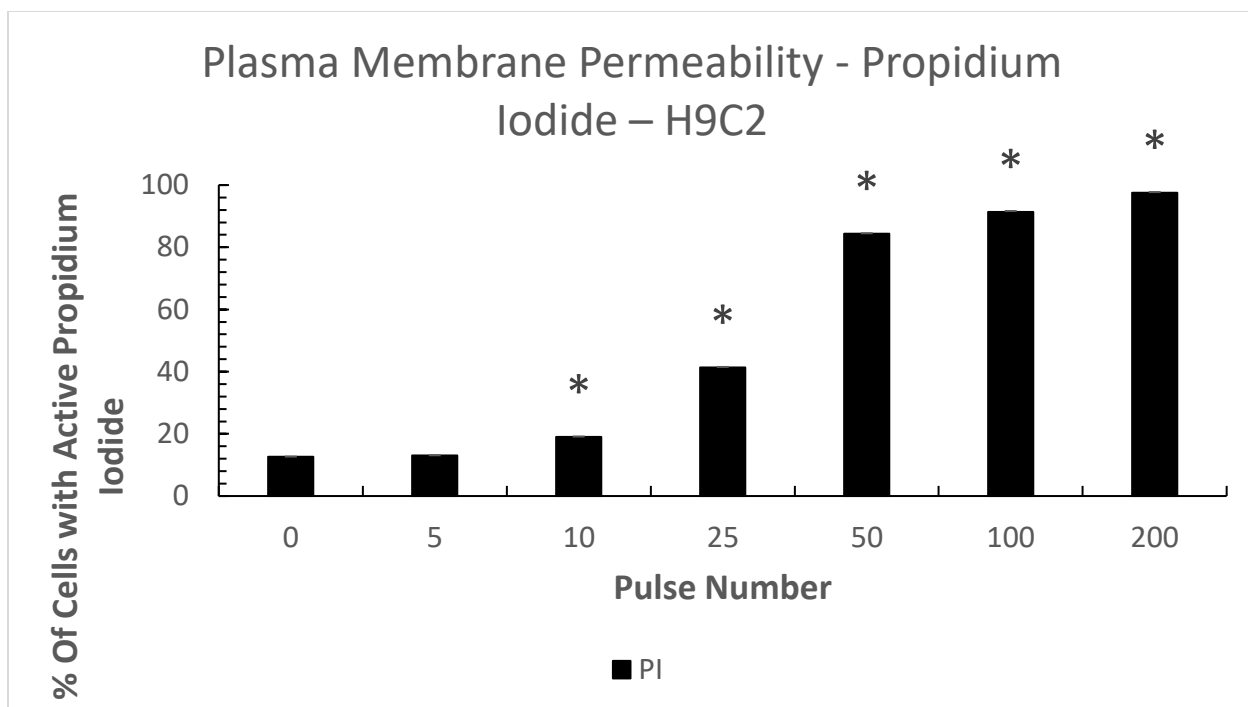


Graph 3: PMRS activity significantly decreases 20 minutes after nsPEF treatment as measured by the WST-8 kinetics assay. Four cell lines (H9C2, MCF10A, 4T1, and HCC1937) were pulsed with a variable amount of 60ns, 40kv/cm, 15ns rise-time pulses - 0, 5, 10, 15, 25, 50, or 100 which correspond to 0, 0.0053, 0.0075, 0.0092, 0.012, 0.016, and 0.024 V*sec/cm and then suspended in growth media. Immediately (0-10 minutes) after treatment, WST-8 (CKK-8) reagent was added to the solution, and fluorescence intensity was recorded at 1.5 second intervals for at least 90 minutes. The absorbance slope of the WST-8 reagent is plotted against Charging Effect (Volt*Sec/cm). Absorbance slope is measured at 450nm by a Spectra Max i3 plate reader set to read for 60 seconds at every 1.5 seconds. Error bars represent 1 standard deviation. (* difference from control with $\alpha= 0.05$, Student's T Test).



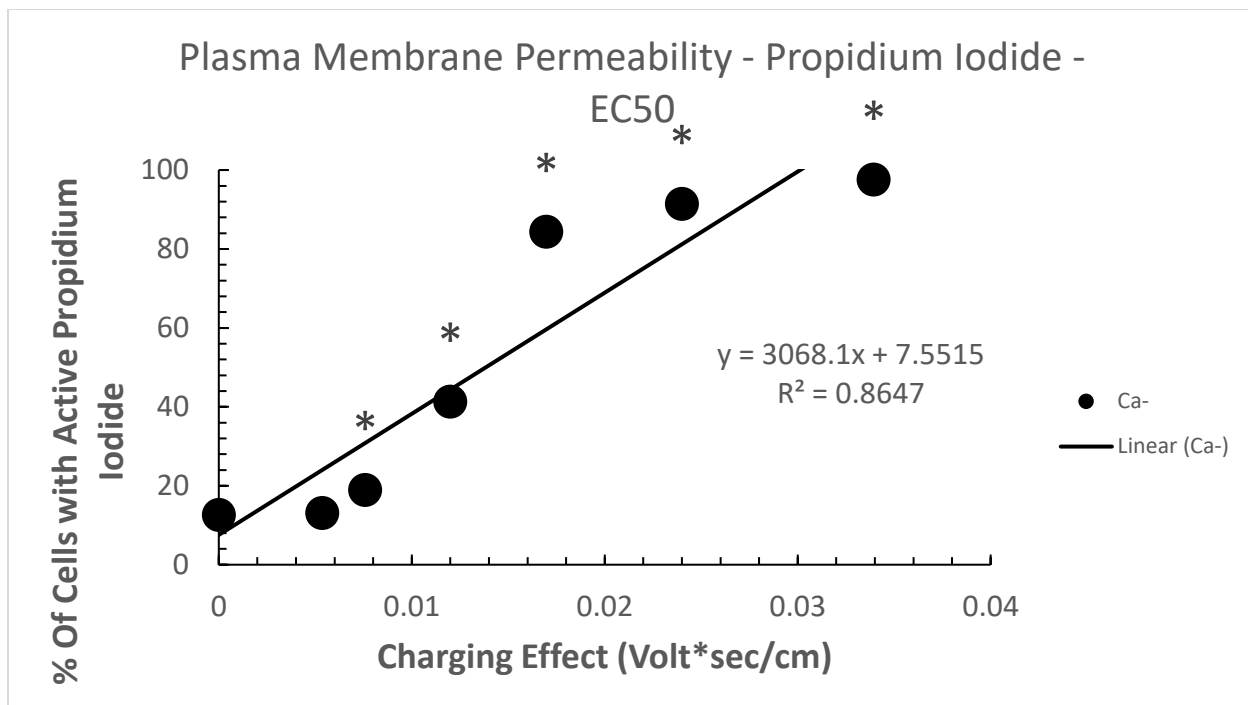
Graph 4: Example PMRS kinetics assay with H9C2 cells (see Graph 3). A representative PMRS Kinetics assay. Absorbance slope is quantified when pulses were administered from 0 to 100 pulses in H9C2 cells. With a higher number of pulses, PMRS activity declines. Error bars represent 1 standard deviation. (*difference from control with $\alpha=0.05$, Student's T Test).

The nsPEF treatment is not only affecting the PMRS activity but also affects another plasma membrane characteristic of the permeabilization of that membrane (Graph 5). To quantify the extent of the cell permeabilization with the nsPEF treatment, it is measured the active propidium Iodide content within the H9C2 cells.



Graph 5: nsPEFs induce a dose-dependent increase in plasma membrane permeability to propidium iodide (PI). H9C2 cells were suspended in PBS and pulsed with a variable amount of 60ns, 40kv/cm, 15ns rise-time pulses - 0, 5, 10, 15, 25, 50, 100, or 200 times. Cells were added immediately after pulsing to flow tubes containing PI with a final concentration of 0.03mM and were incubated for 15 minutes in the dark at room temperature. Then they were analyzed by flow cytometry. Black bars represent the percentage of plasma membrane permeabilization to PI. Error bars (nearly absent) represent 1 standard deviation. (*difference from 0 pulse with $\alpha= 0.001$, Student's T Test).

Pulsing does not affect the plasma membrane permeability for low charging values, then a charging dose-dependent increases the cell permeabilization to reach a plateau with nearly all cells become permeabilized to the dye. The pulse threshold to observe a significant change in plasma membrane permeabilization is approximatively 10 pulses ($0.00759 \text{ V} \cdot \text{sec/cm}$, Graph 6).

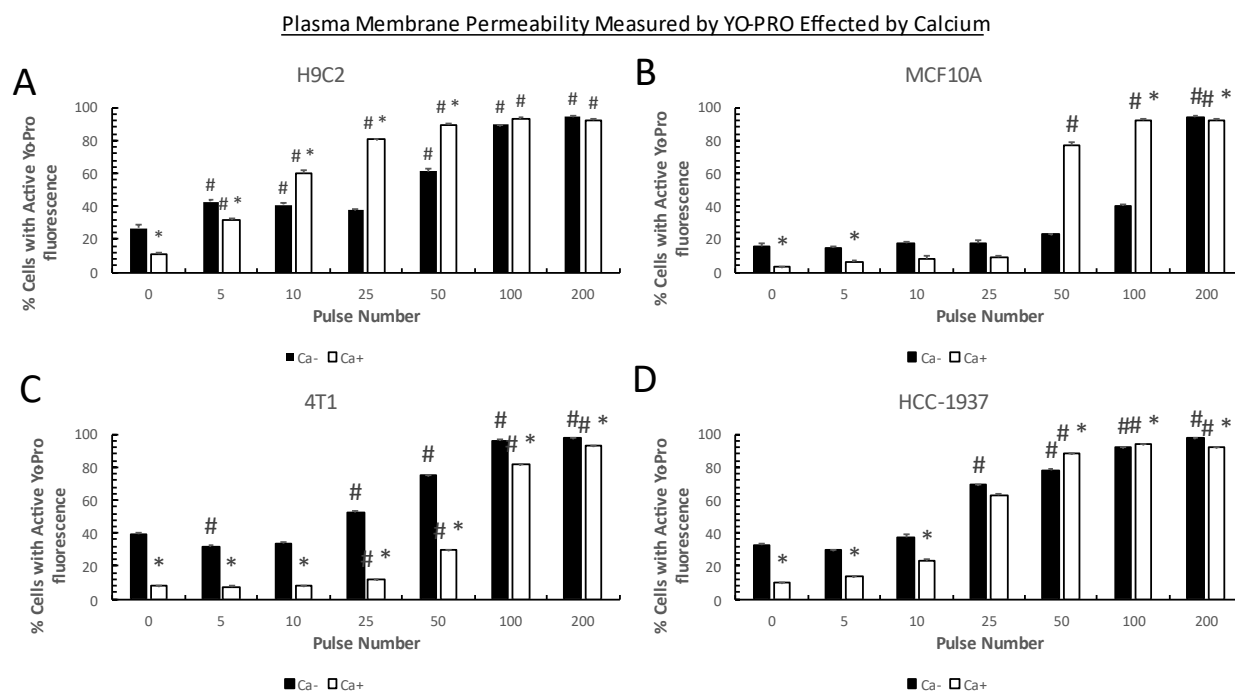


Graph 6: Charging increases the plasma membrane permeabilization in H9C2 cells. H9C2 cells were suspended in PBS and pulsed with a variable amount of 60ns, 40kv/cm, 15ns rise-time pulses - 0, 5, 10, 15, 25, 50, 100, or 200 times. Cells were added immediately after pulsing to flow tubes with a final PI concentration of 0.03mM and were incubated for 15 minutes in the dark at room temperature and then they were analyzed by flow cytometry.

Subsequently, it is investigated how calcium affects the effect of nsPEF treatment on cell permeabilization detected by YO-PRO fluorescence (Graph 7). The cell permeabilization in absence of calcium is compared with that obtained in presence of calcium for different charging values. The black bars represent the cell permeabilization of the control cells which were suspended in PBS with 2 mM EGTA to minimize the effect of calcium on the P2X7 pore. The cells were suspended in DPBS for calcium treatment. Contrary to past evidence in support of no calcium effect on plasma membrane permeability with nsPEF treatment, our and forthcoming results show that there may possibly be some evidence a calcium dose-dependent response to plasma permeability changes measured by YO-PRO for all four cell lines. In a previous study, nsPEF

treatment has not shown a calcium dependence (Pakhomov et al., 2007). Calcium has a biphasic effect on non-cancerous cells where it is inhibitory at low pulse numbers and stimulatory at high pulse numbers. There are only inhibitory effect of Ca^{2+} on cancer cell Yo-Pro-permeability. For all cell lines, the presence of calcium allows to have lower cell permeabilization than that without calcium for pulses less than 10. With an increase of number of pulses, the presence of calcium is stimulatory or less protective against cell permeabilization by nsPEF treatment of H9C2 (Graph 7A) and MCF10A (Graph 7B) cells. In another words, the permeabilization becomes more sensitive to the number of pulses in presence calcium than that without calcium. Calcium effect become negligible when cell permeabilization reaches high value 80-100%. With 100-200 pulses, there is no statistically significant difference in the number of permeabilized cells to YO-PRO between cells treated with calcium and those no treated with calcium. The calcium effect on permeabilization becomes negligible for other cell lines when treated with 200 pulses.

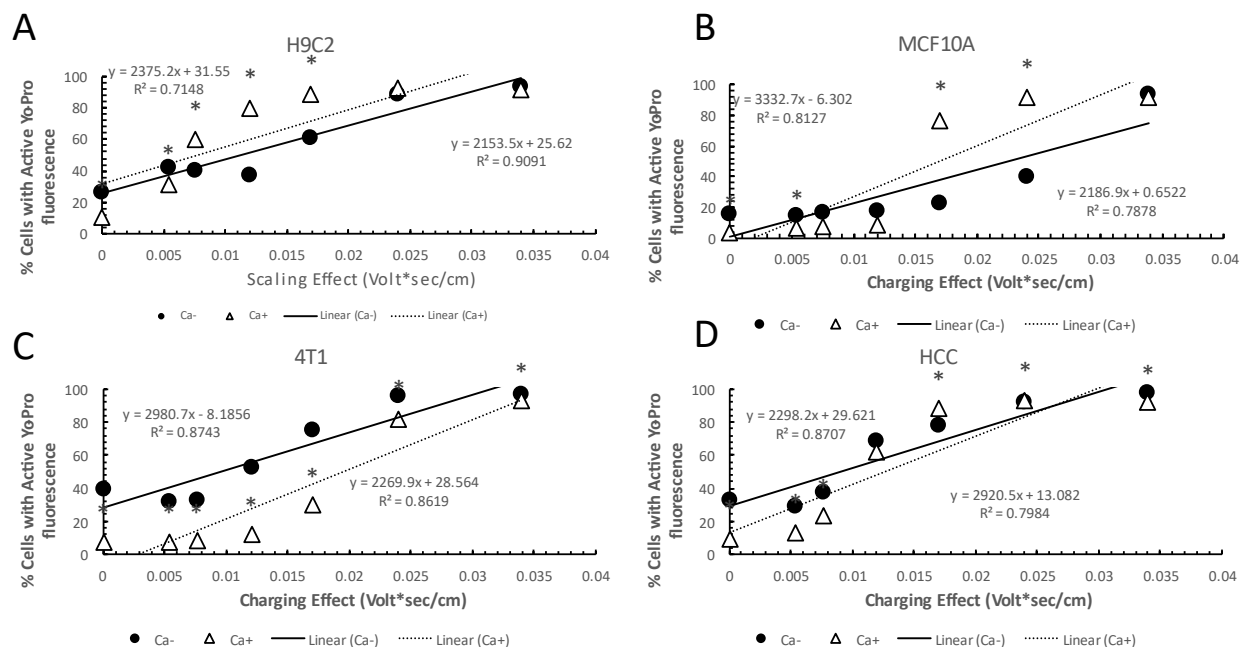
The key finding from this assay are a) the calcium effect on cell permeabilization is depending on pulse number b) the Ca^{2+} effect on Yo-Pro-permeability is different for cancer and non-cancer cells c) all cell lines can be completely permeabilized to Yo-Pro via nsPEF treatment with a sufficient number of pulses.



Graph 7: Exogenous calcium has a cell type-dependent effect on plasma membrane permeabilization quantified by cellular YO-PRO fluorescence uptake. Four cell lines (H9C2, MCF10A, 4T1, and HCC1937) were suspended in PBS with 2mM EGTA (no calcium, black bars) or in DPBS with 2mM calcium (white bars). The samples were then pulsed with a variable amount of 60ns, 40kv/cm, 15ns rise-time pulses - 0, 5, 10, 15, 25, 50, 100, or 200 times. 4uM YO-PRO was added, and cells were incubated for 15 minutes in the dark at room temperature. Then they were analyzed by flow cytometry. The graph shows the percentage of cells (Y axis) with an active YO-PRO fluorescence signal as a function of pulse number (X axis). Error bars represent 1 standard deviation. (* difference between calcium groups, # difference from no nsPEF treatment, $\alpha = 0.001$, Student's T Test).

To calculate the EC50 of the nsPEF treatment on the plasma membrane permeability, a subsection of the graphs is used to generate a linear fitting of the data in the range close to the dosage that caused a permeabilization of 50% of the cells.

YO-PRO Plasma Membrane Permeabilization Linear Interpolation



Graph 8: Calcium modulates YO-PRO fluorescence differently in cancerous and non-cancerous cell lines.

The graph shows the effect of the charging effect (Vs/cm) on cell permeabilization measured by Yo-Pro uptake within the cells. nsPEF treatment of the cells with YO-PRO is performed in the presence (DPBS solution with Ca²⁺, white triangles) or absence of Ca²⁺ (PBS solution with 2mM EGTA, black circles). Yo-Pro fluorescence is determined by flow cytometry and is indicated as a percentage of the control YO-PRO fluorescence signal. The graph shows a subset of the YO-PRO data from Graph 6. The linear regression of the YO-PRO fluorescence data is used to calculate the EC₅₀ (seen in Table 3). Error bars represent 1 standard deviation. (* difference between calcium groups at the same dose, $\alpha = 0.001$, Student's T Test).

Cell Line	Media Type	Charging Effect (V*sec/cm)	Pulse Number (#)	Calcium Effect	R ²
H9C2	Ca-	0.011	22	13	0.91
	Ca+	0.008	9		0.71
MCF10A	Ca-	0.023	163	68	0.79
	Ca+	0.017	95		0.81
4T1	Ca-	0.009	23	-8	0.86
	Ca+	0.02	31		0.87
HCC1937	Ca-	0.009	33	12	0.87
	Ca+	0.013	21		0.80

Table 3: EC50 for YO-PRO in the presence (Ca+) and absence (Ca-) of 2mM of Ca²⁺. The charging effect (column 3) and number of pulses (column 4) to permeabilize 50% of the plasma membrane. The calcium effect on cell permeabilization (column 5) is quantified by the difference in permeability without and with Ca. The R² value of the regression procedure is reported in the last column.

The determination of the EC50 and IC50 provide an index of the cell permeabilization and death as a function of the charging effect. The comparison between EC50 and IC50 values reported in Table 2 and 3, respectively, indicates that cell death occurs after cell permeabilization for all cell lines. However, other than that, there is no correlation between EC50 for cell death and IC50 for cell permeabilization. For the cell lines H9C2, MCF10A, 4T1, and HCC-1937 the IC50 (i.e., death) occurs at 22, 321, 49 and 86 pulses, whereas EC50 (i.e., permeabilization) is observed at 9, 95, 49 and 31. Mitochondria play a more important role in viability than plasma membrane permeability does.

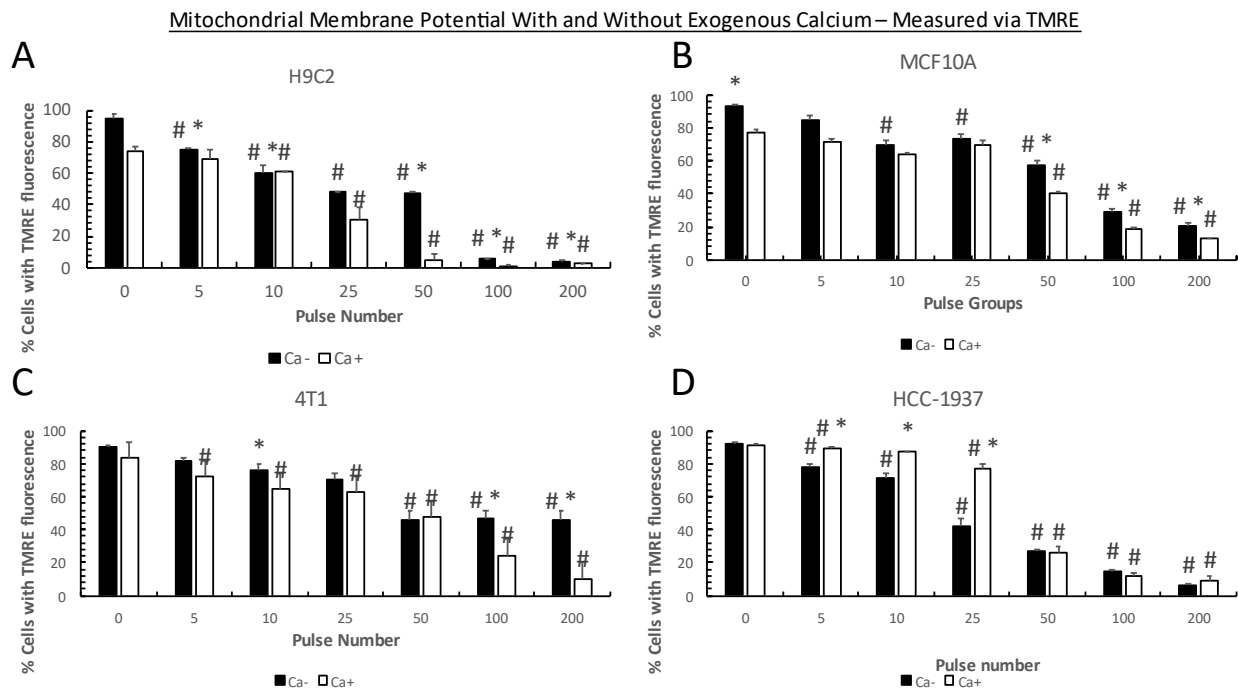
YO-PRO is used to test for plasma membrane permeability, some mammalian cell lines, specifically RAW 264.7, express receptors of the P2X family (North, 2002) endogenously (RAW 264.7 (ATCC, 2021)), and it has been demonstrated that at least one of these receptors (P2X7) allows YO-PRO dye to enter the cell with multiple pathways including that of calcium-dependent permeability to the YO-PRO Dye (Cankurtaran-Sayar et al., 2009). The accumulation of YO-PRO

has been proven to depend on the presence of this receptor (Michel et al., 2009) For this reason, YO-PRO has been used to demonstrate differences in cancerous and non-cancerous cell lines. One feature that could be a future scope of study would be to evaluate the activity of the P2X7 receptor via Yo-Pro (Rat et al., 2017) which can contribute to open large pores in the plasma membrane (> 600Da) (Virginio et al., 1997). Previous studies have established that HCC-1937 (Jardin et al., 2018; Motiani et al., 2010) H9C2 (Chen et al., 2019), 4T1 (Brisson et al., 2020), and MCF10A (Jelassi et al., 2013) cell lines may have a calcium-dependent permeability.

Mitochondrial Membrane

Our study on the effect of nsPEFs treatment on intracellular structure and functions continued with the investigation of the effects on mitochondria because their key role in cell death (viability) and energy metabolism. Specifically, it is important to determine whether there exists a relationship between nsPEF treatment and cellular metabolic function. Indeed, nsPEF treatment effect on cellular membranes can also involve an alteration of the mitochondrial membranes.

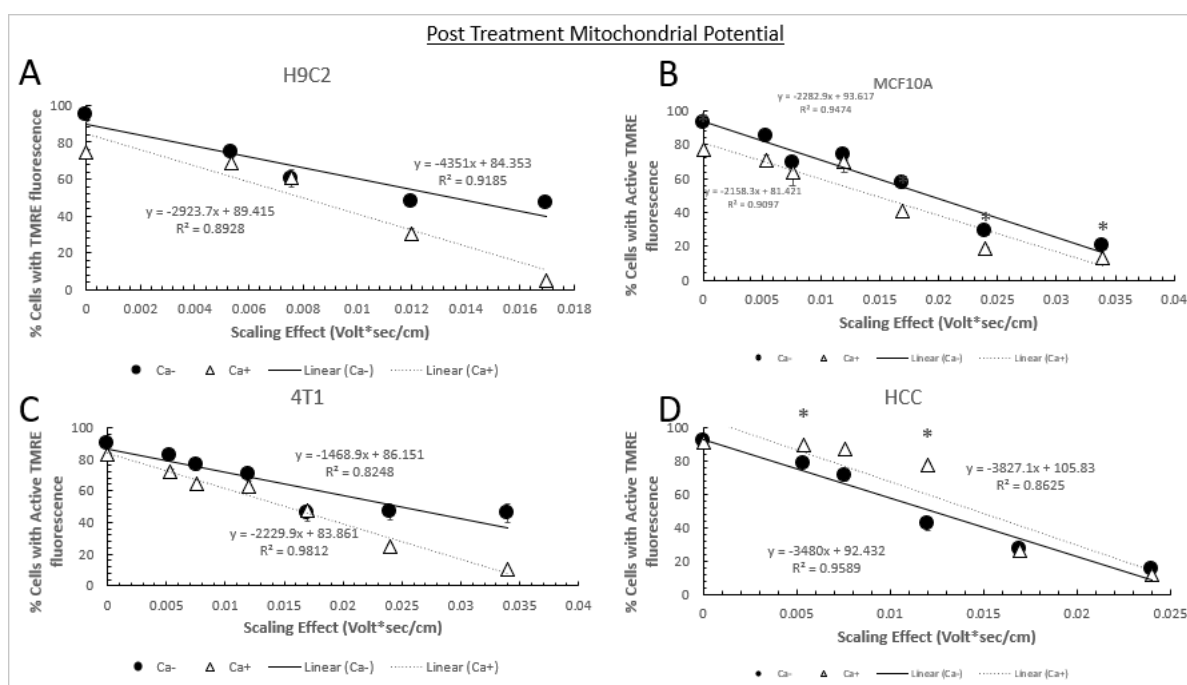
The second series of experiments focused on the mitochondrial membrane integrity to find the conditions under which the inner mitochondrial membrane (IMM) and outer mitochondrial membrane (OMM) are functionally compromised, and so to differentiate the future changes in the ETC complexes from the changes that occur due to permeability- which could be due to either the mechanical breaching of the mitochondrial membranes, or the opening of the mPTP (mitochondrial Permeability Transition Pore) or the VDAC (Voltage Dependent Anion Channel).



Graph 9: Mitochondrial membrane potential (MMP) drop is dependent on calcium at low levels of nsPEF treatment. Four cell lines (H9C2, MCF10A, 4T1, and HCC1937) were suspended in PBS with 2mM EGTA (no calcium, black bars) or in DPBS with 2mM calcium (white bars) The samples were then pulsed with a variable amount of 60ns, 40kv/cm, 15ns rise-time pulses - 0, 5, 10, 15, 25, 50, 100, or 200 times. 2uM TMRE was then added, and cells were incubated for 15 minutes in the dark at room temperature. Then they were analyzed by flow cytometry. The graph shows the changes of cells percentage with an active TMRE fluorescence signal as a function of the pulse number. On the X axis, the pulse number is shown. Error bars represent 1 standard deviation. (* difference between Calcium groups, # difference from no nsPEF treatment with $\alpha= 0.001$, Student's T Test).

The effect of nsPEF treatment on mitochondrial membrane depolarization was measured by detecting the dissipation of TMRE fluorescence signal for different pulse number. H9C2 cells show significant differences in mitochondrial membrane drop both with and without calcium in the solution, as seen in table 4. Within the group of cells with exogenous calcium, H9C2 cells see an IC50 lower than any other group, only requiring 11 pulses to reduce mitochondrial polarization by half. MCF10A and HCC-1937 cells, under that same condition, would require 26 more pulses to reach this IC50 – a factor of around 3.4. The threshold for a nsPEF-induced loss of $\Delta\Psi_m$ was 5 pulses (0.005 V*sec/cm) and the presence of calcium enhanced the loss of $\Delta\Psi_m$, especially at

higher nsPEF conditions (≥ 50 pulses, ≥ 0.017 V*sec/cm. A similar trend is observed for MCF10A Cells which show to be more resilient to nsPEF treatment until the cells absorb high levels of energy where calcium enhanced the effects on loss of $\Delta\Psi_m$. In this particular case, the IC50 for H9C2 cells with calcium chelation is approximately 32 pulses. The same value for MCF10A cells under the same condition is nearly double that at 63 pulses. With exogenous calcium, the difference is even greater- 11 pulses for H9C2 and 37 for MCF10A. 4T1 cells show resilience like MCF10A cells. In contrast, in the HCC-1937 cell line, calcium appears to protect the MMP.



Graph 10: Effect of nsPEFs (charging effect) on the mitochondrial membrane potential with and without Ca^{2+} in cancerous and non-cancerous cell lines. The graph shows the changes of cells percentage with a high TMRE fluorescence signal as a function of Charging Effect (Volt*Sec/cm). The control cells (PBS solution with 2mM EGTA, are represented with black circles) and the cells with calcium (DPBS solution) are represented with white triangles. The linear regression of the data is used to calculate the EC50 (Table 4). Samples did have significant delay in flow cytometry processing due to the number of samples run.

In Graphs 9 and 10, the effect of calcium influences the dissipation of $\Delta\Psi_m$ in the four cell lines tested are demonstrated. The EC50 for dissipation of the mitochondrial membrane potential is reported in Table 4. The H9C2 cells show a drop after 0.015 V*sec/cm - and shows a clear divergence in the samples with and without exogenous calcium available. Specifically, the cells suspended in media with exogenous calcium dissipate $\Delta\Psi$ with substantially less pulsing that cells with EGTA. MCF10A cells show a less pronounced effect. 4T1 cells demonstrate similar behavior but the pulsing conditions appears to be insufficient to cause a complete dissipation of $\Delta\Psi$ in cells without exogenous calcium. HCC-1937 cells have a crossing behavior, implying that calcium can contribute to a response that has different activities at high or low nsPEF dosages.

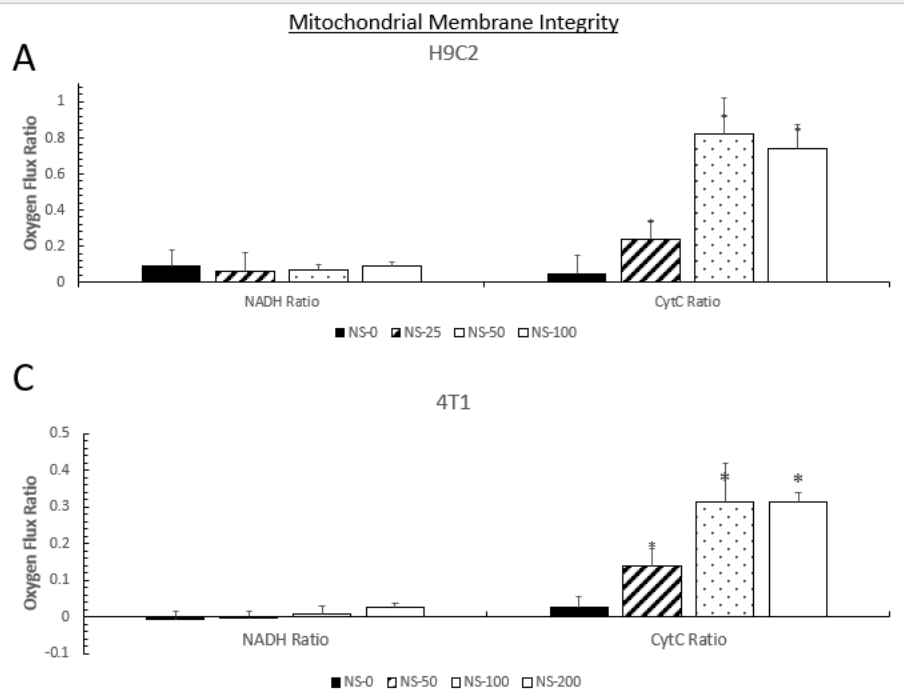
Cell Line	Media Type	Charging Effect (Volt*sec/cm)	Pulse Number (#)	Calcium Effect	R ²
H9C2	Ca-	0.013	32	21	0.89
	Ca+	0.008	11		0.91
MCF10A	Ca-	0.019	63	26	0.95
	Ca+	0.015	37		0.91
4T1	Ca-	0.025	105	65	0.82
	Ca+	0.015	40		0.98
HCC1937	Ca-	0.012	26	-11	0.96
	Ca+	0.015	37		0.86

Table 4: EC50 for dissipation of the mitochondrial membrane potential with and without Ca²⁺. The charging effect (column 3) and number of pulses (column 4) to dissipate 50% of the mitochondrial membrane potential. The R² value of the regression procedure is reported in the last column.

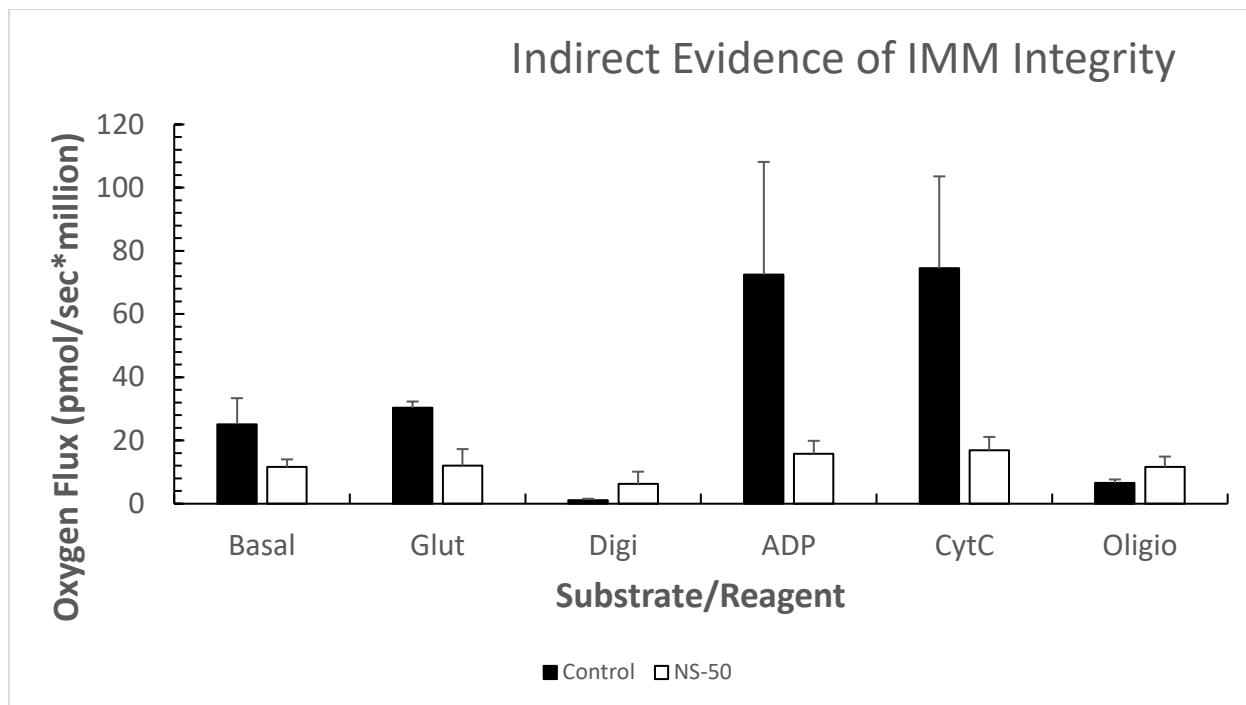
The next set of experiments focus on the evaluation of the functional integrity of the outer and inner mitochondrial membranes by polarographic measurements. H9C2 cells were exposed to half the pulse doses used for the other cell lines. In both the H9C2 and the 4T1 cell lines, there is

a notable lack of any increase in oxygen consumption rate after the addition of NADH regardless the pulse number, indicating that nsPEFs do not alter the integrity of the IMM, even with 50 and 100 pulses where 80-90% of cell would be dead 24h later (see Graph 2). In presence of an altered integrity of IMM, an increase of oxygen consumption should have occurred because the IMM would have been permeable to NADH that can freely reach mitochondria for its utilization. In contrast, the oxygen flux ratio increased dramatically in response to the addition of CytC, indicating that the integrity of the OMM was compromised. The outer mitochondrial membrane in both H9C2 and 4T1 cells began to permeabilize significantly with administration of 50 pulses or more. The release of Cytochrome C from the mitochondria is far from trivial – the release of CytC as a part of caspase-dependent programmed cell death is usually part of multiple regulatory mechanisms and can amplify other RCD signals (Yong-Lin et al., 2008)

The approach proposed in our work to evaluate the IMM integrity was similar to (Hyo-Jung Choo, 2017). This indirect analysis of the IMM by using oligomycin was done to quantify some changes in the IMM. But this data also did not point to significant permeabilization of the IMM. This is seen in Graph 12.



Graph 11: nsPEF treatment can effectively disrupt OMM integrity without compromising the IMM of H9C2 and 4T1 cells. Two cell lines (H9C2, and 4T1) were suspended in growth media and treated with variable numbers of pulses with 60ns durations, 15ns rise-and electric fields of 40kv/cm, time pulses. Cells were then suspended in Mir05 electrode media and analyzed in the oxygraph by sequentially exposure to Digitonin, ADP, NADH, CytC, and DOC (see Methods). To obtain oxygen flux ratio, the respiration rate obtained with NADH or CytC was subtracted from that with digitonin and normalized to the respiration rate with DOC. Error bars represent 1 standard deviation. (* difference from control with $\alpha=0.05$, Student's T Test).



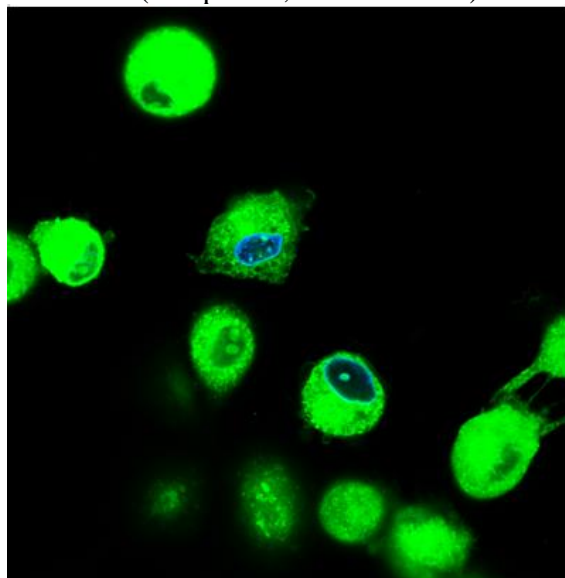
Graph 12: Inhibition of Complex V by Oligomycin provides indirect evidence of IMM integrity. For this experiment, H9C2 cells were suspended in growth media. The samples were then pulsed with a variable amount of 60ns, 40kv/cm, 15ns rise-time pulses (0 or 50 times). Cells were then suspended in Mir05 electrode media and sequentially exposed to Glutamate, Digitonin, ADP, CytC, and then oligomycin. The change in oxygen flux from the elevated levels under CytC and the decrease after oligomycin was added to provide an indirect measure that the ATP synthesis in the IMM is still intact. The smaller change in oxygen flux for the treated cell is likely an indicator of the effect of nsPEFs on that lowers the basal rate respiration in the cells. Error bars represent 1 standard deviation. (No significance calculated – N=2 for both groups)

The IMM condition was analyzed with the microscopy in cells after nsPEF treatment. A pilot study with Mitotracker green was done to verify that mitochondrial dyes that were somewhat dependent on $\Delta\Psi$ could be used. This pilot study demonstrated it was possible to visualize the mitochondrial membrane of H9C2 cells treated with 200 pulses 2 hours after treatment. These results demonstrate that Mitotracker green was able to bind to the mitochondrial membrane even after the administration of pulses that should cause total loss of $\Delta\Psi$ (as shown through TMRE). The full assay was done by dyeing H9C2 cells (Control or 200p treated) with DAPI and either

Mitotracker Green or NAO (10 nonyl acridine orange), a stain for cardiolipin, which is located solely in the IMM. Unfortunately, both dyes are green and so cannot be used to co-locate in the same sample.

Mitochondrial Membrane Microscopy – MitoTracker Green

A Control (Not pulsed, 0 volt*sec/cm)



B 200 Pulses (0.034 volt*sec/cm)

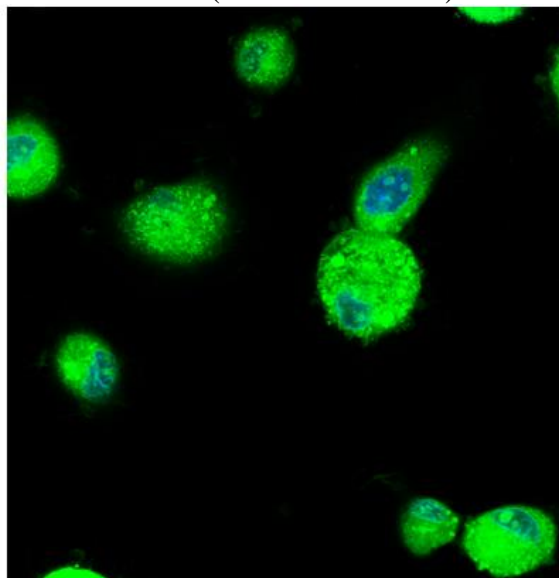


Figure 4: Effect of nsPEF on general mitochondrial morphology. DAPI (nuclear stain) is visualized in blue, and Mitotracker (mitochondrial stain) is in green. Panel A (left-hand side) shows control cells resuspended with sham treatment and stained. Panel B (the right-hand side) shows cells pulsed 200 times and stained.

The primary goal of visualizing the mitochondria after cells nsPEF treatment, was to determine whether the nsPEF treatment could reduce the mitochondrial $\Delta\Psi$ to non-functional levels. In figure 4, it can be demonstrated that despite the near total loss of $\Delta\Psi$, the IMM is still at least present and cardiolipin has not been degraded to the point where it cannot be stained and visualized. Additionally, the punctate structure of H9C2 cells after treatment is visible. However, the resolution is not enough to make more conclusive statement.

The next goal was to visualize specifically the IMM of the treated cells to see if the IMM was still at least present, or if any visual difference in the treated or control cells could be seen. This is seen in Figure 5, which is similar to Figure 4, with the primary exception that green fluorescence shows the dye NAO, which attaches to the protein cardiolipin, a structural component of the IMM.

Mitochondrial Membrane Microscopy – NAO

A Control (Not pulsed, 0 volt*sec/cm)

B 200 Pulses (0.03394 volt*sec/cm)

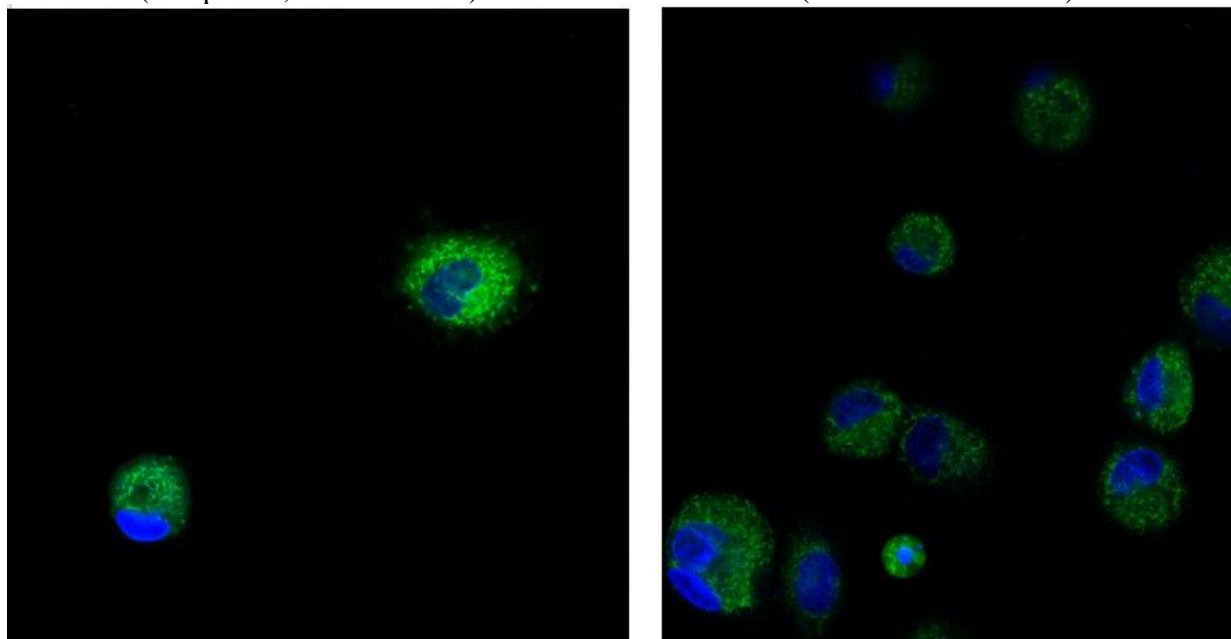
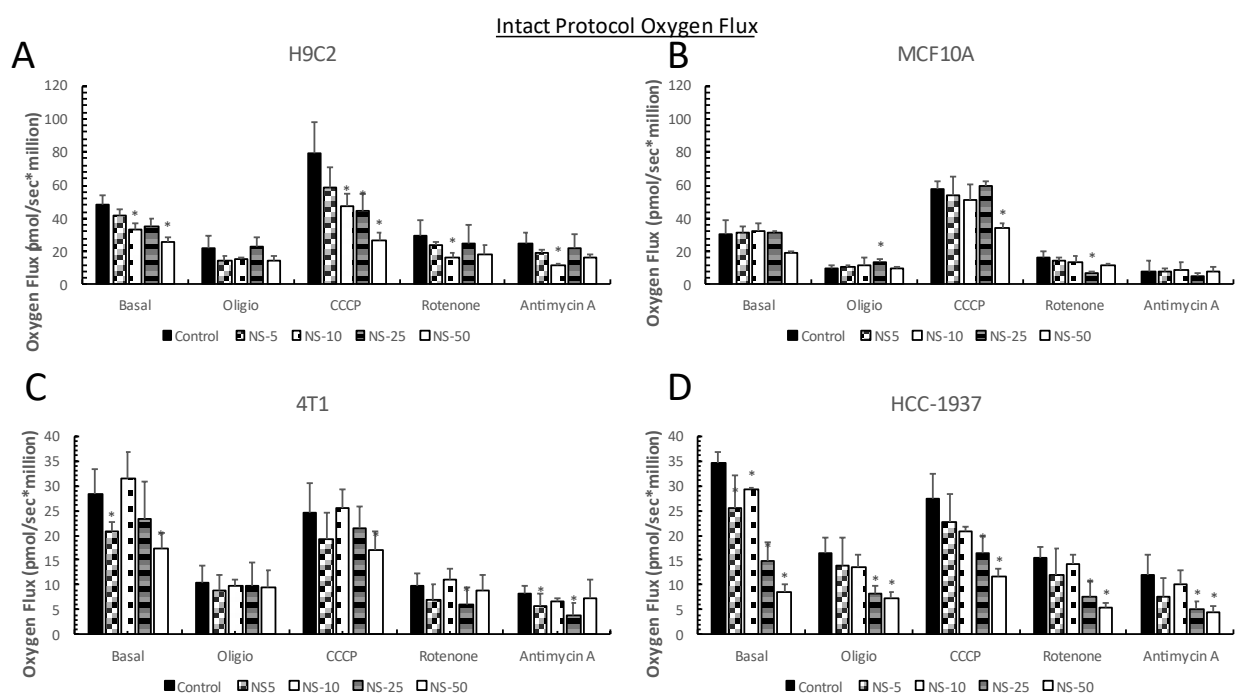


Figure 5: Effect of nsPEF on mitochondrial cardiolipin staining. DAPI (nuclear stain) is visualized in blue, and NAO (cardiolipin stain) is in green. Panel A (the left-hand side) of the figure shows control cells that were resuspended, given sham treatment, and then stained. Panel B (the right-hand side) shows cells that were pulsed 200 times and then stained.

Mitochondrial ETC Complex Changes

Since nsPEF affected electron transport in the PMRS (as detected with WST-8 and PMS), it was determined whether nsPEF could affect electron transport in the mitochondrial ETC. This

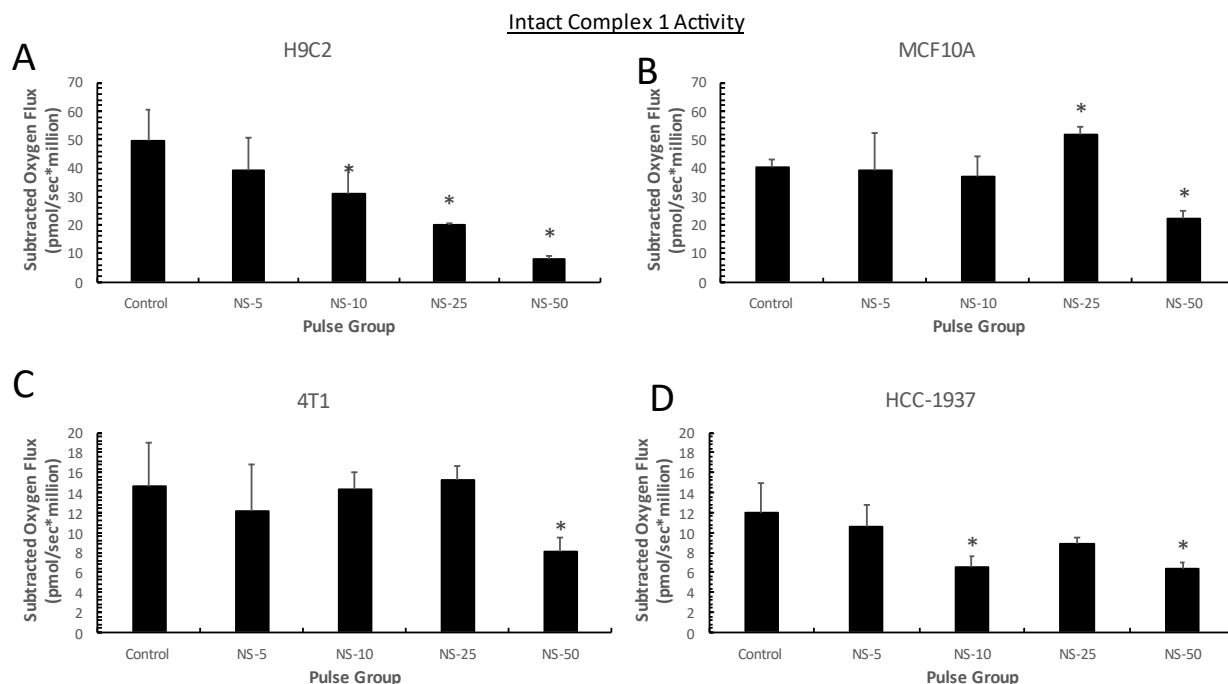
could be detected by metabolically related changes in oxygen consumption. The first attempt to do this relied on cell-permeable reagents, oligomycin (an inhibitor of ETC Complex V), CCCP (an ionophore of the mitochondrial membrane), rotenone (an inhibitor of ETC Complex I), and antimycin A (an inhibitor of ETC Complex III), and the resultant oxygen flux in each case can be seen in Graph 13.



Graph 13: nsPEFs attenuate oxygen flux in 4 different cell lines with intact plasma membranes. 4 cell lines were suspended in growth media. The samples were then pulsed with a variable amount of 60ns, 40kv/cm, 15ns rise-time pulses (0, 5, 10, 25, and 50 pulses for all four lines). Cells were immediately suspended in Gemish electrode media and sequentially exposed to Oligomycin (Complex V inhibitor), CCCP (ionophore/uncoupler), Rotenone (Complex I inhibitor), and Antimycin A (Complex III inhibitor) (see Methods section for concentrations). The oxygen consumption of the 4 tested cell lines in the basal state and after treatment with 5 different nsPEF conditions. Oxygen fluxes were recorded after addition of 4 different reagents (see legend for pulse conditions). Error bars represent 1 standard deviation. (* = significance with $\alpha = 0.05$, Student's T Test). Note that the Y axis for H9C2 and MCF10A are 120 pmol/sec*million, and for 4T1 and HCC1937 the Y axis is only 40 pmol*sec/million.

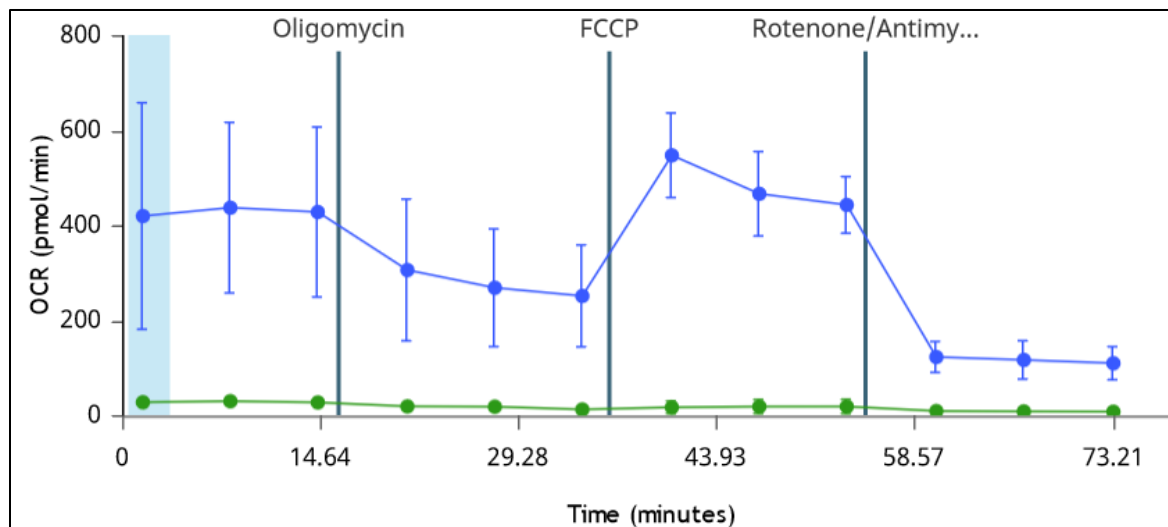
50 nsPEF pulses significantly inhibited basal respiration rates in 3 of the four cell lines (H9C2, 4T1 and HCC1937). The oxygen consumption rate of the uncoupled mitochondria with nsPEF treatment was lower than control group for all cell lines. Oligomycin (Complex V inhibitor) caused no significant differences across treatment dosages. The specific effects of nsPEFs on Complex I is quantified by subtracting the oxygen consumption rate under the effect of rotenone, an inhibitor of complex I function from the oxygen consumption rate under the effect of the ionophore CCCP. The effect of nsPEF treatment on Complex I was reported in Graph 11. These experiments indicate that for all cell type the metabolic function was reduced for 50 nsPEF pulses at 60ns, 40kv/cm, 15ns rise-time. This result was obtained even when the effect of Antimycin A, an inhibitor of Complex III, was subtracted from the oxygen consumption rate.

In H9C2 cells, a significant dose dependent decrease in Complex I activity is noted in every test condition greater than 10 pulses or 0.008 Vs/cm, which is near the threshold for nsPEF-induced increase in plasma membrane permeability in these cells (Graph 6).



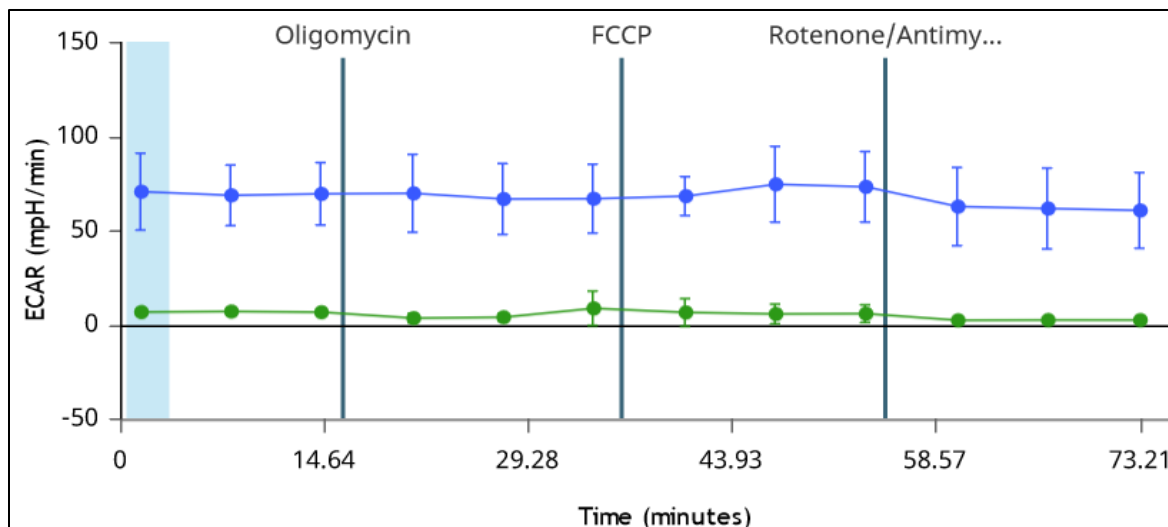
Graph 14: nsPEF treatment shows a dose-dependent decrease in ETC Complex I activity for H9C2 cells. From the data in Graph 13 (previous), the total oxygen flux rate when the sample is exposed to the Complex I inhibitor Rotenone is subtracted from the oxygen flux rate when the sample is exposed to the ionophore CCCP for all experimental samples. Black bars represent the oxygen flux difference, and this difference is split by pulse group along the abscissa. Again, note that the Y axis differs between H9C2 and MCF10A non-cancer cells (70 pmol/sec*million) vs. 4T1 and HCC1937 cancer cells (20 pmol/sec*million). Error bars represent 1 standard deviation. (* difference from control, $\alpha=0.05$, Student's T Test).

In addition to the bioenergetic assays carried out with the Oroboros instrument that does not provide information on the cell glycolytic capacity, additional tests were obtained with the Agilent Seahorse XF analyzer to have both oxygen consumption rate and hydrogen ion production rate. The latest measure provides an indirect measure of glycolysis by lactate production. A pilot study of H9C2 cells (control cells being non-pulsed, and treated cells pulsed 25 times at 40kV/cm, 60ns pulses) was done (Graph 16 and 17). The temporal profile of the oxygen consumption rate (OCAR) and extracellular acidification rate (ECAR) of the cells are reported in Graphs 16 and 17, respectively.



Graph 15: The temporal profile of Oxygen Consumption Rate (OCAR) for H9C2 cells. The blue dots and line are representative of the oxygen consumption rate of unpulsed (control) H9C2 cells, and the green dots and line is representative of the oxygen consumption rate of cells treated with 25 nsPEF pulses (40kV/cm, 60ns). The assay used was the commercially available “Mito Stress Test” (Agilent, 2019). This kit uses Oligomycin, FCCP (a similar ionophore to CCCP) and a combination of the CI and CIII inhibitors – Rotenone and Antimycin A – which are injected at the same time.

The Seahorse XF Analyzer, in terms of producing OCAR results, shows similar trends as the earlier implemented Oroboros O2K unit. However, as can be seen by the complete lack of activity in the test group (green) 25 40kV/cm, 60ns pulses renders the H9C2 cell unable to form an intact monolayer of cells within a 2-hour time frame. The lack of this monolayer in turn reduces the ability of the Seahorse XF to adequately measure the OCAR and ECAR of the cell samples. The standard operating protocol is to incubate the cells at a specified seeding density for 24 hours before testing. The flaw in these tests is that the Seahorse XF analyzer requires cells be actively adherent. A 25-pulse dose for H9C2 cells is foremost more than the EC50 dose for viability. Secondly, the cells that do remain take more time to adhere to the bottom of the plate used for the Seahorse XF analyzer. This makes investigations of the cells after nsPEF treatment difficult. However, by counting the adherent cells it is possible to accurately OCR and ECAR

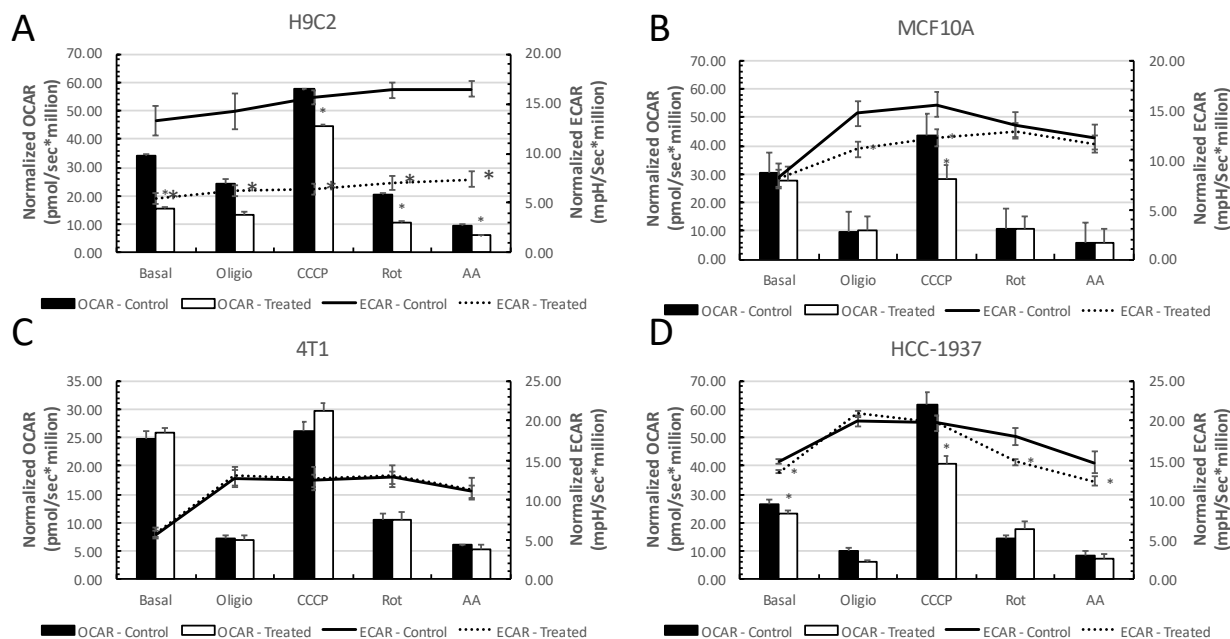


Graph 16: The temporal profile of Extracellular Acidification Rate (ECAR) for H9C2 cells. The blue dots and line are representative of the Hydrogen Ion production rate of unpulsed (control) H9C2 cells, and the green dots and line is representative of the Hydrogen Ion production rate of cells treated with 25 nsPEF pulses (40kV/cm, 60ns). The assay used was the commercially available “Mito Stress Test” (Agilent, 2019). This kit uses Oligomycin, FCCP (a similar ionophore to CCCP) and a combination of the CI and CIII inhibitors – Rotenone and Antimycin A – which are injected at the same time.

The frequently studied Warburg effect (the tendency for cancerous cell to utilize glycolysis even under normal, aerobic conditions (Potter et al., 2016; Warburg et al., 1927) could not be analyzed at those conditions because using a condition with the viability greater than the IC50 and the problem related to the cell adherence. For the full investigation of the oxygen consumption and glycolytic activity, the dose was decreased to 10 40kV/cm, 60ns pulses for all cell types. The plotting style was changed to better fit the earlier intact assay (see Graph 18).

The glycolytic shift in metabolically stressed cells is observed through the administration of oligomycin, which blocks the function of Complex V. This inhibition causes the cell to increase its glycolytic activity until the ionophore CCCP is administered.

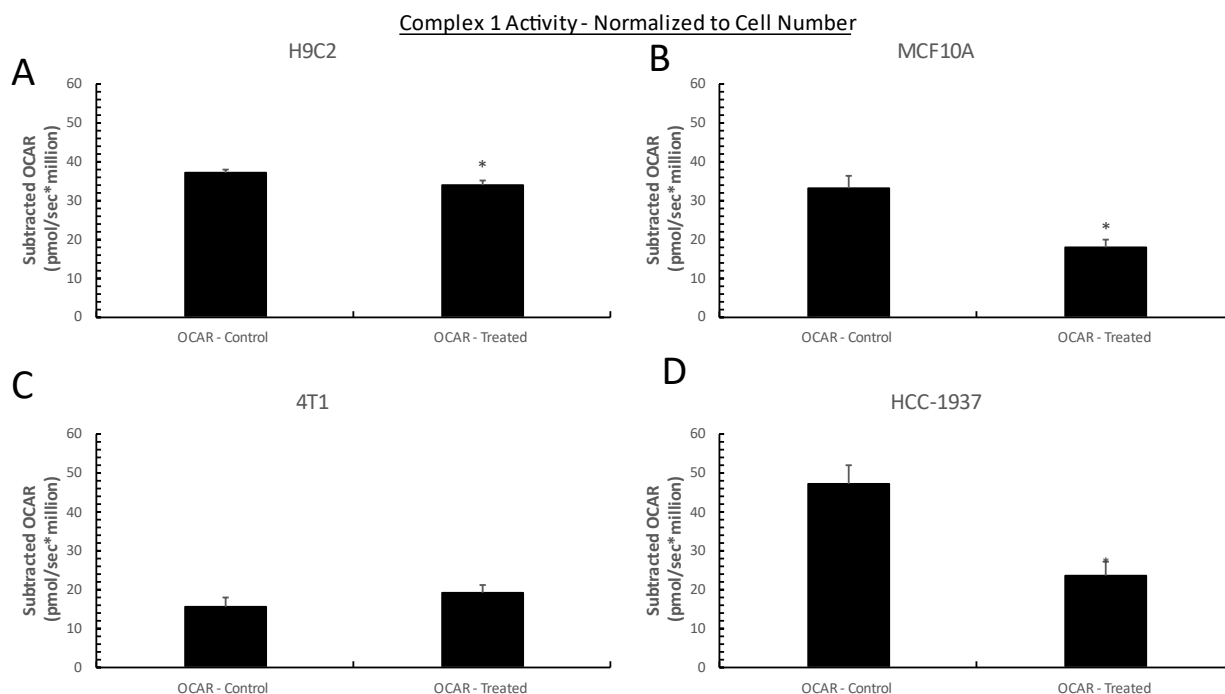
Intact Oxygen Consumption and Hydrogen Ion Production - Normalized to Cell Number



Graph 17: OCAR and ECAR rates of nsPEF treated cells show significant changes. Cells were suspended in growth media and pulsed 0 or 10 times with 60ns, 40kv/cm, 15ns rise-time pulses. Cells were then resuspended in Seahorse XF media Agilent sourced DMEM media, and supplemented with 1 mM pyruvate, 2 mM glutamine, and 10 mM glucose. Given 1 hour to attach to the plate bottom. Once attachment and viability were verified, cells were inserted into the Seahorse XF analyzer. The Acute Injection Mito Stress Test was used, with the injection order being Oligomycin (0.5uM), CCCP (2uM), Rotenone (0.5uM), and Antimycin A (0.5uM). OCAR and ECAR measurements were taken every 5 minutes. OCAR measurements are in bars and aligned with the left-hand axis. For 4T1 cells this value is 35, for the other three graphs it is doubled. Black bars are for control (non-treated) cells, and white bars are used for treated cells. ECAR measurements are plotted as lines and aligned with the right-hand axis. Solid and dotted black line are used for ECAR of the control and treated cell, respectively. The left axis indicates OCAR (pmol/sec*million cells) and the right axis indicates ECAR (mpH/sec/million cells). Error bars represent 1 standard deviation. (* difference from control $\alpha=0.05$, Student's T Test).

The two derived values from this series of experimentation are the OCAR attributable to Complex I and the ECAR production (attributable to Complex V) are reported in graph 19. The OCAR was statistically reduced for H9C2, MCF10A and HCC1937, but the difference was not observed for 4T1 cells. For this cell line it is possible that the pulses administered were not sufficient to have a notable effect on the oxygen consumption rate. The seahorse method can be

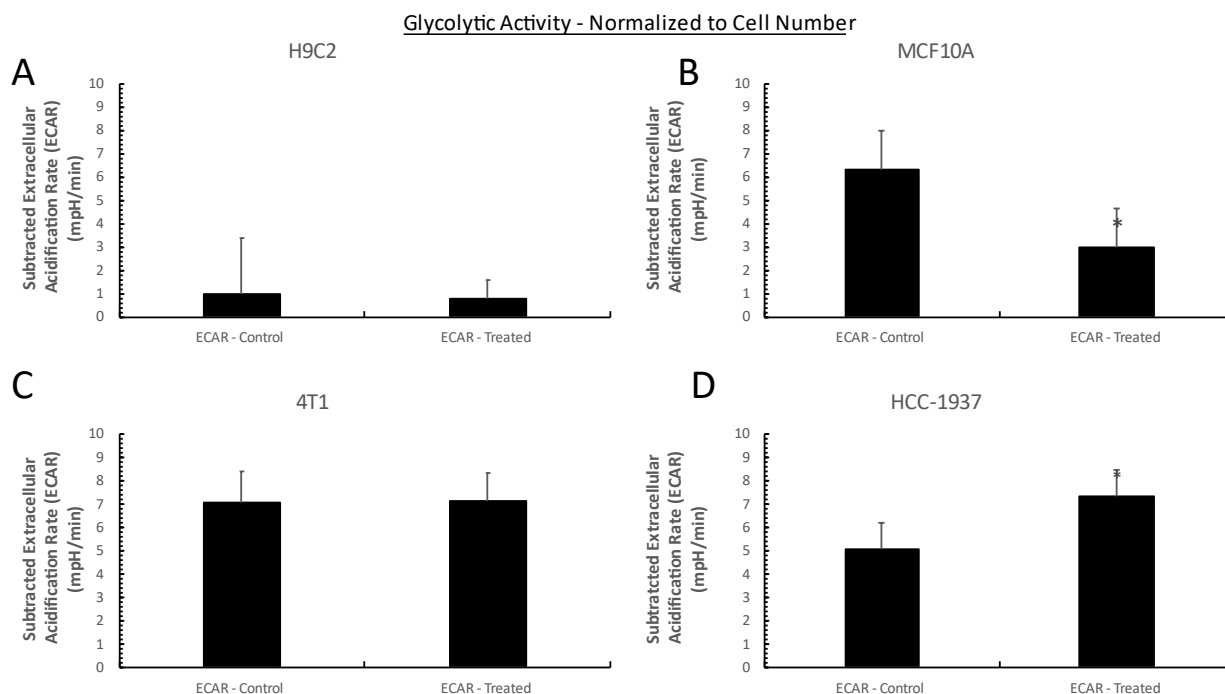
used to detect very slight changes in oxygen consumption rate whereas the procedure is somewhat inconvenient because it requires the cell monolayer formation to perform the assay, which is not necessary in the oxygraph.



Graph 18: OCAR from Seahorse XF significantly drops in 3 cell lines. The normalized OCAR (OCAR normalized to the number of cells placed into the well) under the effect of rotenone was subtracted from the normalized OCAR under the effect of CCCP. The Normalized OCAR difference is plotted in black lines and separated by control and treated (10 nsPEF pulses, 60ns, 40kv/cm, 15ns rise-time). The Y axis for all plots is set to 60 pmol/sec*million). In 3 cases (H9C2, MCF10A, and HCC1937), the result of nsPEF treatment was a significant decrease in oxygen flux. For 4T1 cells, oxygen flux increased, but not significantly. Error bars represent 1 standard deviation. (* = significance with $\alpha = 0.05$, Student's T Test).

The nsPEF treatment effect on the glycolytic activity of the cells was assayed (Graph 20). Neither of the murine samples, the non-cancerous H9C2 nor the cancerous 4T1, demonstrate a significant change in glycolytic metabolism. The H9C2 sample have very low glycolytic capacity, and the 4T1 glycolytic output high – and nsPEF treatment does not change this. As far as the

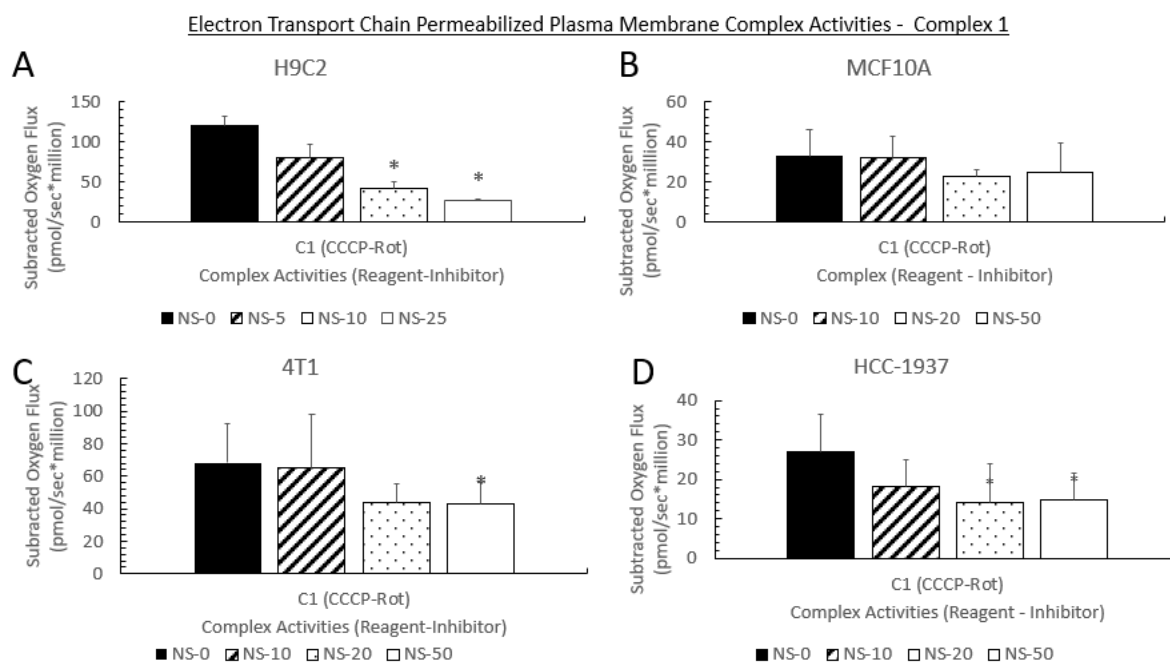
human cell lines - a significant decrease to glycolytic capacity in MCF10A cells due to nsPEF treatment is seen, as well as a significant increase in HCC1937 cells. This change in glycolytic activity in HCC-1937 cells aligns with past experimentation (Juvekar et al., 2016).



Graph 19: ECAR from Seahorse XF significantly drops in 2 human-based cell lines. The normalized ECAR (ECAR normalized to the number of cells placed into the well) under the effect of oligomycin was subtracted from the normalized ECAR at basal levels. The normalized ECAR (normalized to the number of cells) under the effect of oligomycin was subtracted from the normalized ECAR at basal levels. In 2 cases (MCF10A, and HCC1937), the result was a significant change in hydrogen ion production. MCF10A cells produced less H⁺ (as did H9C2 cells, though not significantly). HCC1937 cells produced more H⁺ ions. For 4T1 cells there was essentially no change. (* = significance with $\alpha=0.05$, Student's T Test).

After the study of the effect of nsPEF treatment on glycolytic activity, a series of experiments were designed to determine whether the effect of nsPEF treatment observed on the metabolic activity was related to the alteration of the ETC components or of the substrates. The cells were permeabilized and stimulated with substrates that were not pulsed and assayed via high

resolution polarography in a similar manner. Therefore, the activity that may have been ascribed to Complex III could be referred to as Residual O₂ Flux – because Complex III was not shown to be sufficiently stimulated. Complex III data was thus obtained but not duplicated here.

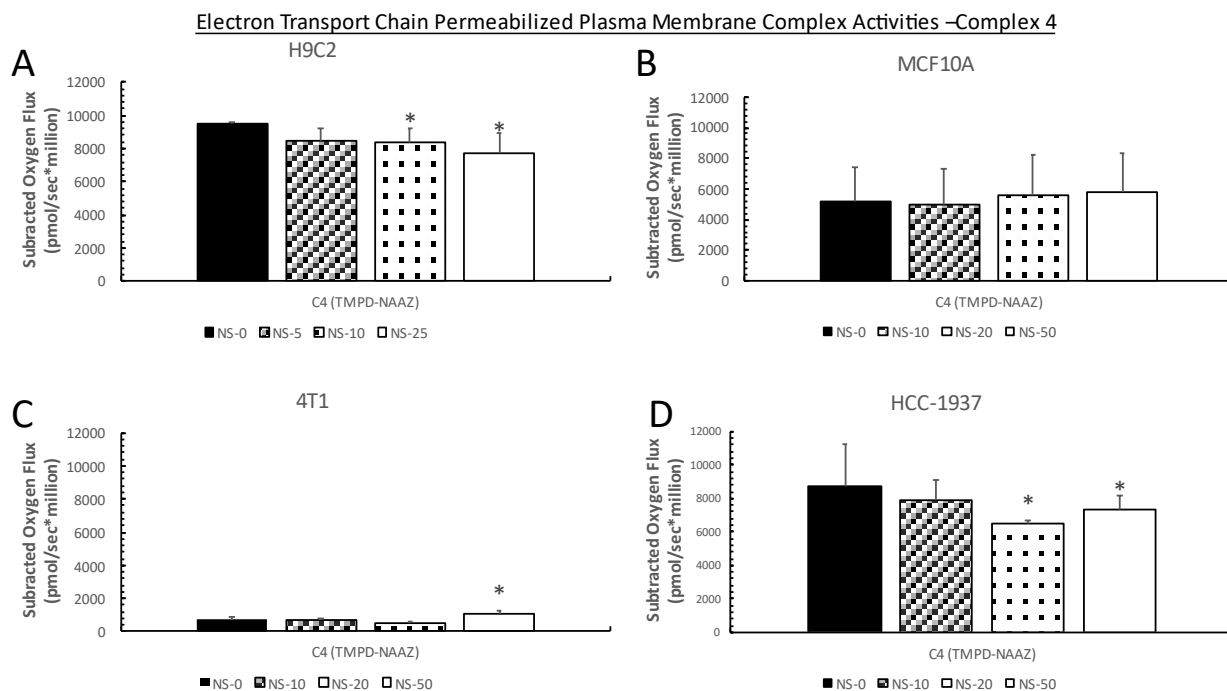


Graph 20: Three cell lines suspended with exogenous mitochondrial substrates and treated with nsPEF show significant change to Complex I activity. 4 cell lines were suspended in growth media. The samples were then pulsed with a variable amount of 60ns, 40kv/cm, 15ns rise-time pulses. For H9C2 cells, 0 (Control), 5, 10, and 25 pulses were given. For the other cell lines, 0 (Control), 10, 20, and 50 pulses of the same parameters were given. Cells were incubated for 20 minutes under SIP after treatment and then suspended in Mir05 electrode media and sequentially exposed to a series of substrates and digitonin to chemically permeabilize the plasma membrane and ensure contact of the substrates with the mitochondria (see Methods section for concentrations). Once the substrates were added, CCCP was used to uncouple mitochondrial function. Once CCCP was titrated to maximal levels, rotenone was added to inhibit Complex I function. The difference between oxygen consumption rate values under rotenone and CCCP were subtracted to find C1 (CCCP-Rot) values. The left axis shows the oxygen flux value (which is set to 140 pmol/sec*million). Error bars represent 1 standard deviation. (* = significance with $\alpha=0.05$, Student's T Test).

In permeabilized cells, Complex I activity has significant decreases in 3 of the four cell lines tests (H9C2, 4T1, and HCC-1937 cells). There are no significant changes to MCF10A activity. For H9C2 cells a dose-dependent decrease in Complex I is visible.

The oxygen consumption rate associated to the Complex IV activity is reported in graph 20. The analysis of the oxygen consumption rate related to the Complex IV activity was separated from the other oxygen consumption rate because of the higher activity of Complex IV.

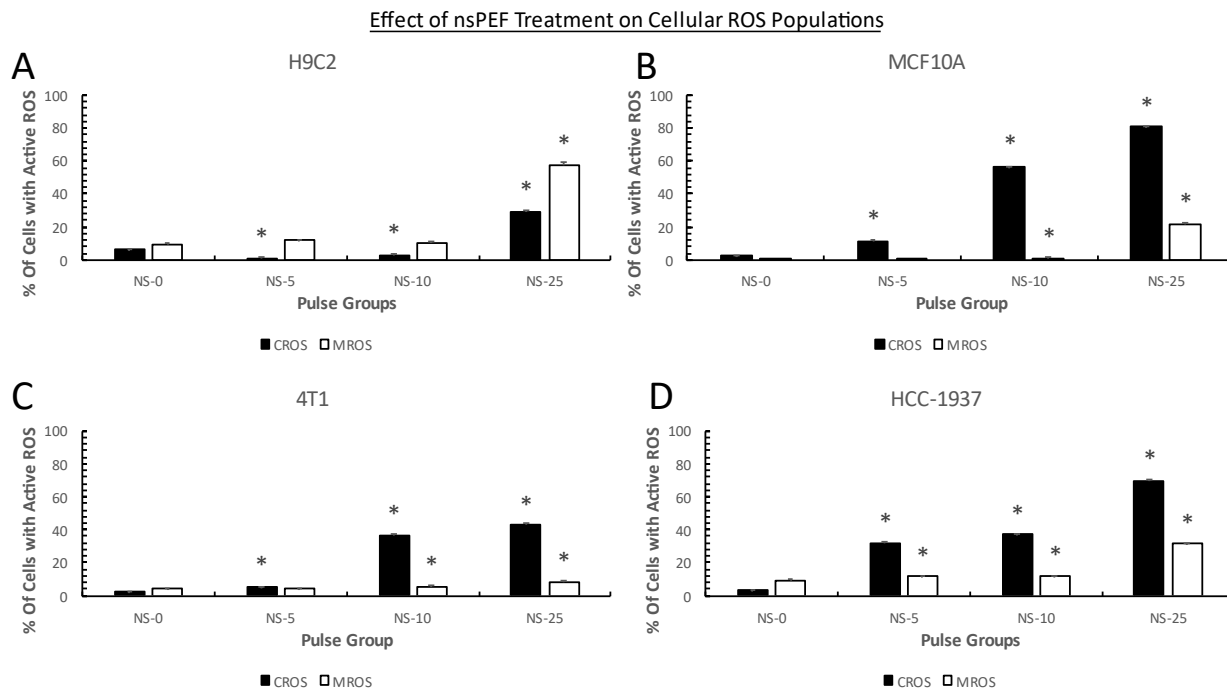
H9C2 and HCC-1937 cells show a significant decrease in Complex IV activity at the two highest pulse conditions. 4T1 cells show a lower activity in Complex IV in comparison to the other cell lines. At high number of pulses Complex IV activity increases in comparison to the activity observed at rest. A linear increase of the Complex IV activity with the number of pulses can be observed with an increase of the pulses at 35 and 100 pulses (Data not shown). H9C2 and HCC1937 cells had significantly reduced function. MCF10A cells showed no effect of Complex IV activity.



Graph 21: Three cell lines suspended with exogenous mitochondrial substrates and treated with nsPEF show significant change to Complex IV activity. 4 cell lines were suspended in growth media. The samples were then pulsed with a variable amount of 60ns, 40kv/cm, 15ns rise-time pulses. For H9C2 cells, 0 (Control), 5, 10, and 25 pulses were given. For the other cell lines, 0 (Control), 10, 20, and 50 pulses of the same parameters were given. Cells were incubated for 20 minutes under SIP after treatment and then suspended in Mir05 electrode media and sequentially exposed to a series of substrates and digitonin to chemically permeabilize the plasma membrane and ensure contact of the substrates with the mitochondria (see Methods section for concentrations). Once the substrates were added and Complex I were determined (see previous graph), Complex III was inhibited with antimycin, then ascorbate (2mM) and TMPD (N,N,N',N'-Tetramethyl-p-phenylenediamine dihydrochloride, , 0.5mM) were added. Once maximal respiration was reached, Sodium Azide (Na-Az, 200M) was added. The difference between respiration of the two states are reported here. The left axis shows the oxygen flux value (which is set to 12000 pmol/sec*million). Error bars represent 1 standard deviation. (* = significance with $\alpha=0.05$, Student's T Test).

Mitochondrial ROS ETC Effects

To quantify the sources of ROS in cells treated with nsPEF treatment, dyes for both mitochondrial ROS (mROS) and cytosolic ROS (cROS) were administered. This was repeated for all four cell lines. The same pulse groups were used for all cell lines - 0 (control), 5, 10, and 25.



Graph 22: nsPEF treatment leads to elevated cellular ROS. Type of ROS is dependent on cell line. Four cell lines (H9C2, MCF10A, 4T1, and HCC1937) were suspended in unmodified DPBS. The samples were then pulsed with a variable amount of 60ns, 40kv/cm, 15ns rise-time pulses - 0, 5, 10, or 25, times. 2 μ M MitoSOX and 2 μ M Carboxy-H2DCFDA was then added, and cells were incubated for 15 minutes in the dark at room temperature. Then they were analyzed by flow cytometry. The Y axis shows the percentage of cells with an active fluorescence signal. On the X axis, the pulse number is shown. The percentage of cells that expressed CytosolicROS (cROS) is in black and the percentage of cells that expressed Mitochondrial ROS (mROS) is in white. Error bars represent 1 standard deviation. (* = significance with $\alpha= 0.001$, Student's T Test).

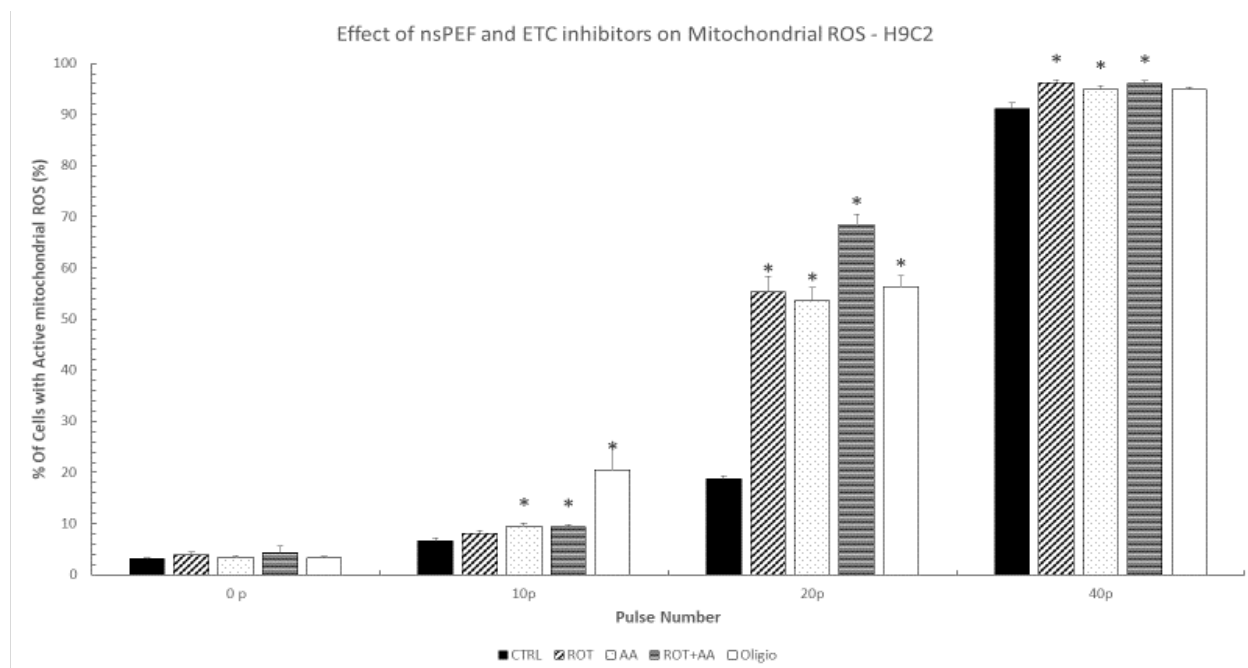
H9C2 cells showed a notable increase in mitochondrial ROS – at 25 pulses there is nearly a twofold increase in proportion of mROS over cROS. This pattern is not replicated in any other cell type. At 25 pulses for MCF10A, 4T1, and HCC-1937, the proportion of cROS over mROS is a 3.7, 5.2, and 2.2-fold increase (respectively).

nsPEF treatment in H9C2 cells induced a dose-dependent significant increase in mitochondrial ROS, reaching a maximum of 57% of cells showing mROS activity at 25 pulses. In the other three cell lines, cROS increased in a dose-dependent manner reaching varying levels of

activity. No other cell line reached the same level of mROS activity as H9C2s – and the trend for the other cell types was to increase cytosolic ROS activity before mROS was increased.

This exploratory study used inhibitors of Complex I, 3, and 5, and tracked the production of mitochondrially produced superoxide (by using MitoSOX Red). Since H9C2 showed the most mitochondrially produced superoxide, it was decided to use this line for the remaining studies. Thus, for this next study, the production of mROS was assayed with the combination of nsPEF treatment and ETC inhibitors.

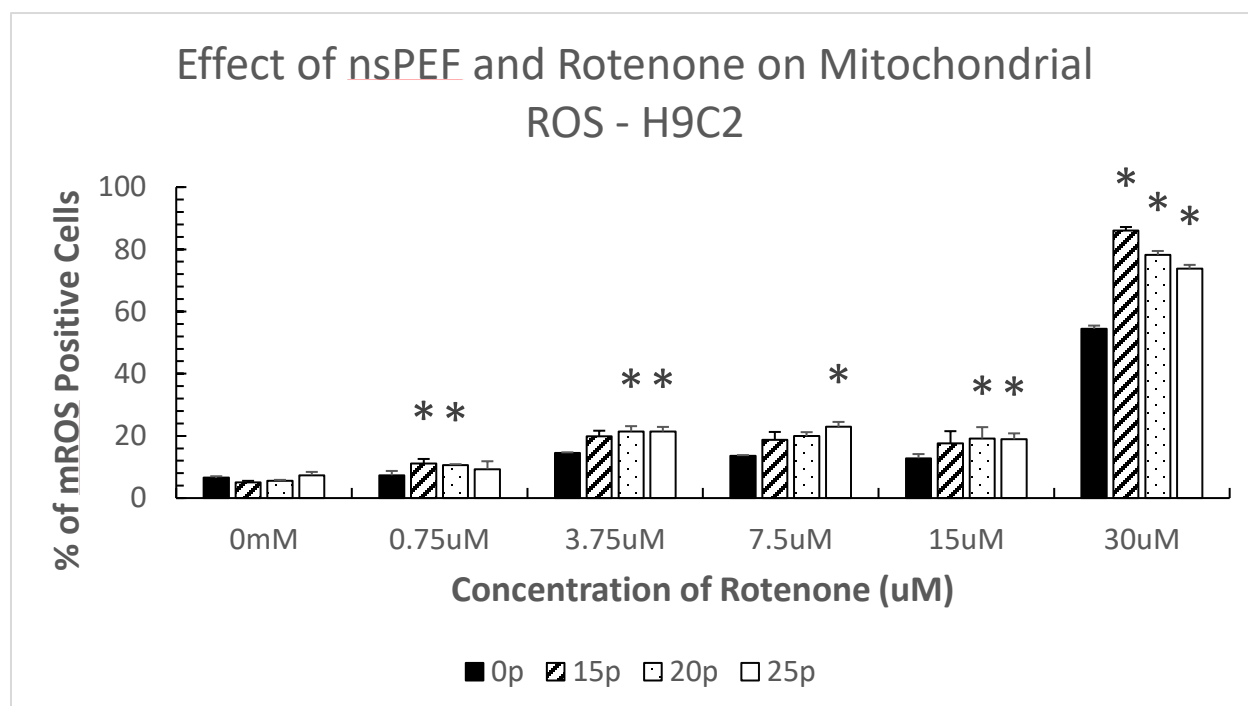
Without nsPEF treatment, no significant rise in mitochondrial ROS was detected regardless the presence of ETC inhibitor. At 10, 20, and 40 pulses, mROS production increased in presence of pulse and inhibitors. At 10 pulses, oligomycin showed a dramatic increase in mROS. At 20 pulses, it was observed the largest change of the fraction of cells with active mitochondria mROS in comparison to the control group. The fraction of cells changes was about 40% at 20 pulses whereas was only 5% at 40 pulses. At 20 pulses, the greatest differences in mitochondrial ROS produced from control to treated samples were found with the combination of rotenone and antimycin A. Since mitochondrial superoxide should be produced by Complex I, it is possible that the effect of Antimycin A was to act as a bottleneck and cause reverse electron transport to Complex I.



Graph 23: nsPEF treatment and ETC complex inhibitors demonstrate compounding effects on mROS in H9C2 cells. H9C2 cells were suspended in unmodified DPBS. The samples were then pulsed with a variable amount of 60ns, 40kv/cm, 15ns rise-time pulses - 0, 10, 20, or 40, times. 2uM MitoSOX and inhibitors were added: Rotenone (0.015mM), Antimycin A (0.01mM), oligomycin (2.5 uM), and a final group that added only Rotenone and Antimycin A at the concentration previous reported and cells were incubated for 15 minutes in the dark at room temperature. Then they were analyzed by flow cytometry. The Y axis shows the percentage of cells that showed active mROS indicator. Control cells (given no inhibitor) are shown in black bars, followed by cells administered rotenone (diagonal stripes), cells administered Antimycin A (dots), cells administered rotenone and Antimycin A (horizontal stripes), and cell administered oligomycin (white bars). Error bars represent 1 standard deviation. (* = significance with $\alpha= 0.001$, Student's T Test).

Afterwards, it was investigated the effect of rotenone concentration on mROS for different pulses groups. Dose-dependent behavior is not observed as a function of rotenone concentration until the very last group – with the same amount of rotenone that was administered in the previous experiment. However, a particular issue was noted – with the number of added trials, the time to analyze each test point was increased. Specifically, the fluorescence of the control condition (0 pulse, 0 uM rotenone) was higher than previous trials. To determine if this issue was due simply to the time that it took to analyze the condition, a final experiment was done to determine the

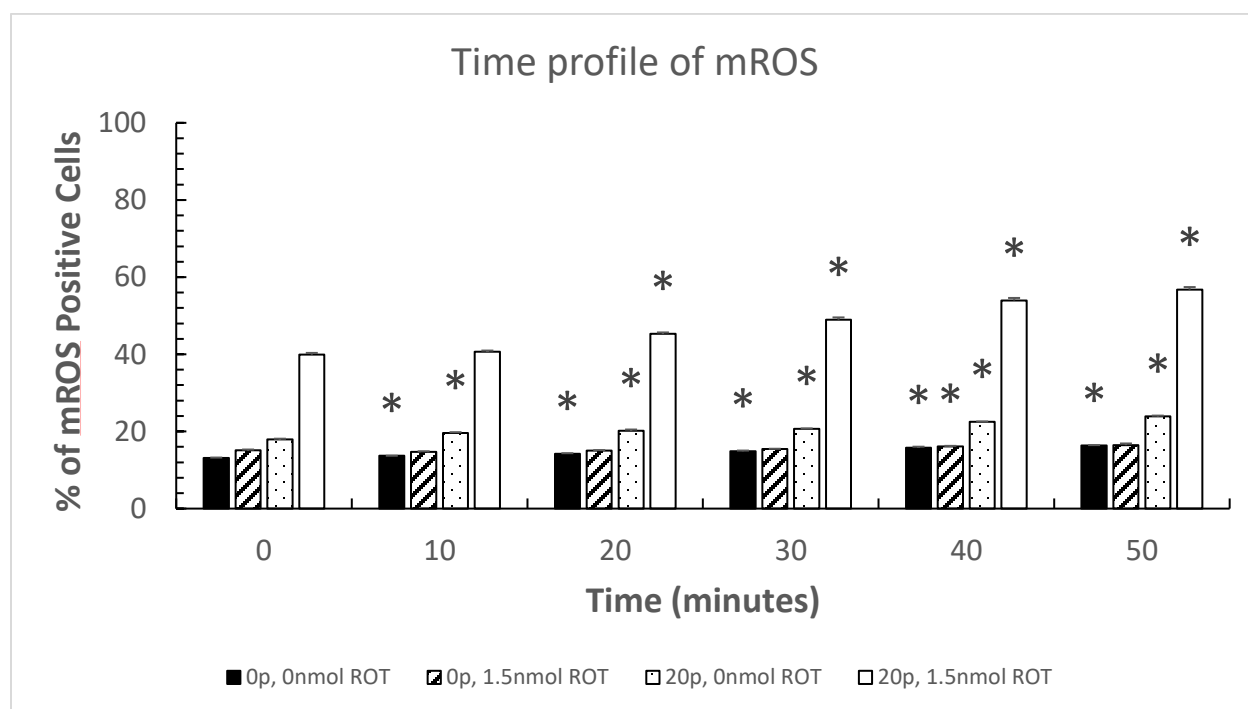
change over time of the mitochondrial ROS. Using only 30uM of rotenone and 20 pulses as test conditions, the mitochondrial ROS was calculated over 50 minutes at 10-minute increments.



Graph 24: nsPEF treatment and Rotenone (Complex I inhibitor) demonstrate rotenone dose-dependent effects on mROS for rotenone concentration above 15 uM in H9C2 cells. H9C2 cells were suspended in unmodified DPBS, and preincubated with different amounts of Rotenone (for 10 minutes - see X axis for amounts). The samples were then pulsed with a variable amount of 60ns, 40kv/cm, 15ns rise-time pulses - 0, 15, 20, or 25, times. 2uM MitoSOX was then added, and cells were incubated for 15 minutes in the dark at room temperature. Then they were analyzed by flow cytometry. The Y axis shows the percentage of cells that showed active mROS indicator. The X axis shows the concentration of rotenone preincubated with the samples. Control cells (no nsPEF treatment) are shown in black bars, followed by cells administered 15 nsPEF pulses (diagonal stripes), 20 nsPEF pulses (dots), and 25 nsPEF pulses (white bars). Error bars represent 1 standard deviation. (* = significance with $\alpha= 0.001$, Student's T Test).

This time course demonstrates that there may be synergism between the effects of rotenone and nsPEFs, especially with 30 μ M rotenone, indicating that they are acting at different sites in

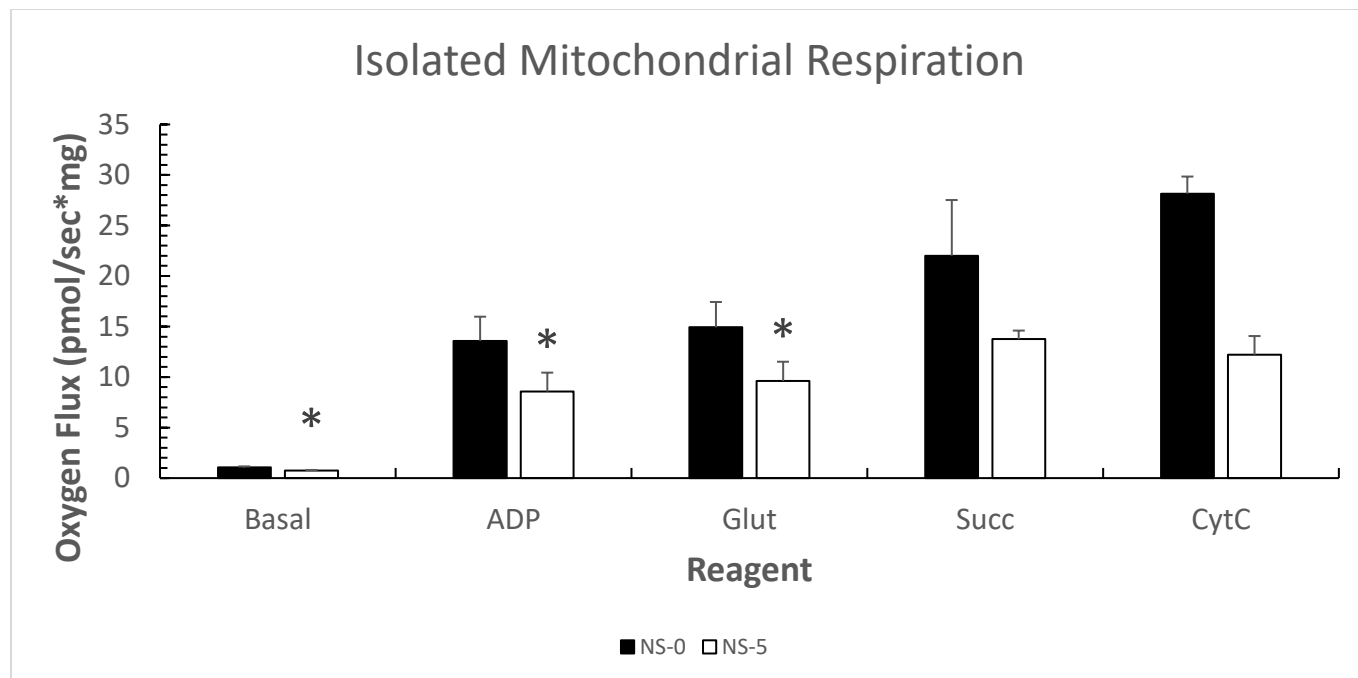
Complex I. This warrants further study. However, it is clear that the appearance of synergism is greater with increasing incubation time (Graph 25). Therefore, this synergism may be illusory. Thus nsPEFs appears to act at a site different than the transfer of electrons from iron-sulfur centers in Complex I, , to ubiquinone., where rotenone acts. While the exact site of nsPEF action in Complex I is not specified, this is perhaps the best specified mechanism and site of action in Complex I of the ETC for nsPEFs to inhibit electron transport and generate ROS.



Graph 25: Effect of time after nsPEF treatment on mitochondrial ROS production. The mROS indicator activity (MitoSOX) raises with time. The Left axis, like graph 19, shows the percentage of cells with active mitochondrial ROS. The X axis shows the time points at which this mROS was measured. This shows a time-dependent increase in synergistic interaction between rotenone and NPS for effects on Complex I. When cells were treated with rotenone (or 1.5 nM) with and without 20 pulses was a time dependent increase on synergism from 8% to 41% during the 5 min time course. Error bars represent 1 standard deviation. (* = significance with $\alpha=0.001$, Student's T Test).

Isolated Mitochondria

The final assay to study the effects of nsPEF treatment on cellular metabolism was performed in isolated mitochondria. Mitochondria were isolated as described in previous work (Ye & Hoppel, 2013). The cells treated with nsPEF showed a lower basal rate than that observed in the unpulsed isolated mitochondria (see Graph 13, 20). This is likely due to the absent effects of the Krebs cycle present in intact and permeabilize cells. For both mitochondria untreated and treated cells the addition of CytC did not significantly affect the oxygen consumption rate. This evidence suggests that the OMM integrity was not compromised for both groups of mitochondria. However, nsPEFs at 5 pulses (0.005 V*sec/cm) is significantly below the conditions to affect OMM integrity in intact cells ~50 pulses (~0.017 V*sec/cm (Graph 11).



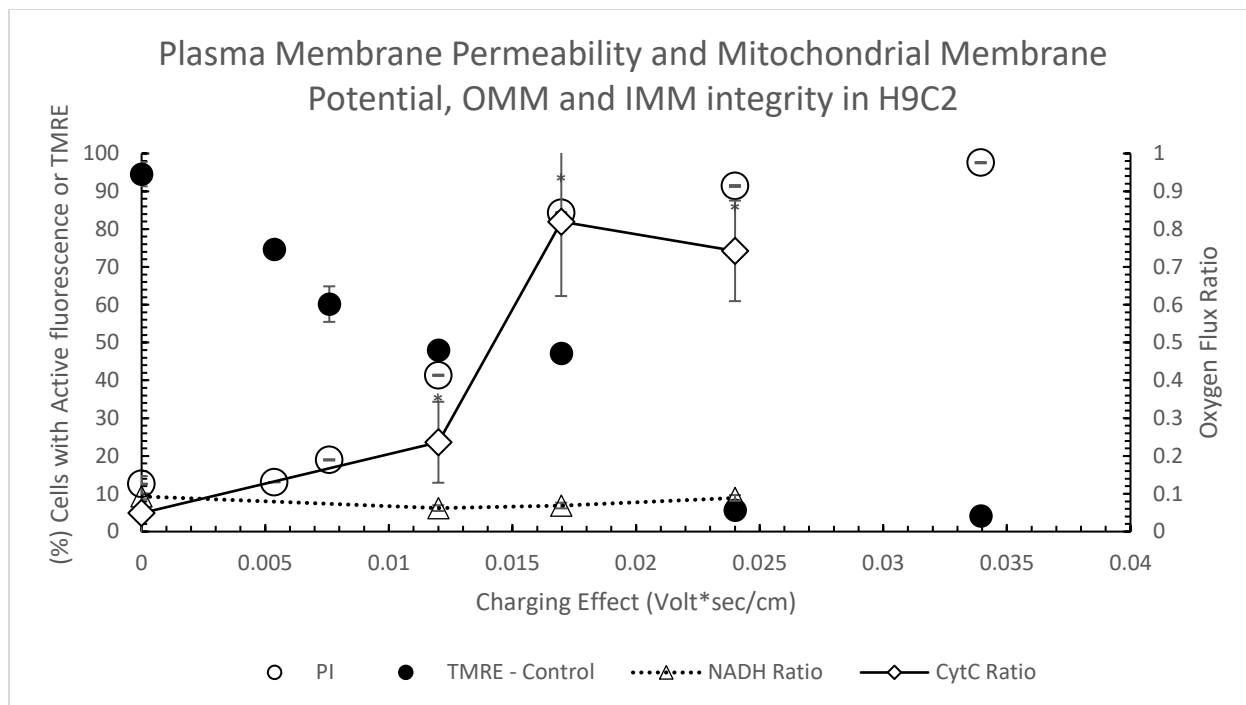
Graph 26: nsPEF treatment has an effect on the ETC complex activity of isolated mitochondria. The Y axis indicates the oxygen consumption rate per mg of the isolated mitochondria from murine samples. Five nsPEF pulses = 0.005 V*sec/cm. Error bars represent 1 standard deviation. (* = significance with $\alpha = 0.06$, Student's T Test).

CHAPTER 4: ANALYSIS OF THE CHARGING EFFECT

To facilitate the comparison of the results obtained with different pulse parameters, most of the graphs reported in the following section are proposed in terms of the charging effect of nsPEFs as a continuous variable rather than using the number of pulses. This strategy allows to highlight the biological effects of nsPEF treatment among different pulse numbers (charging conditions) and among different cell lines.

Effect of nsPEF Treatment on H9C2 Cells

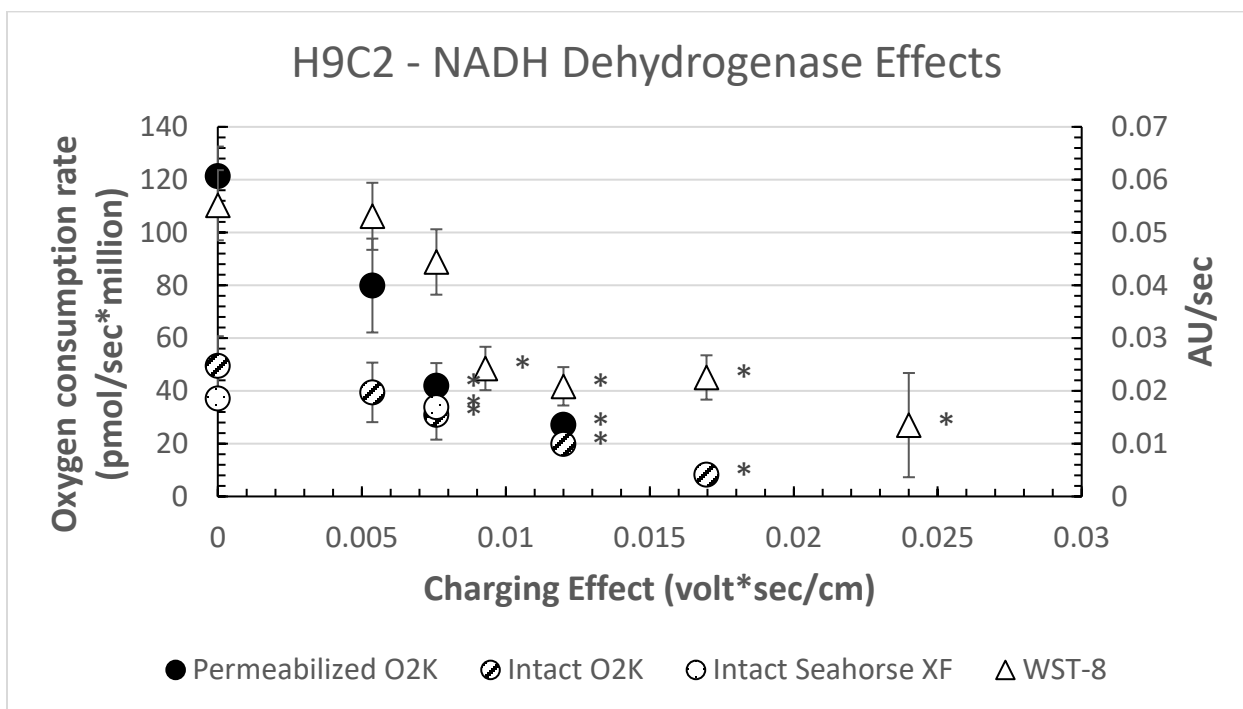
The charging effect on plasma permeability was compared with that on mitochondrial membranes of H9C2 cells that were selected because of their high content of mitochondria. Thus, a flow cytometric assay with TMRE was used to evaluate the effect of nsPEFs on the mitochondrial membrane potential ($\Delta\Psi_m$), and with PI to evaluate plasma membrane permeability. Also, the polarographic assay with NADH or CytC was used to evaluate the integrity of the IMM and OMM, respectively (Graph 28). All flow cytometric measurements were performed nearly immediately after treatment while the duration of the polarographic measurements was approximatively of 1 hour. The plasma membrane permeability increased for higher charging effect (10^{-2} Volt*Sec/cm) than that required to observe a decrease of $\Delta\Psi_m$ ($5 \cdot 10^{-3}$ Volt*Sec/cm). Also, the plasma membrane permeability changes and the OMM integrity loss occurred for the same charging effect (10^{-2} Volt*Sec/cm). This is reasonable because the protein:lipid ratio of both membranes are the same (50:50). In contrast, the protein:lipid ratio of the IMM is very different (80:20) (Comte et al., 1976).



Graph 27: H9C2 cells show non-simultaneous effects of nsPEF treatment on the plasma membrane (PI) and the OMM without an effect on the IMM. Here the data from H9C2 cells are combined. The left axis shows the fraction of cells that show PI (Plasma membrane permeability, open circle) and TMRE signal ($\Delta\Psi$, solid circle) dependent on the nsPEF treatment dose (shown as the Charging Effect on the X axis). The TMRE signal is normalized to the control condition. The right axis is the oxygen consumption rate ratio for the NADH (open triangle) and CytC (open diamond) (Graph 11) The treatment which shows that at 0.017 Volt*Sec/cm (50 pulses) only OMM of the mitochondria becomes permeable. The dissipation of $\Delta\Psi$ does not occur as quickly as past experimentation (Unpublished Data). This may be due to the cells being used at a higher confluency than those used in past experiments.

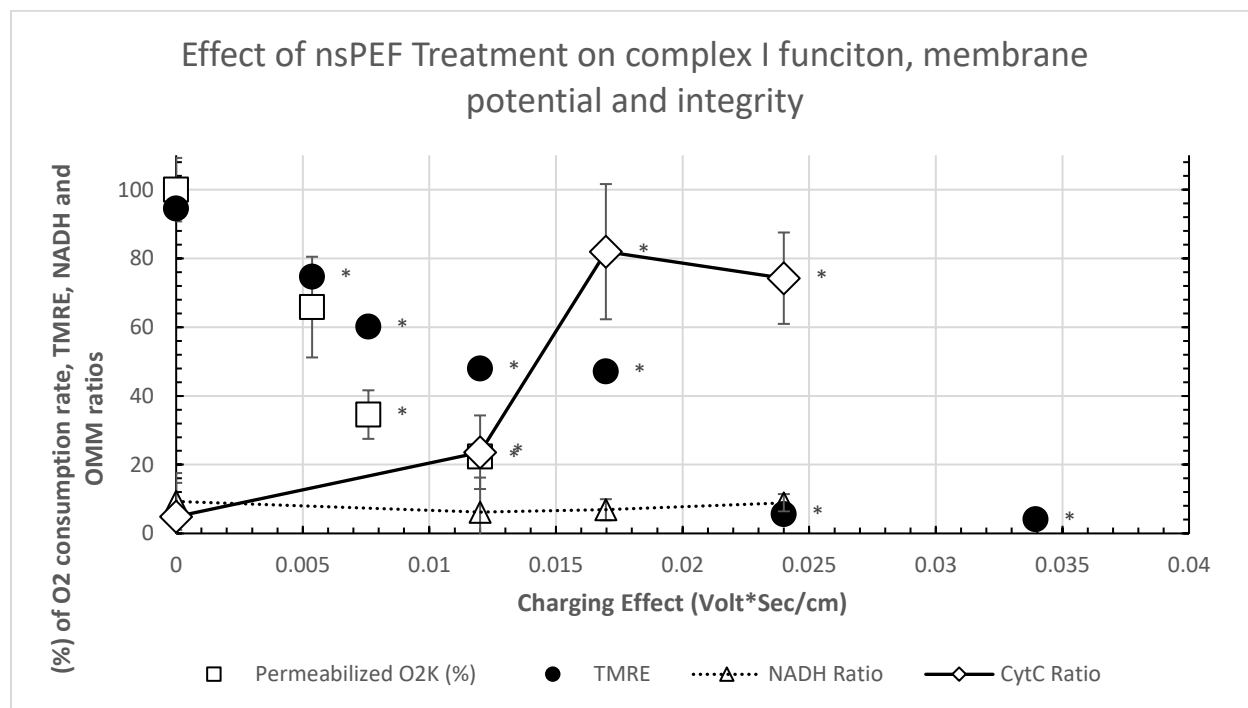
This suggests that the effect of nsPEF treatment on the OMM is responsible for the release of Cytochrome C, and relative accessibility of this compound exogenously under this study. Afterwards, it was investigated the effects of the nsPEF treatment on the NADH hydrogenase protein of Complex I and in the plasma membrane (Graph 29). The decrease in CI function and PMRS activity is dose-dependent and decreasing with an increase of the nsPEF dose. A significant decrease of the oxygen consumption rate (ET) occurs approximately at 0.008 Vs/cm, 10 pulses) Volt*Sec/cm (Graph 13) and the tPMET activity in the PMRS is affected at the same value 0.008

Vs/cm, 10pulses) (Graph 3), indicating that as soon as nsPEFs affects ET in the PMRS it also affects ET in the mitochondrial ETC. It should be noted that the decrease of the Complex I function occurs for lower value of the charging effect than that causing an alteration of the OMM integrity. The decrease of Complex I function was systematically observed in permeabilized and intact cells. To highlight the differential charging effect on the metabolic function and membrane potential and integrity, it was compared the charging effect on Complex I activity, membrane potential and IMM and OMM integrity (Graph 29).



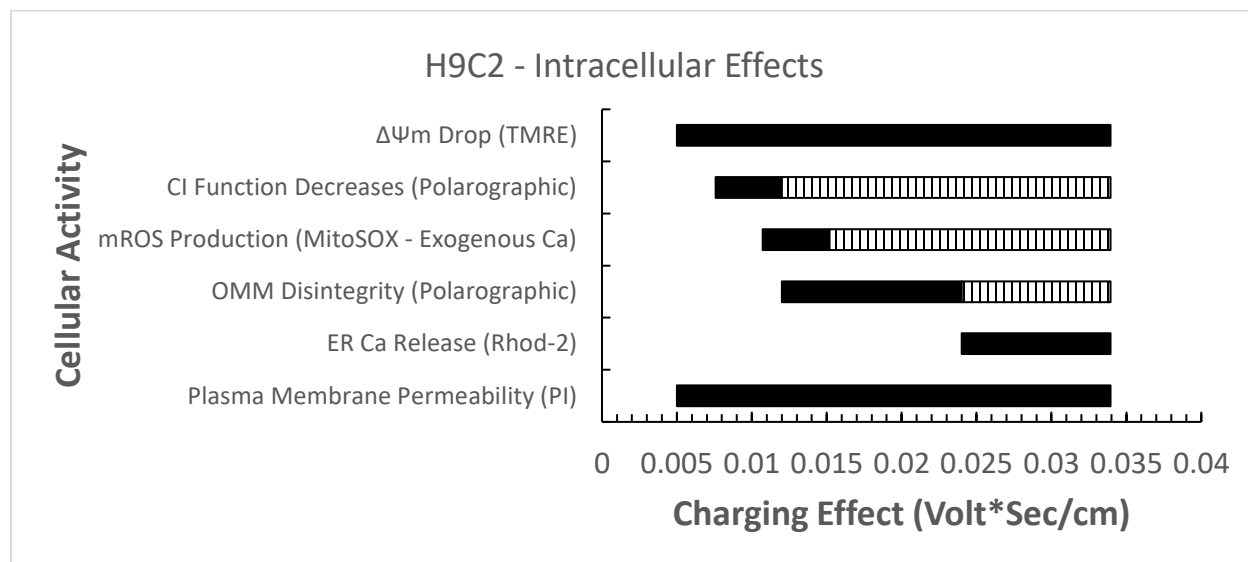
Graph 28: H9C2 cells show significant decrease in function around $10 \text{ } 40\text{kV/cm}$, 60ns monopolar pulses ($7.6 \text{ } 10^{-3} \text{ Volt*sec/cm}$). Oxygen consumption rate in permeabilized (solid circle), and intact (open circle with diagonal strings, O2k; open circle, seahorse) (Graphs 20, 13, 17) cells was compared with the plasma membrane redox system (PMRS) activity (open triangle) (Graph 3). The Y axis indicates the net oxygen consumption rate between the total and the one associated to Complex I. The PMRS activity was assayed by the WST-8 reagent. The nsPEF effects on mitochondria occurs at $7.6 \text{ } 10^{-3} \text{ volt*sec/cm}$ whereas those on the PMRS occurs at a higher treatment levels of $9.3 \text{ } 10^{-3} \text{ volt*sec/cm}$.

The $\Delta\Psi_m$ and Complex I function decrease for low nsPEF dose ($<7.6 \cdot 10^{-3}$ Volt*Sec/cm – (or 0.008 V*sec/cm (10 pulses) whereas the OMM integrity declines for a higher nsPEF dose ($0.012 \cdot 10^{-2}$ Volt*Sec/cm - 25 pulses). It should be noted that the nsPEF dose responsible for the decline of the OMM integrity is similar to that corresponding to the EC50 (22 pulses, Graph 6). As noted in Figure 3, NADH Dehydrogenase may not be the only mechanism for electron transport in the PMRS.



Graph 29: Mitochondrial membrane potential loss precedes the alteration of OMM integrity in permeabilized H9C2 cells. Both the oxygen consumption and the TMRE signal were normalized to the control conditions whereas the oxygen consumption rate ratio for NADH (open triangle) and CytC (open diamond) are the same of those reported in Graph 27. The oxygen consumption, TMRE fractions as well as the oxygen consumption rate ratio for NADH and OMM dependent on the nsPEF treatment dose (shown as the Charging Effect on the X axis).

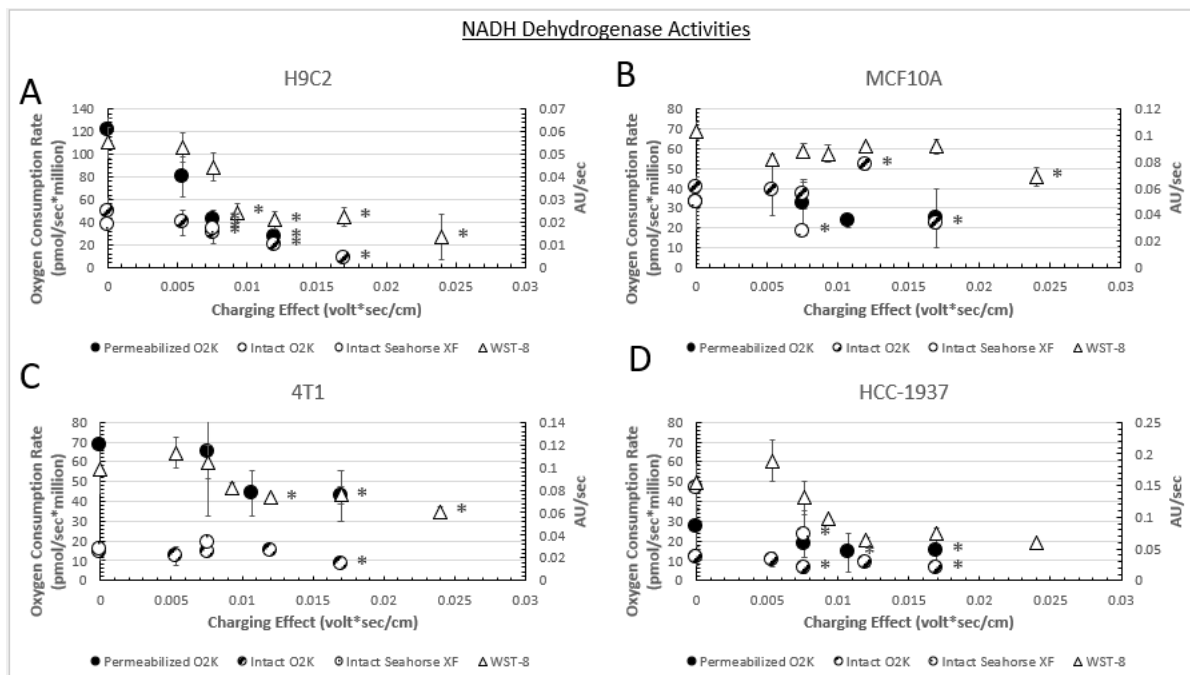
To summarize the effects of the nsPEF treatment and the scales at which each separate effect takes place, the Graph 31 was constructed.



Graph 31: Charging effect levels for several intracellular effects. H9C2 cells show a series of intracellular effects due to nsPEF treatment at 40kV/cm, 60ns, monopolar pulses with fast rise/fall times when the cells are suspended in media with EGTA. The charging effect is used to normalize the effects of the intracellular activity on the X axis. The Y axis is sorted by the different effects tested. The black bars indicate the range of charging effect was significant whereas the striped bar indicates the range of conditions not tested but are likely to have the same effect observed for the black bar range. It is expected that CI activity is decreased via the mPTP at the same dose as $\Delta\Psi$ dissipation occurs but is not able to be reliably detected via the polarographic method used.

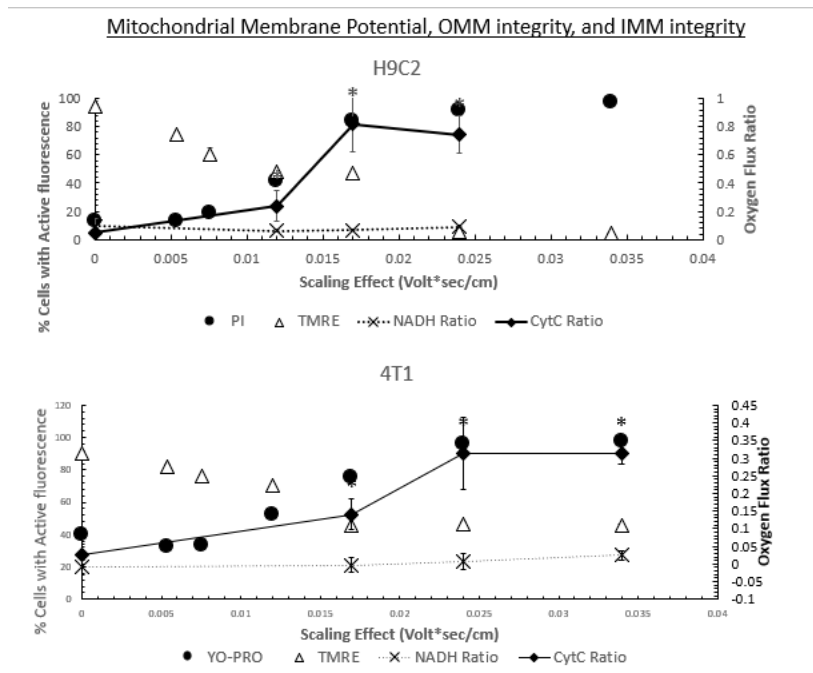
$\Delta\Psi$ and plasma membrane permeability decreased and increased at roughly the same experimental conditions as shown by graphs 7 (Exogenous calcium attenuates plasma membrane permeabilization quantified by cellular YO-PRO fluorescence uptake) and 9 (Mitochondrial membrane potential (MMP) drop is dependent on calcium at low levels of nsPEF treatment). The activity of Complex I decrease before the OMM integrity declines as demonstrated by graph 28 (H9C2 cells show significant decrease in function around 10 40kV/cm, 60ns monopolar pulses ($7.6 \cdot 10^{-3}$ Volt*sec/cm)) and graph 11 (nsPEF treatment can effectively disrupt OMM integrity without compromising the IMM of

H9C2 and 4T1 cells” and graph). Only for large dose of nsPEF treatment, does ER-stored released calcium into the mitochondria directly (see Graph 44).



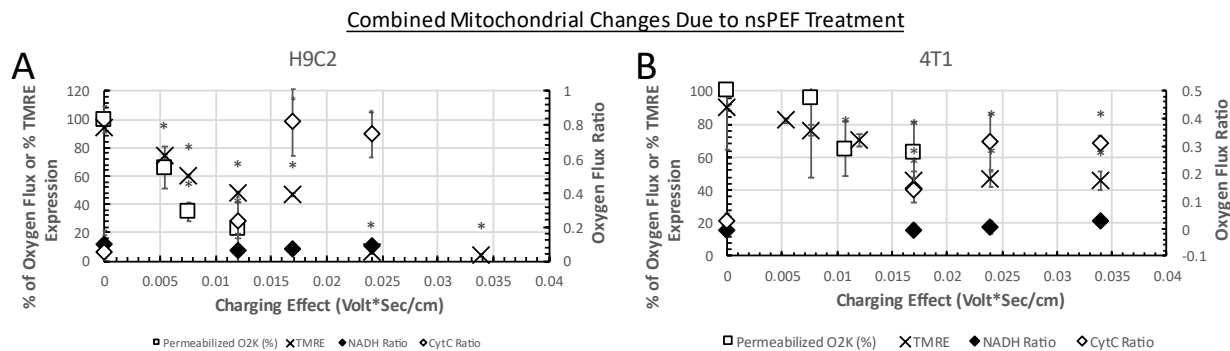
Graph 32: Comparison of the Complex I function and PMRS activity for 4 cell lines. The notation of this graph is the same of the Graph 28.

The effect of charging effect on NADH dehydrogenase activity in Complex I and PMRS activity was also analyzed for all 4 cell lines. The decrease of the PMRS activity occurs at roughly the same charging effect for three of the four cell lines investigated. Only MCF10A cells did not show any significant effect.



Graph 33: The decrease of OMM integrity and membrane potential occurs at similar pulse conditions as the increase of the plasma membrane permeability. The notation of this graph is the same of the Graph 27.

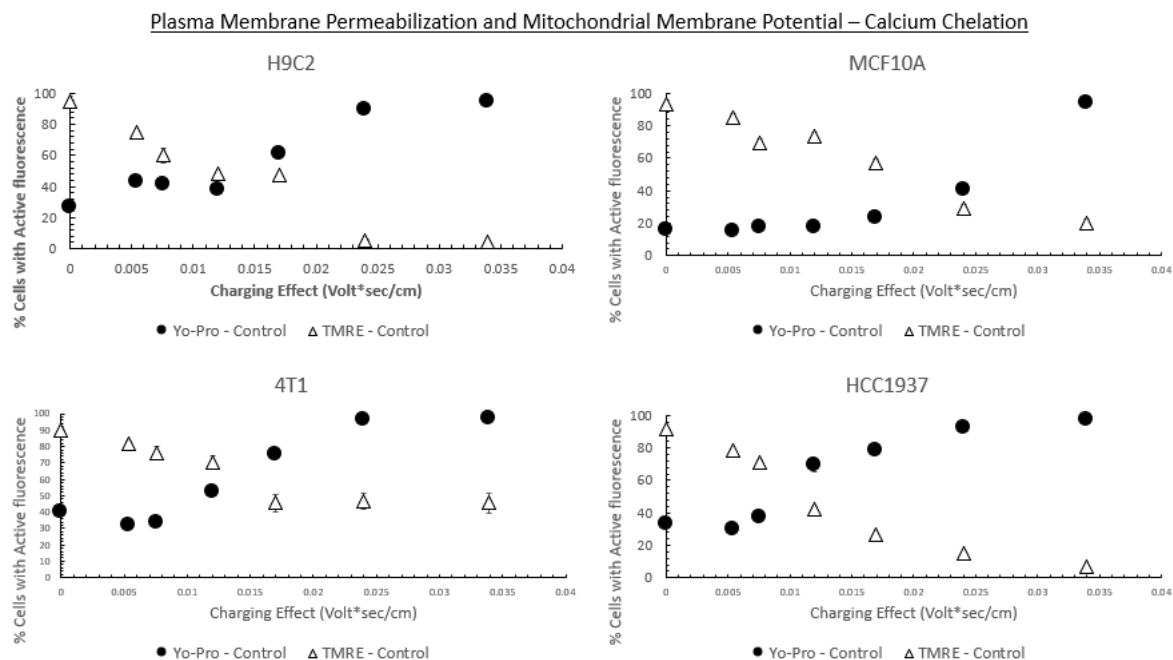
This pattern of the collapse of mitochondrial potential, the permeabilization of the plasma membrane, and the permeabilization of the OMM to CytC as seen in quadrant A of Graph 33 holds true for 4T1 cells (seen in quadrant B), though the dose of nsPEF treatment required is much higher (approximately doubled) and the normalized oxygen flux is halved. Normalized permeabilized oxygen flux change of CI is plotted with the resultant OMM and IMM integrity flux values and TMRE decrease, only H9C2 and 4T1 cells are plotted.



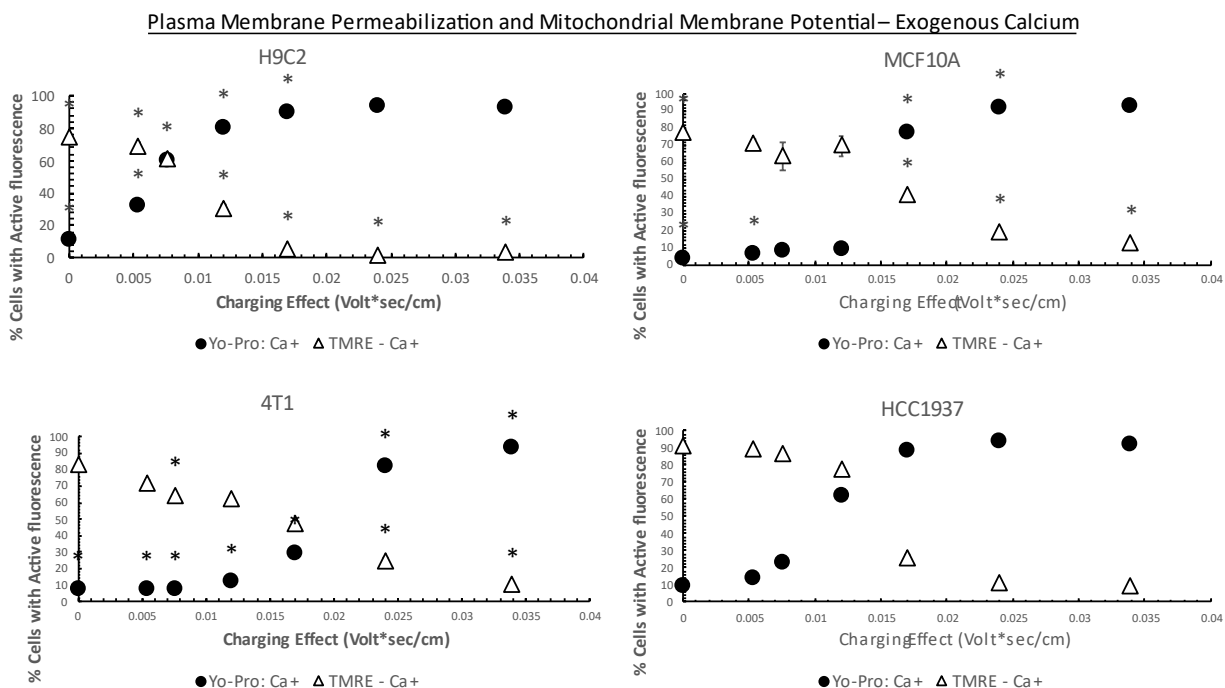
Graph 34: nsPEF treatment across H9C2 and 4T1 cells shows that Mitochondrial Membrane Potential drop precedes OMM permeabilization - and CI function decreases with similar sensitivity.

The effect of calcium on the permeability of YO-PRO to the plasma membrane and the polarization of the mitochondrial membrane was investigated (Graph 35). In the absence of calcium, the mitochondrial membrane potential appears to collapse for the charging effect value that permeabilized the plasma membrane (Graph 35).

The depolarization of the mitochondrial membrane become more sensitive to the nsPEF treatment in presence of calcium (Graph 35) for all cell lines, whereas plasma membrane permeability does not appear to be affected by calcium.



Graph 35: The decrease of the mitochondrial membrane potential ($\Delta\Psi$) and the increase of the Plasma Membrane permeability tends to occur almost for the same charging effect for all cell lines. Plasma Membrane Permeability and Mitochondrial Membrane Depolarization in absence of calcium. The calcium's chelator EGTA was used in this experiment. The permeability of the cell tested to YO-PRO is reported in black circles, and the fraction of polarized mitochondria are visualized in white triangles.



Graph 36: Calcium has an effect on both $\Delta\Psi$ and Plasma Membrane Permeability. Plasma Membrane Permeability and Mitochondrial Membrane Depolarization with Ca⁺. The permeability of the cell tested to YO-PRO is seen in black circles, and the number of cells with depolarized mitochondria are visualized in white triangles. Data points that differ significantly from the calcium chelating group that was pulsed at the same dose are marked (*).

CHAPTER 5: DISCUSSION

nsPEF Treatment Effect on Cell Viability, Plasma, and Mitochondrial Membranes

nsPEF treatment with a 40kV/cm electric field and 60ns pulse duration caused a substantial viability loss in all the tested cell lines at high doses (Graph 1 and 2, Table 2). The cells death could be related in part to their mitochondrial sensitivity to high nsPEF treatment leading to the the destruction of the outer mitochondrial membrane. This is demonstrated by the loss of mitochondrial membrane potential (Graph 9 and Table 4), and the increased oxygen flux ratio in the presence of cytochrome C (Graph 11). In contrast, at low levels of NS pulse exposure, H9C2, HCC-1937, MCF-10A cells exhibited an increase in viability which was probably related to a mild, excitatory effect of nsPEF treatment. The stimulatory effect was statistically significant only for MCF-10A cells. This stimulatory effect currently rests on an untested hypothesis that nsPEFs affect the PMRS, which affects proliferation mechanisms.

nsPEF caused changes in redox proteins in the plasma membrane: at low levels no significant changes of the PMRS activity was observed, but at higher levels of treatment a significant decrease of the PMRS activity was followed by a loss of viability (Graph 3 and 4).

It was additionally demonstrated via YO-PRO that nPEF cause an increase of permeability in all cell lines, and this permeability may be related to calcium because of the dye selected (YO-PRO) which has a noted interaction with calcium in the presence of the P2X7 receptor (Table 3, Graph 5 and 6).

Both nsPEF treatment and calcium cause a decline in $\Delta\Psi$ (Graph 7 and 8) for most cell lines. Specifically, H9C2 (25-50 pulses), MCF10A (50-200 pulses), and 4T1 cells (100-200 pulses) showed a significant decrease in $\Delta\Psi$ that points to a calcium dependence. Particularly, the presence of exogenous calcium in cell samples treated with nsPEF tends to lower the dose required

for nsPEF to collapse mitochondrial membrane potential. The point at which the calcium is not a significant factor in the depolarization of the mitochondrial membrane is dependent on the cell line. For instance, in H9C2 for 100-200 pulses, there is so few cells with $\Delta\Psi$ left that there is no detectable difference in the EGTA and calcium media (Graph 7-8). This is supported by the evidence of mitochondrial blebbing in Figure 4, where the exterior surface of the mitochondrial are essentially ablated by such high doses of nsPEF treatment.

The study on the integrity of the IMM and OMM highlights that nsPEF treatment cause only an alteration of the outer mitochondrial membrane integrity with a concomitant cell death. The release of CytC could be related to apoptotic signaling, and this could be governed by the composition of the OMM (Renault & Chipuk, 2014). The nsPEF treatment effects on the disruption of the OMM presents similarity with the electroporation that causes a poration of the plasma membrane. This is relevant to the ROS release from mitochondria which may be related to opening of the mPTP. The mPTP may also regulate the transfer of mitochondrial ROS into the cytosolic compartment. The generation of mitochondrial ROS could be regulated by a feedback loop onto the state of the mitochondria, which can cause the collapse of the mitochondrial membrane potential (Zorov et al., 2014). The generation of ROS and the rupture of the OMM in this way are related. However, it seems that nsPEF treatment is not able to cause permeabilization of the inner mitochondrial membrane to NADH.

The mPTP is a theorized, non-specific pore of <1.5kDa, located in the IMM. Its exact construction is uncertain, though it does behave as an uncoupler of mitochondrial function – as does CCCP (Halestrap, 2009). One possibility is that the mPTP is a formation of multiple ATP synthase (Complex V) proteins which breach the IMM (Long et al., 2015). The mPTP plays a significant role in RCD in both apoptotic and necrotic pathways (Kim et al., 2003). Early models

of the mPTP assumed that the VDAC was a component of the mPTP, though this has been shown to not be the case (Bonora & Pinton, 2014). VDAC is a channel on the OMM that regulates mitochondrial communication with the rest of the cell – and is involved with several cell death and cell survival signaling pathways (Shoshan-Barmatz et al., 2010). Importantly the VDAC permeabilizes the OMM independently of the mPTP (Doran & Halestrap, 2000), and the blockage of the VDAC can result in the release of CytC from the mitochondria (Madesh & Hajnóczky, 2001). This implies that a key target of therapies involving the mitochondria could be this ion channel (Camara1 et al., 2017).

Microscopy imaging of NAO demonstrates that the inner mitochondrial membrane protein cardiolipin is still intact after pulse conditions that would result in complete loss of cellular viability. However, greater magnification is required to show this in detail. Electron microscopy is recommended, but a visual microscope could, theoretically, be used. The ability to visualize cardiolipin is of exceptional importance, due to the importance of cardiolipin to mitochondrial bioenergetics (Paradies et al., 2014; Ren et al., 2014) and mitochondrial protein transport (Dudek, 2017).

Changes in Mitochondrial ETC Protein Behavior Due to nsPEF Treatment

When H9C2 cells are left intact and not supplied with exogenous substrates, Complex I does demonstrate changed function in the cell at higher levels of pulsing than would cause the cell to lose significant function – and in some cases demonstrates changes at lower levels, implying that changes to the ETC proteins occurs either at the same time or even before in cardiomyocytes. This change to ETC protein function is also evidenced in the three other cell types used – though only at higher levels.

Yet, with only 10 pulses, significant decreases in oxygen consumption are seen by using a more delicate method – the Seahorse XF analyzer. The changes are still dependent on cell line (4T1 cells, for instance, did not significantly decrease their function). H9C2 cells see a decrease in both oxidative phosphorylation AND glycolysis after nsPEF treatment. Except for 4T1 cells, all cell lines saw significant decreases in OCAR, fitting with the framework that nsPEF treatment can decrease ETC protein function. ECAR observations were inconclusive in most cases – in H9C2 cells glycolytic activity decreased (not significantly), with MCF10A cells there was a significant decrease in glycolytic activity, and HCC1937 cells were the only cell type to upregulate glycolysis after exposure to nsPEF treatment. 4T1 cells did not change glycolytic activity.

When the cells were treated with nsPEF treatment, had their plasma membranes permeabilized, and were supplied with exogenous substrates, the overall oxygen flux increased when compared to the intact cell methods (as expected). This increase in oxygen flux made it somewhat easier to identify the significant decreases in nsPEF function observed across cell lines. However, it must be reiterated that Complex III was not adequately supplied, so the effects of nsPEF treatment on Complex III is only indirect evidence of an effect on that specific protein.

Changes in Mitochondrial ROS Production Due to nsPEF Treatment

When cells are treated with equivalent amounts of pulsing, a discrepancy in the amount of ROS produced via the mitochondria and ROS present in the cytosol is noted in 3 of the cases. The single exception to this rule is H9C2 cells. This is not entirely unexpected, considering that the H9C2 line has such a high concentration of mitochondrial mass. However, due to this discrepancy, the rest of the assays focusing on mitochondrial ROS use only this line to elucidate the nature of the nsPEF mROS effect.

The second experiment tracking the production of mitochondrial ROS found that administering Rotenone (an inhibitor of Complex I) by itself did not appreciably raise ROS (~5% of cells showed signs of mitochondrial ROS). Yet administering 20 nsPEF pulses at 40kV/cm and 60ns raised ROS production to about 20% of all cells, and the combination of rotenone and antimycin A raised this to around 60%. This points to a synergism between rotenone and nsPEF treatment, which in turn points to the notion that the effects of nsPEF treatment on the mitochondrial generation of ROS is not the same effect of rotenone.

Limiting the range of doses (via the selection of a narrower section of pulse groups) and using a dose-response curve of only rotenone accomplished the goal of establishing that there was not a simple dose-dependent curve upon which the synergism of rotenone and nsPEF treatment acted. However, the time-dependent nature of the indicator used may have effected these outcomes.

When evaluating the mROS produced over time, two effects are clearly seen. First, the synergism between rotenone and mROS is clear – being more than additive from the effect of Rotenone and nsPEF treatment at all time points. Unfortunately, the proportion of mROS active cells show that either the indicator become more active over the course of 1 hour, or that the cells expressing mROS increases with time. This is not so much a barrier to using this assay as it is another facet of testing mROS to be controlled – the time at which groups are tested may have a significant effect on the proportion of mROS found. This is simply one more confounding variable to be accounted for.

Changes in Mitochondrial ETC Protein Behavior Due to nsPEF Treatment on Isolated Mitochondria

Isolated hepatocyte mitochondria were useful in determining that nsPEF treatment could change Complex I and V activity as shown via changes in oxygen flux rate under glutamate and ADP. However, the addition of calcium to the isolated sample was likely destructive to the mitochondrial structure, and so the effect of calcium directly on Complex I of the mitochondria in the context of nsPEF treatment is still unknown. However, it was determined that the changes that CI undergoes due to nsPEF does not rely on anything outside the mitochondrial environment.

CHAPTER 6: PILOT STUDIES AND SUGGESTED EXPERIMENTS

Effect of Picosecond Pulsed Electric Fields (psPEF) on Viability

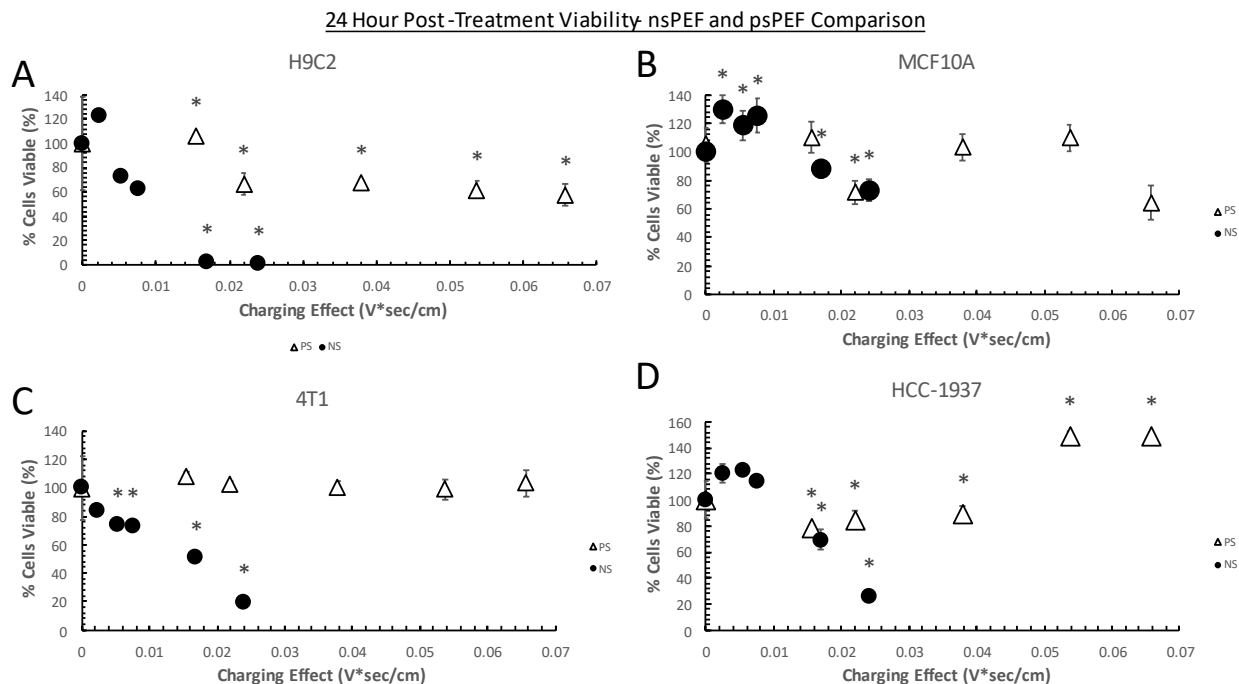
The efficacy of nsPEF treatment on cell death was determined in this thesis using the assay with the WST-8 reagent. An aspect that has not been fully investigated is the effect of using a shorter time-scale electrical stimulation. It is unknown the effect of using a time scale of the electrical pulse of picosecond (psPEF) on the cellular metabolic fate. psPEF treatment has shown to change cell proliferation and gene expression in human stem cells and may also affect (ThermoFisher, 2021) the mitochondrial metabolic activity (Petrella et al., 2018). The conclusion of work relies on the assumption that the mitochondria is responsible for the majority of the cellular metabolic activity which may not entirely be the case. Thus, similarly to the assay to evaluate the effect of nsPEF treatment on viability (Graph 2 – nsPEF Viability), a psPEF pulser was used to investigate the effect of psPEF on cell viability. Cells were suspended in growth media, placed in glass bottomed microwell (100uL) dished and pulsed with a 40kV/cm feed field (resulting in at 2kV/cm exposure), at 1kHz, for varying amounts of time (0 to 90 minutes). To compare nsPEF and psPEF results the charging effect was calculated with a modification of Equation 1:

$$\text{Charging Effect} = E_{\text{Field}} \left(\frac{kV}{cm} \right) * \text{Pulse Duration}(ns) * \sqrt{\text{Frequency (Hz)} * 60 \left(\frac{sec}{min} \right) * (\text{Minutes})} \rightarrow \frac{volt * sec}{cm}$$

Equation 2: psPEF pulse frequency Charging effect equation

The equation used for nsPEF treatment was adapted for the psPEF generator. However, individual pulses could not be counted, so the frequency was used to estimate dose.

The results of the monopolar nsPEF pulse treatment on viability were compared with the effect of the psPEF pulsing on viability for the same cell line (Graph 37).



Graph 37: psPEF treatment affects cell viability via the Charging effect. The viability is plotted on the Y axis and represents the percentage of the treated cells that remained viable after 24 hours. The percentage is relative to the control (unpulsed/sham treatment) cells. The abscissa represents the Charging Effect (Volt*Sec/cm) as a continuous variable used to compare different experimental condition. Pulse numbers for nsPEF treated cells were 0 (Control), 1, 5, 10, 50, and 100. Pulse time for psPEF treated cells were 0, 5, 10, 30, 60, and 90 minutes. Solid black circle and white, triangular symbols denote the nsPEF and psPEF treated samples, respectively. Error bars represent 1 standard deviation. Asterisks (*) denote significance as calculated by a Student's T Test with an alpha of 0.05.

A bipolar psPEF treatment does not significantly affect 4T1 cells viability, whereas at high doses of treatment the viability increases in HCC-1937 cells. A confounding factor in this experimental setup is that the nsPEF treatment was monopolar (Figure 2) whereas the psPEF treatment was bipolar. The bipolar pulses effect on plasma membrane permeabilization has previously been documented (Ibey et al., 2014). A mechanism explaining these bipolar effects (Pakhomov et al., 2021) using a “reverse electrophoresis” has been proposed to account for this change (Schoenbach et al., 2015). It is possible, that the lack of significant effects and dose-dependent response in some of the cell lines could be related to a less efficient electronic exchange

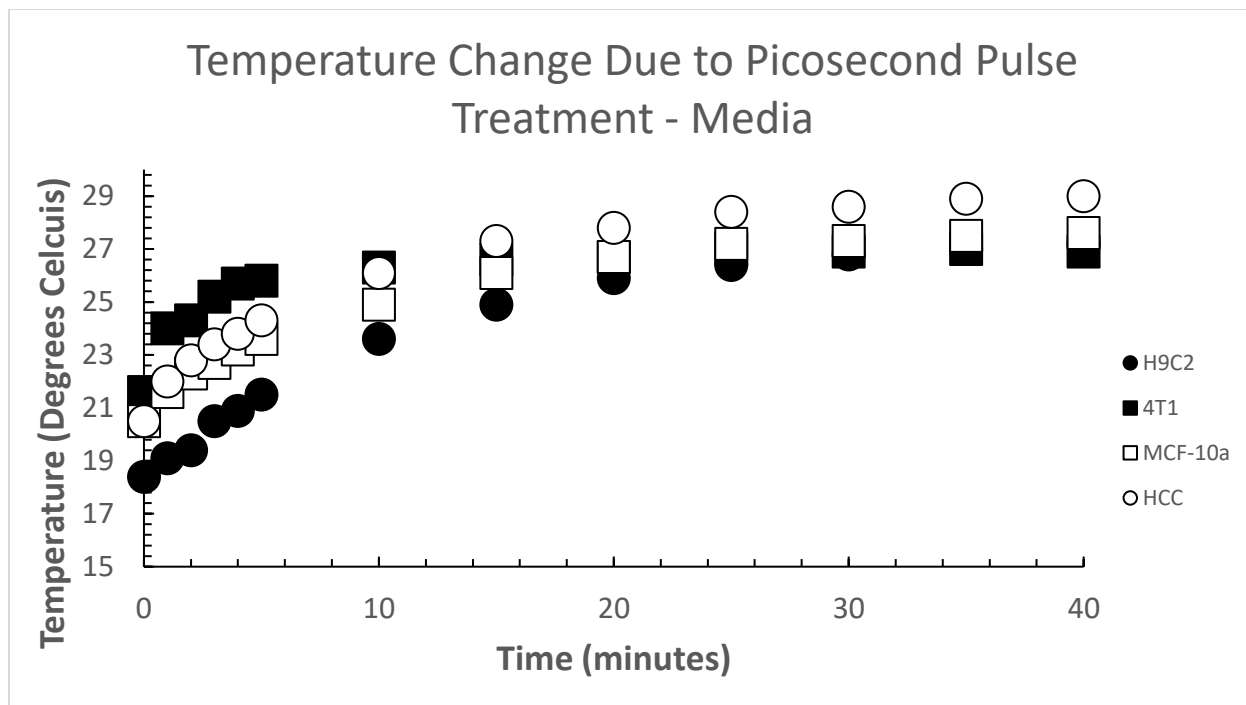
of the bipolar pulses than that with a monopolar pulse. Because the effective field is much lower than in the case of the nsPEF pulses, the electronic exchange is drastically reduced. Therefore, a monopolar discharge of psPEF treatment could have had a more effective effects to the plasma membrane with less energy than the bipolar psPEF treatment.

The mono/bipolar nature of the pulse and the charging effect could be a misattribution of the actual effect of the nsPEF treatment, especially as it pertains to changes in the mitochondrial membranes. If the plasma membrane is seen as a capacitor, and the mitochondrial membrane capacitors within that circuit, then it is possible that the frequency effects are not the main cause of biochemical change. Spectral analysis in this vein has already been done with respect to uni/bipolar nsPEF pulses (Merla et al., 2017). Instead, it is the charge deposited in that membrane that may be the primary effective agent in changing the behavior of the membrane or proteins. Since this effective charge is reduced in the case of a bipolar pulse, the deposition of the charge on the membranes is lessened. To confirm this in a modeling perspective, the Fourier transform of a fast-rise time, monopolar nsPEF pulse of low voltage, and a monopolar psPEF pulse of high voltage could be compared. Once the voltage-time signal is found, then the area under the curve of the nsPEF and psPEF pulse ought to be found. Then the voltage of both could be altered until the integral of the voltage with respect to time signal could be normalized so that each could deliver approximately the same amount of energy. For instance, if the nsPEF treatment was an ideal step function that went to 0.1kV/cm, then the total charge of a single pulse would be $6E-6 \text{ V*sec/cm}$. To match this charging effect, then an ideal psPEF pulse of 500ps would need to be 12kV/cm. In theory, the membrane permeabilizations for both ought to be similar. Earlier experimentation that used long-rise time waveforms may not have captured the differences in mitochondrial changes as the treated samples would have had their plasma membranes charged due to the slow time it took

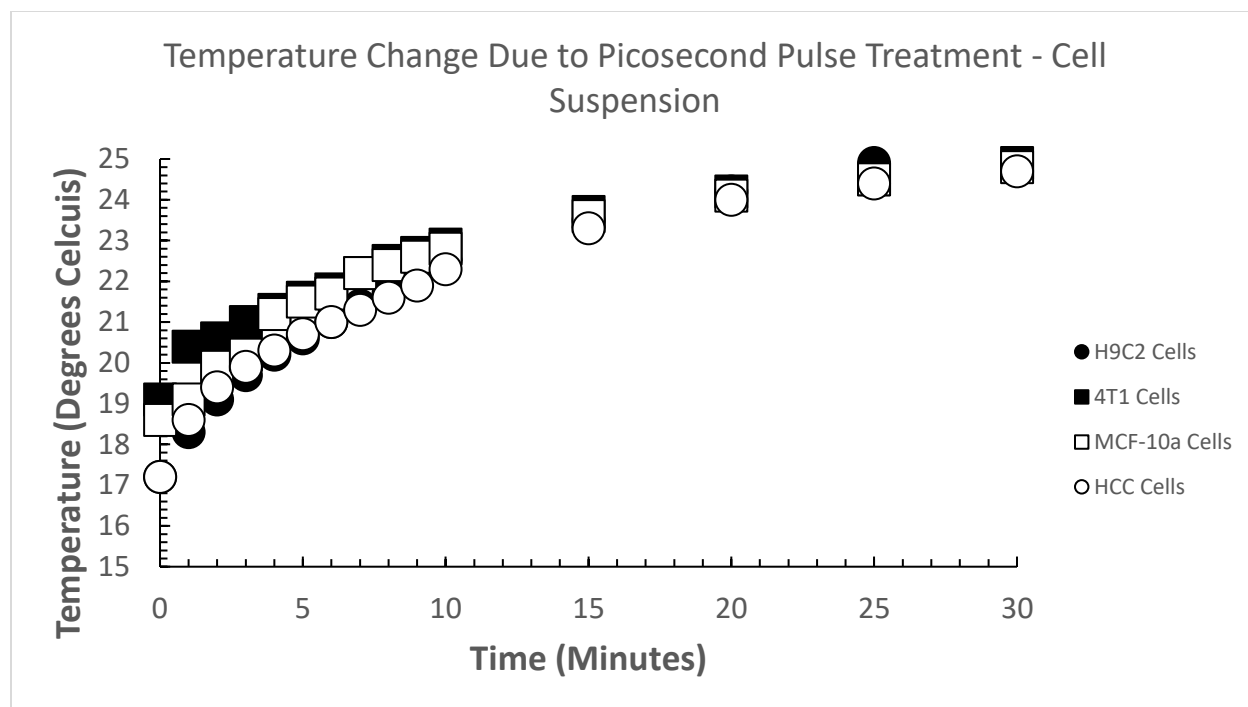
for the cell to reach its end electric field – and so the charge bypassed the mitochondrial membrane, or at least the voltage seen by the mitochondrial membranes were altered by the plasma membrane.

One theory of psPEF treatment is that the effects of temperature rise could contribute to changes in cell physiology. In graph 38, the effect of psPEF treatment on temperature in cell media with respect to time is visualized, and in graph 39, the effect of psPEF treatment on temperature in cell media with cell suspension with respect to time is visualized.

Yet, the media itself varies in composition across the different cell lines used – and so the real temperature rise of a cell sample would be different. With the addition of $1E6$ cells/mL into the 100uL cuvette, the following temperature curves were obtained. The same methods were used – the only difference is now there were cells suspended in the media that was subjected to bipolar psPEF treatment.



Graph 38: Temperature change in cell growth media when treated with psPEF shows less than 5 degrees Celsius of variability over 40 minutes. 500 mL containers of growth media were placed in the hot water bath for 20 minutes. 0.5mL of the growth media was placed in aliquots and then allowed to cool in ambient temperature for 20 minutes. The PS pulser with antenna was set to 1 kilohertz (kHz) and 30 kilovolts/cm (kV/cm). The plate was filled with 100uL of the respective cell line's growth media and pulsing was carried out with for at least 40 minutes. The temperature probe was directly placed in the media. To utilize the temperature probe, the recording unit of the probe was placed inside a faraday cage and readings were recorded manually. The temperature probe used was a Neoptix ReFlex fiber optic temperature sensor. After each experiment, the probe was removed from the pulser, and all items were given 20 minutes to return to ambient temperature. Ambient air temperature was measured at approximately 18 C. The decrease in media temperature with cells is primarily related to the increase of the thermal mass of the sample. The circle symbols represent the temperature readings for each media exposure to the PS pulser electric field. Square symbols represent the temperature profile of each media with cells suspended. The media without cells reached a steady-state temperature of approximately 27-28 degrees Celcius at about 30 minutes.



Graph 39: Temperature change in cell growth suspension shows less than 3 degrees Celsius of variability.

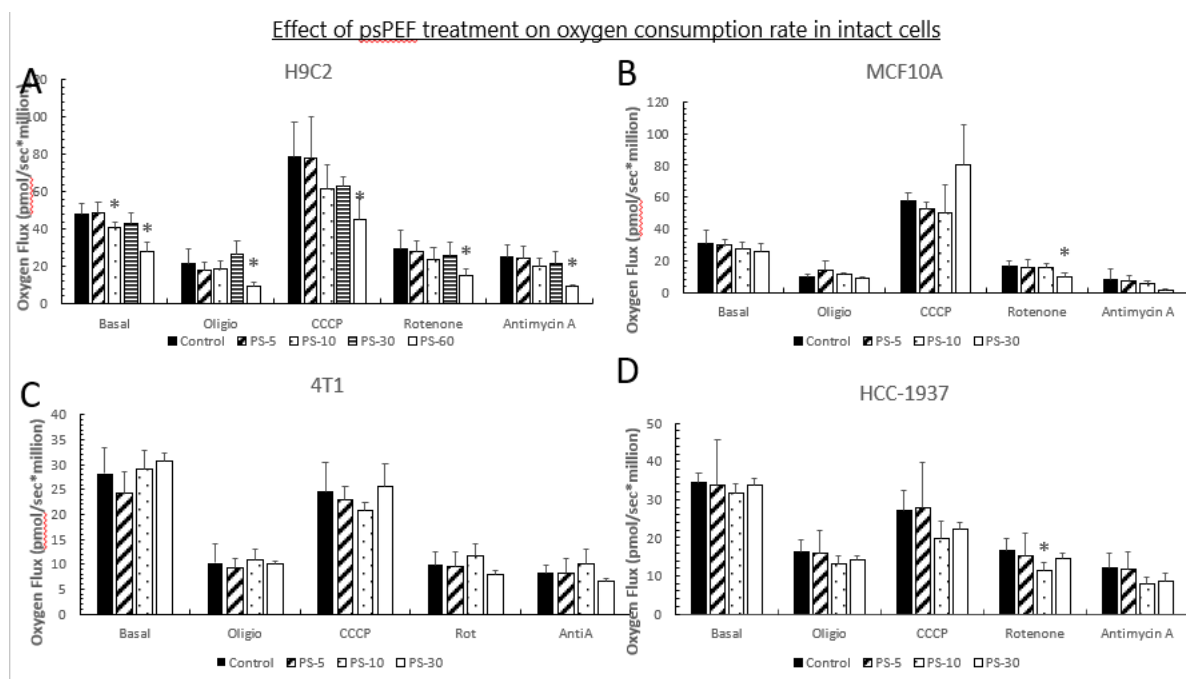
500 mL containers of growth media were placed in the hot water bath for 20 minutes. 0.5mL (500uL) of the growth media was placed in aliquots and then allowed to cool in ambient temperature for 20 minutes. For this experiment, the PS pulser with antenna was set to 1 kilohertz (kHz) and 30 kilovolts/cm (kV/cm). The plate was filled with 100uL of the respective cell line's growth media and pulsing was done with a minimum of 40 minutes. The temperature probe was placed in the media directly. To utilize the temperature probe, the recording unit of the probe was placed inside a faraday cage and readings were recorded manually. The temperature probe used was a Neoptix ReFlex fiber optic temperature sensor. After each experiment was completed, the probe was removed from the pulser, and all items were given 20 minutes to return to ambient temperature. Ambient air temperature was measured at approximately 18 C. The decrease in temperature in media with cells present is ascribed primarily to the increased thermal mass of the sample. In the scatter plot, the circular symbols represent the temperature readings in each kind of media during its exposure to the PS pulser electric field. Square symbols represent media that had its respective cells suspended with it. Media with cells reached a steady-state temperature of approximately 24.25 degrees at about 20 minutes.

From Graphs 38 and 39, the temperature of media with and without cells converges on similar values with psPEF treatment in 20-40 minutes. This variability is less pronounced with the addition of cell in the sample. While thermal effects of psPEF pulsing could very well be a

significant factor in how psPEF treatment effects cell physiology, it does not seem to vary significantly at 20-40 minutes of treatment when cells are added.

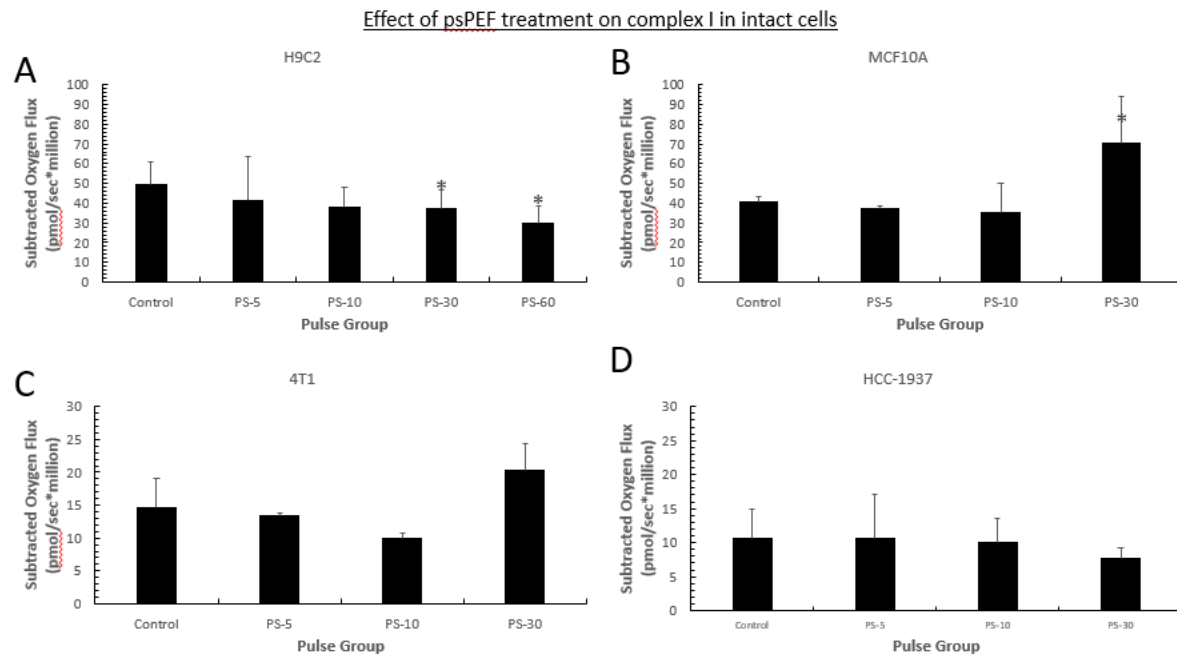
Effect of Picosecond Pulsed Electric Fields (psPEF) on Complex I Activity

It was assessed the effect of the psPEF treatment on the metabolic activity in intact cells with a high resolution respirometry. The decrease in oxygen consumption rate observed for higher pico pulses treatment in H9C2 cells was not present for the other cell lines investigated.



Graph 40: psPEFs do not affect the oxygen consumption rate in all intact cell lines. 4 cell lines were suspended in growth media and pulsed for a variable amount of time. Cells were immediately suspended in Gemish electrode media and sequentially exposed to Oligiomycin (Complex V inhibitor), CCCP (ionophore/uncoupler), Rotenone (Complex I inhibitor), and Antimycin A (Complex III inhibitor) (see Methods section for concentrations). The oxygen consumption rate was measured for all cell lines after the treatment with different nsPEF conditions. Oxygen fluxes were recorded after addition of 4 different reagents (see legend for pulse conditions). Error bars represent 1 standard deviation. (* = significance with $\alpha = 0.05$, Student's T Test). It should be noted that the Y axis scale for H9C2 and MCF10A is higher than that for 4T1 and HCC1937.

To evaluate the effect of the psPEF treatment on Complex I function, the oxygen consumption rate of the uncoupled mitochondria was subtracted from that in presence of rotenone (Graph 41).



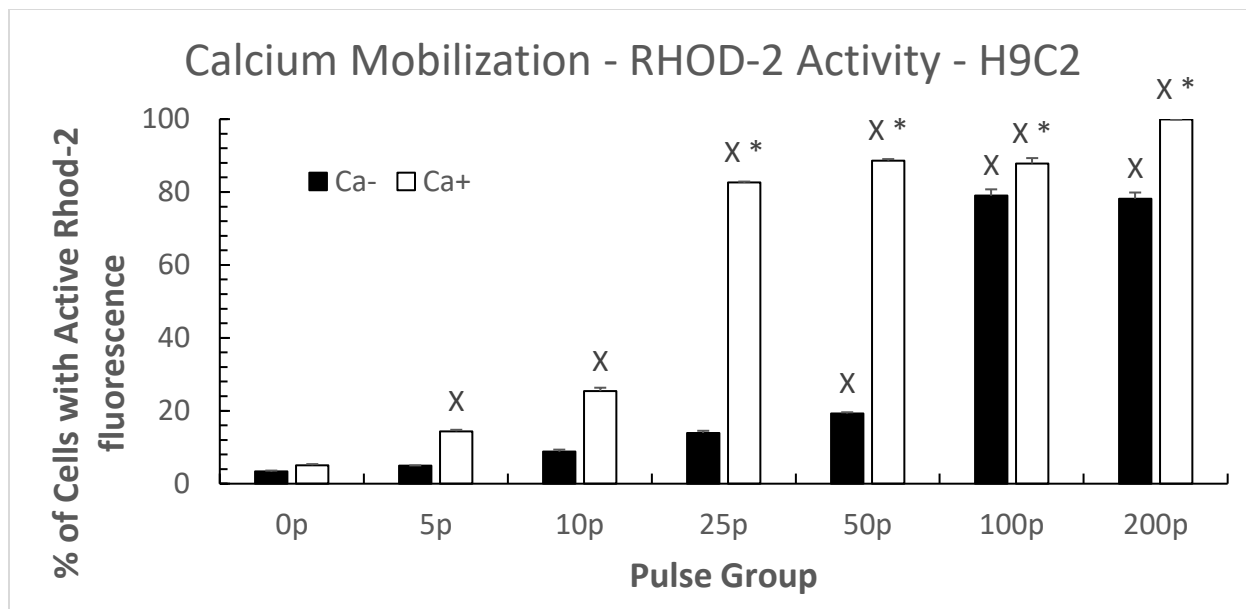
Graph 41: psPEF treatment do not affect the Complex I function in all cell lines. The oxygen consumption rate in intact cells with uncoupled mitochondria is subtracted from that measured in presence of rotenone (black bar). The Y axis scale for H9C2 and MCF10A cells is higher than that used for 4T1 and HCC1937 cells. Error bars represent 1 standard deviation. (* significance with $\alpha = 0.05$, Student's T Test).

A significant effect of the psPEF treatment can be observed for a number of pulses greater than 30. This could be related to the bipolar characteristics of the psPEF waveform. The psPEF treatment was administered by suspending cells in a cuvette with metal plates 0.1 cm apart whereas the pulses were delivered via an antenna (Petrella et al., 2016). The form used to deliver electric field may be in part responsible for the outcome of the results. Thus, the lack of a monopolar

waveform, and the delivery mechanism could be the reason for the inconsistent effect of psPEF treatment on different cell lines. Some issues were noted in the design of nsPEF signal delivery electrodes (Chen et al., 2009).

Rhod-2 for Ca in Mitochondria

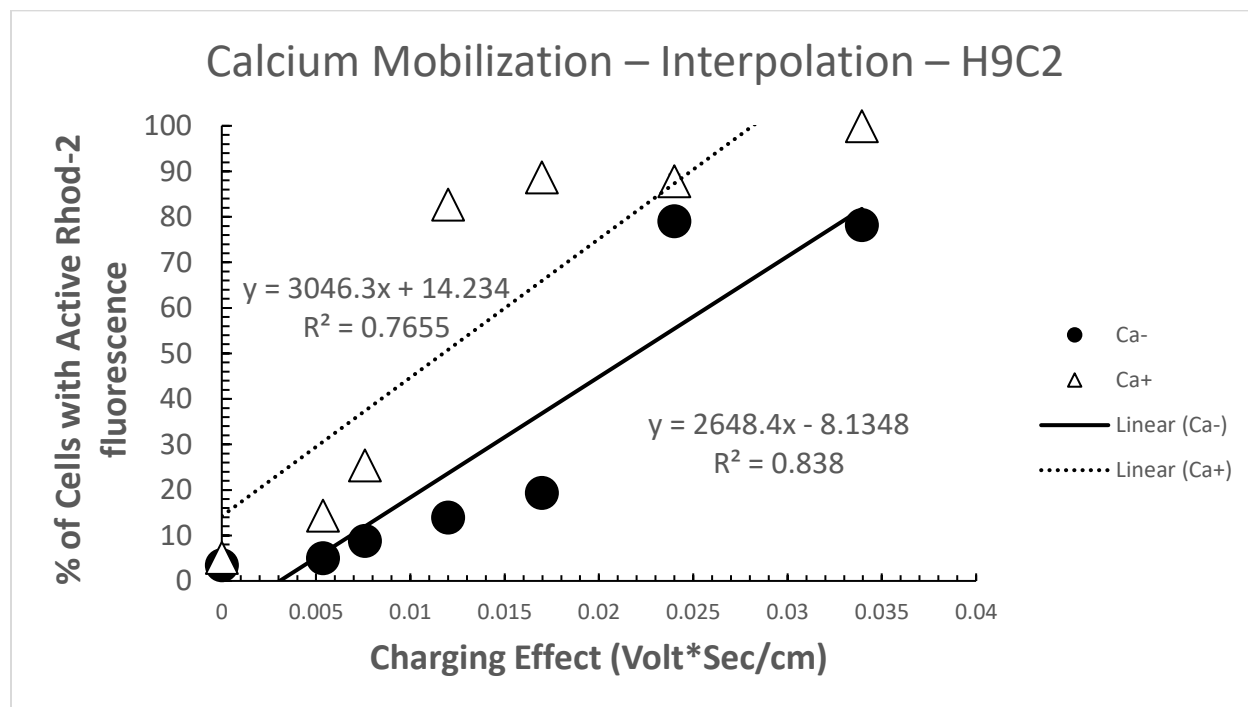
The detection of extramitochondrial calcium flux due to the formation of the mtPTP has previously been reported, although indirectly, with the tools used in this work (Nászai et al., 2019). Rhod-2 is a cell-permeant dye with fluorescence properties in presence of calcium (ThermoFisher, 2021). It has been used to study the function of the mtPTP (Mironov et al., 2005) and apoptosis (Ramachandran et al., 2020). It has particularly been used with microscopy (Tenorio & Niggli, 2016). The investigation of mitochondrial calcium in our work is important because previous study reported an association between an excess of mitochondrial calcium and $\Delta\Psi$ loss (Lu & Armstrong, 2007).



Graph 42: Calcium release into the mitochondria occurs at high doses of psPEF treatment, even when exogenous calcium is chelated. H9C2 cells were suspended in PBS with 2mM additional EGTA (Ca-, black bar) or in unmodified DPBS (Ca+, white bar). The samples were then pulsed with a variable amount of 60ns, 40kv/cm, 15ns rise-time pulses - 0, 5, 10, 15, 25, 50, 100, or 200 times. 2uM Rhod-2 was then added, and cells were incubated for 15 minutes in the dark at room temperature and then analyzed by flow cytometry. The Y axis shows the percentage of cells with an active Rhod-2 fluorescence signal and the X axis shows the pulse number. Error bars represent 1 standard deviation. (* significant difference between groups with the same pulse, X significant difference from 0 pulse condition, with $\alpha= 0.001$, Student's T Test).

H9C2 cells show a two-threshold effect of calcium mobilization. One threshold occurs approximately at 25 (0.008 Vs/cm) and 100 pulses (0.24 Vs/cm) with and without calcium, respectively. Regardless, this threshold, it is important to determine the source of mitochondrial calcium observed with the psPEF treatment in the absence of extracellular Ca²⁺. A possible explanation is an influx of calcium through the PM at 25 pulses and the release of intracellular calcium at 25 pulses. To demonstrate that ER is responsible for the calcium release, is possible to determine whether calcium stores are still present in ER by inducing calcium depletion from ER with thapsigargin (Rogers et al., 1995).

The transport of calcium into mitochondria is important because it might regulate the superoxide fate by the enzyme SOD1 in mitochondria (Estácio et al., 2015) (see Figure 1).



Graph 43: Calcium effects the mobilization of Rhod-2 into the mitochondria. The Rhod-2 fluorescence changes with the charging effect. The Y axis shows a subset of the Rhod-2 data from graph 44. On the X axis, the Charging Effect (calculated as Volt*Sec/cm) is shown. A linear interpolation of data of the control group (PBS with 2mM EGTA, black circles), and exogenous calcium group (DPBS, white triangles) is used to determine the EC50 (derived from Graph 40).

It has been reported that EGTA and nitrendipine were effective in blocking the entry of Ca^{2+} into the cell (Vernier et al., 2008) whereas the rise in intracellular Ca^{2+} was observed with caffeine or thapsigargin. nsPEF treatment with pulse duration was less than 30ns demonstrated calcium “bursts” in Jurkat T lymphoblasts (Vernier et al., 2003).

Cell Susceptibility to nsPEF Treatment

The goal is to determine whether cells sequentially exposed to nsPEF treatment would eventually become susceptible to nsPEF treatment. The experimental design to accomplish this goal is described in this section. The cells are treated at the number of pulses corresponding to the EC50 of cells determined in this work and then resuspended under growth conditions. The EC50 of H9C2 cells at low passage numbers was 22 pulses of 40kV/cm, 60ns, fast rise-time pulses. Cells would be trypsinized, pulsed, and resuspended in growth media. The primary assay would be WST-8, to determine the viability and polarographic assay to determine the integrity of the mitochondrial membranes. The control cell passaged but not pulsed could be used to detect changes in IMM integrity due to aging. Changes in protein rearrangement in the mitochondrial membranes due to aging has been previously noted and could be the missing link to discover IMM disintegration by nsPEF treatment (Kuhlbrandt, 2015).

Modeling nsPEF Effects on Mitochondrial Membranes

A computational approach was the first methods that provide a quantitative description of the nsPEF treatment effects on the cells (Esser et al., 2010) and mitochondrial membrane (Lopes et al., 2018). The first models of cells as passive receptors of membranes (Smith & Weaver, 2008) has been enhanced, but the effects of the nsPEF treatment on cellular activity are not completely quantified. An ongoing collaboration with Ravi Joshi of Texas Tech University is currently in progress, and the preliminary results are reported in the following section.

Specifically, a simplified model of a cell's plasma membrane, OMM, and IMM (with only 2 invaginations in the IMM, or cristae) was produced as seen below. This model includes the cell's plasma, outer mitochondrial, and the inner mitochondrial membranes. A spherical geometry of the

plasma membrane, OMM and IMM was assumed to obtain preliminary simulation and are not necessarily reflective of the actual IMM structure (Figure 6).

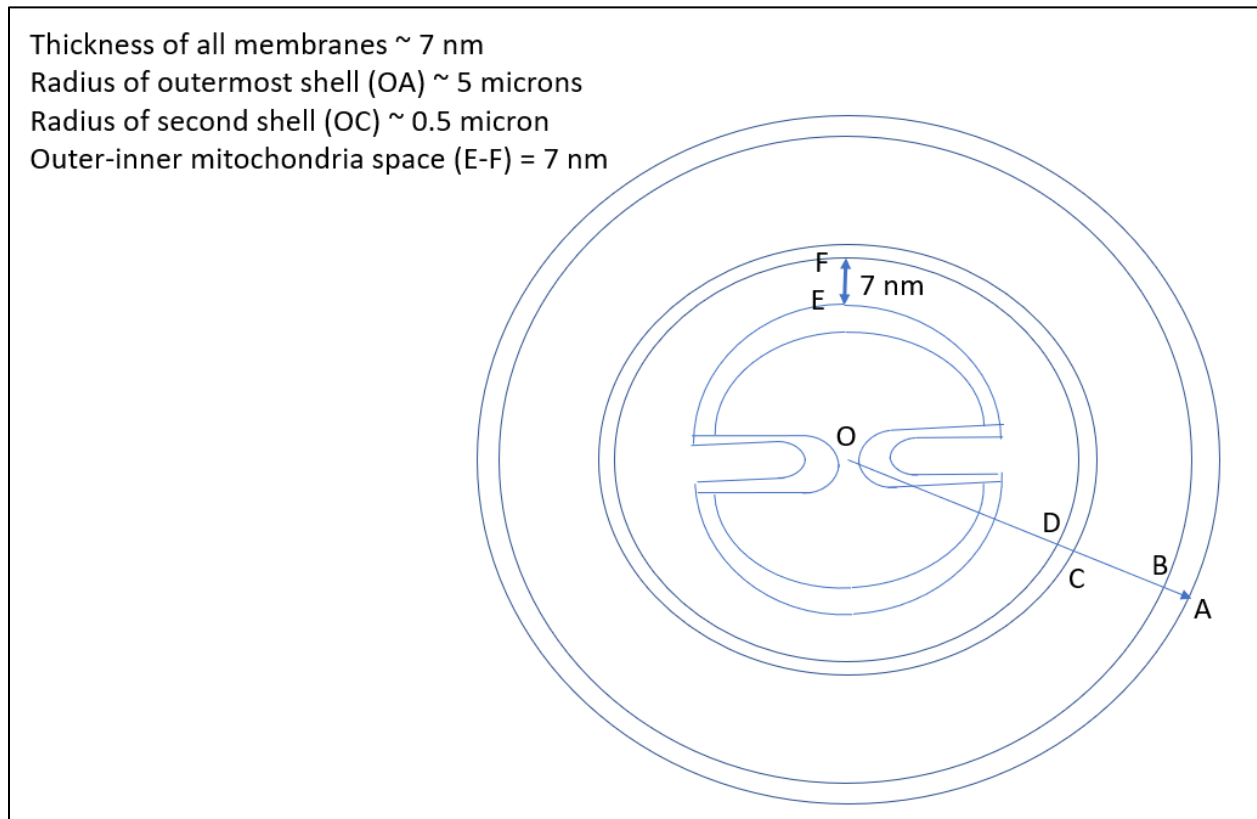


Figure 6: A schematic representation of the geometry of cellular membranes for the Electrical Model of these membranes. The geometry of the membranes is not necessarily reflective of actual morphology. However, the spherical models are used as an approximation of the nsPEF effect across the mitochondrial membranes, particularly to immediate effect of the pulse to the two difference cristae. A 5-micron radius spherical cell with the mitochondrial structure used in the simulations. Only two folds for the inner mitochondrial membrane (IMM) were considerate (*Joshi, 2021*).

The rise/fall times were similar to a monopolar pulse that reached a maximum field strength of 70kV/cm for a duration of 60ns and with short rise/fall times (5ns). Then the normalized field across the OMM and IMM were plotted as reported in Figure 7.

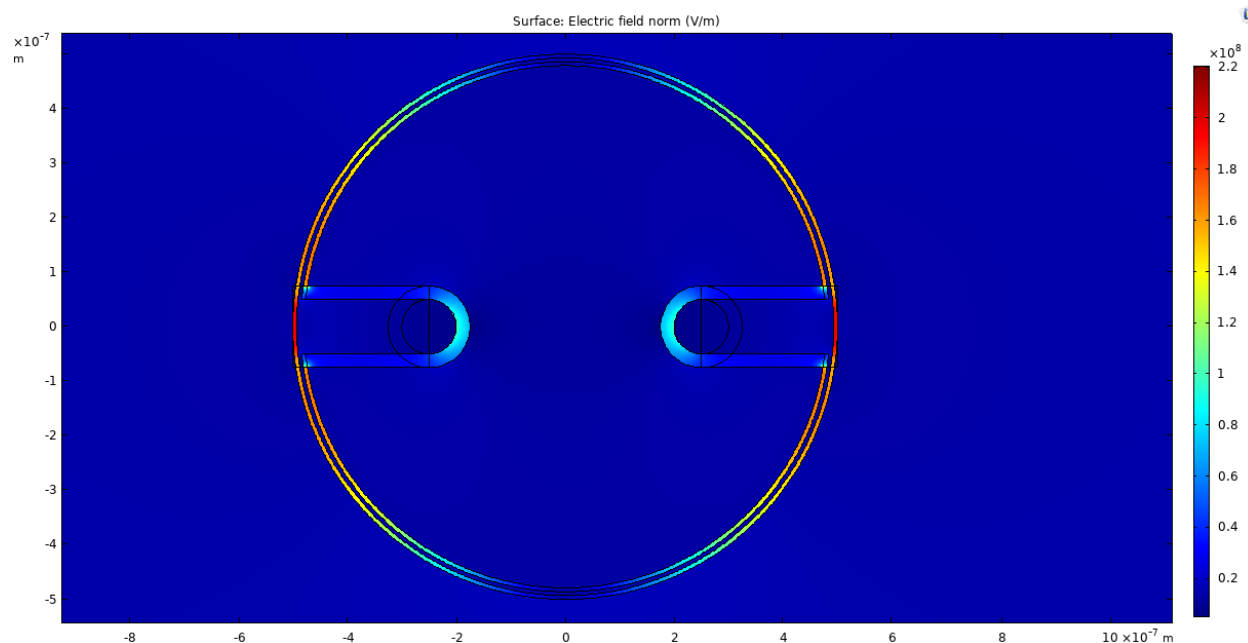


Figure 7: Effect of a monopolar, 70kv/cm, 60ns, fast rise/fall time pulse on individual mitochondrial cristae. Model simulation results for the spatial development of the transmembrane potential (TMP). An external trapezoidal electric pulse with a rise and fall times of 5 ns and a ON time of 60 ns and a peak electric field strength of 70 kV/cm. A 40 ns snapshot of the simulated electric field spatial distribution in the mitochondrial structure. For convenience, the plasma membrane region was not included in the Figure. An electric field is predicted to exist in the outer mitochondrial membrane at the 9- and 3-o'clock positions, while the field magnitude at the IMM and the invaginated region is quite low (*Joshi, 2021*).

The presence of a low voltage in the IMM (the inner layer) provides computational evidence in support of a lack of physical changes in the IMM. NAO was able to bind to cardiolipin and NADH did not cross the IMM are evidence for IMM integrity.

The pulse effect on IMM could be enhanced by considering the cristae electrically independent or insulated, as noted in the experimental works (Schlame, 2019; Wolf et al., 2019). An additional modification in the model could include the resistive and capacitive elements (proteins and bilayers). It should be noted that the protein: lipid ratio in the OMM is 50:50 and in the IMM, is 80:20 (Stefan, 2001) (Shaikh & Brown, 2013). This composition should influence the charge distribution and the ability of the membranes to hold charge.

Proposed Experiments for Future Works.

nsPEF effect on ETC substrates. One aspect that of nsPEF treatment that was not verified was the effect that nsPEF may have on the substrates used for the ETC. The main reason this experimentation was not undertaken was the simple unlikelihood of the amount of energy involved causing a conformational change in the substrates. To consider this effect, the protocol to assess cellular bioenergetics (see methods section Permeabilized ETC Complex Activity) should be carried out with ETC substrates previously treated with pulses.

nsPEF Effect on Duroquinone (Complex III).

The activity of Complex III was not investigated. Previous experiments used duroquinone harvested from murine samples such as Tetramethylhydroquinone to stimulate Complex III. This reagent should be tested and include in the protocol to assess the activity of the complexes of the ETC. (FisherScientific, 2021).

Testing of Apototic Signaling.

The first experiment in this work specified the amount of cell death that was undergone by cells when exposed to varying levels of nsPEF treatment. However, due to the variable ROS proportions that cells are exposed to, it is likely that each of the four cell lines tested could undergo different cell death types (apoptosis, necrosis, etc.). To test this aspect, the Caspase-Glo

family of reagents could be used (ProMega, 2021). The type of cell death could be identified with the release of a specific caspase protein (Galluzzi et al., 2016)) and related to the generation of ROS and loss of $\Delta\Psi$.

Cytosolic ROS indicator with Complex III.

In parallel with the experiment proposed above, the production of ROS attributable to Complex III could be an interesting area of research. Antimycin A as inhibitor of Complex III could be used in conjunction with Carboxy- H₂DCEFDA to detail the production of ROS from Complex III across different cell lines. This experiment could provide information on the mechanisms for ROS formation in cells exposed to nsPEF treatment.

Electron Microscope for Mitochondrial Structure.

The light microscopy was not sufficient to have conclusive results, to overcome the limitations the electron microscopy could be used as accomplished with murine skeletal muscle (Lai et al., 2018). Electron microscopy methods should provide information on the effect of nsPEF treatment on the internal structure of the mitochondria. Electron Microscopy has previously found fascinating facets of the structure of mitochondria (Kuhlbrandt, 2015). Electron microscopy can detect mitochondrial morphology changes in response to nsPEF treatment and provide information on mitochondrial fission and fusion processes. M1 (Sigma-Aldrich, 2021) is a mitochondrial fusion promoter. This has been shown to attenuate oxidative stress in diabetic rats (Ding et al., 2020). M-DIVI-1 (Sigma-Aldrich, 2021) prevents the original fission of the mitochondria decrease oxidative metabolism in cancer cells (Dai et al., 2020). The potential effects of the promotion or prevention of mitochondrial fusion and fission in cancer cells could be investigated with the electron microscopy.

ROS Production Sites.

A total of 11 sites produce superoxide (O_2^-) and/or hydrogen peroxide (H_2O_2) have been found in the ETC proteins of the mammalian mitochondria (Brand, 2016). The mitochondrial ROS formation from different sites can be identified using different inhibitors of the ETC. If all inhibitors show synergistic effects on the ROS production, then it is possible that the nsPEF treatment affect the arrangement of supercomplexes of the mitochondrial respiratory environment. The importance of Complex I dysfunction to diseased states is well-supported (Schapira, 2010).

CHAPTER 7: CONCLUSION

The deleterious effect of nsPEF treatment on mitochondrial Complex I across cell lines is important in two ways: from a clinical perspective, it offers a mechanism for the inhibition of the oxidative metabolism by nsPEF treatment; and from biochemical perspective offers an opportunity to enhance our understanding of Complex I function (Hummer & Wikström, 2016) and its assembly (Mimaki et al., 2012). Our current understanding relies on the experimental approaches available and computer modeling that progresses slowly due to the size and complexity of Complex I.

The evidence of CytC release and the observation that cardiolipin is still present in the mitochondria of H9C2 cells after nsPEF treatment offers an interesting explanation for the mechanistic effects of apoptosis in certain cell lines because CytC and cardiolipin are suggested to participate in programmed cell death mechanisms (Kagan et al., 2009). In this case, one explanation for the specific sequence of events after a cell is exposed to a lethal dose of nsPEF is that the OMM disintegrates relatively quickly, while the IMM is relatively conserved.

The effects of the nsPEF treatment reported in this work at sub-lethal and lethal doses have a potential for clinical application to offer selective and target treatment in different tissue organ systems and expand treatment options.

REFERENCES

- Agilent. (2019, May 1). *Agilent Technologies Agilent Seahorse XF Cell Mito Stress Test Kit*. Retrieved June 28, 2021, from Agilent.com: https://www.agilent.com/cs/library/usermanuals/public/XF_Cell_Mito_Stress_Test_Kit_User_Guide.pdf
- Agilent. (2020, November 1). *Seahorse XF HS Mini Extracellular Flux Analyzer*. Retrieved July 30, 2021, from <https://www.agilent.com/cs/library/usermanuals/public/user-manual-flux-analyzer-xf-hs-mini-extracellular-5994-1961en-agilent.pdf>
- Albano, R., Raddatz, N. J., Hjelmhaug, J., Abajer, D., & Lobner, D. (2015). Regulation of System Xc-by Pharmacological Manipulation of Cellular Thiols. *Oxidative Medicine and Cellular Longevity*, 2015. doi:10.1155/2015/269371
- Aminzadeh, A., & Mehrzadi, S. (2018). Cardioprotective effect of levosimendan against homocysteine-induced mitochondrial stress and apoptotic cell death in H9C2. *Biochemical and Biophysical Research Communications*, 507(1-4), 395-399. doi:10.1016/j.bbrc.2018.11.049
- Aryaman, J., Johnston, I. G., & Jones, N. S. (2019). Mitochondrial Heterogeneity. *Front. Genet.*, 9, 718. doi:10.3389/fgene.2018.00718
- ATCC. (2021, June 22). *4T1*. Retrieved from ATCC.org: <https://www.atcc.org/products/crl-2539>
- ATCC. (2021, June 22). *H9c2(2-1)*. Retrieved from ATCC.org: <https://www.atcc.org/products/crl-1446>
- ATCC. (2021, June 22). *HCC1937*. Retrieved from ATCC.org: <https://www.atcc.org/products/crl-2336>
- ATCC. (2021, June 22). *MCF-10-2A*. Retrieved from ATCC.org: <https://www.atcc.org/products/crl-10781>
- ATCC. (2021, June 23). *RAW 264.7*. (ATCC) Retrieved June 23, 2021, from <https://www.atcc.org/products/tib-71>
- Awasthi, K., Nakabayashi, T., & Ohta, N. (2016). Effects of Nanosecond Pulsed Electric Fields on the Intracellular Function of HeLa Cells As Revealed by NADH Autofluorescence Microscopy. *ACS OMEGA*, 1, 396-406. doi:10.1021/acsomega.6b00090
- Balaban, R. S. (2002). Cardiac Energy Metabolism Homeostasis: Role of Cytosolic Calcium. *Journal of Molecular and Cellular Cardiology*, 34(10), 1259-1271. doi:10.1006/jmcc.2002.2082
- Baradaran, R., Berrisford, J. M., Minhas, G. S., & Sazanov, L. A. (2013). Crystal structure of the entire respiratory complex I. *Nature*, 494(7438), 443-448. doi:10.1038/nature11871
- Beebe, S. (2016). Preclinical Studies with Nanosecond Pulses. In D. M. (Ed), *Handbook of Electroporation* (pp. 1543-1562). Springer. doi:978-3-319-26779-1
- Beebe, S. (2016). Regulated and Apoptotic Cell Death after Nanosecond Electroporation. In e. D. Miklavčič, *Handbook of Electroporation*. Springer. doi:978-3-319-26779-1
- Beebe, S. J. (2015). Considering Effects of nanosecond pulsed electric fields on proteins. *Bioelectrochemistry*, 103, 52-59. doi:10.1016/j.bioelechem.2014.08.014

- Beebe, S. J. (2015). Mechanisms of Nanosecond Pulsed Electric Field (NsPEF)-Induced Cell Death in Cells and Tumors. *Journal of Nanomedicine Research*, 2(1), 16. doi:10.15406/jnmr.2015.02.00016
- Beebe, S. J., Chen, Y.-J., Sain, N. M., Schoenbach, K. H., & Xiao, S. (2012). Transient Features of Nanosecond Pulsed Electric Fields Differentially Modulate Mitochondria and Viability. *PLOS One*, 7(12), e51349.
- Beebe, S. J., Ford, W. E., Ren, W., Chen, X., & Schoenbach, K. H. (2009). Non-ionizing radiation with nanosecond pulsed electric fields as a cancer treatment: in vitro studies. *2009 Annual International Conference of the IEEE Engineering in Medicine and Biology Society*, (pp. 6509-6512). doi:10.1109/IEMBS.2009.5333139.
- Beebe, S. J., Fox, P. M., Rec, L. J., Willis, L. K., & Schoenbach, K. H. (2003, August). Nanosecond, high-intensity pulsed electric fields induce apoptosis in human cells. *FASEB*, 17(11), 1-23. doi:10.1096/fj.02-0859fje
- Beebe, S. J., Sain, N. M., & Ren, W. (2013). Induction of Cell Death Mechanisms and Apoptosis by Nanosecond Pulsed Electric Fields (nsPEFs). *Cells*, 2(1), 136-162. doi:10.3390/cells2010136
- Beebe, S. J., White, J., Blackmore, P. F., Deng, Y., Somers, K., & Schoenbach, K. H. (2003). Diverse Effects of Nanosecond Pulsed Electric Fields on Cells and Tissues. *DNA and Cell Biology*, 22(12), 785-796. doi:10.1089/104454903322624993
- Beebe, S., Fox, P., Rec, L., Willis, L., & Schoenbach, K. (2003). Nanosecond, High intensity Pulsed Electric Fields Induce Apoptosis in Human Cells. *FASEB J*, 17(11), 1493-5.
- Behrend, M., Kuthi, A., Gu, X., Vernier, P., Marcu, L., Craft, C., & Gundersen, M. (2003). Pulse generators for pulsed electric field exposure of biological cells and tissues. *IEEE Transactions on Dielectrics and Electrical Insulation*, 10(5), 820-825. doi:10.1109/TDEI.2003.1237331
- Berg JM, T. J. (2002). Chapter 17: The Citric Acid Cycle. In *Biochemistry. 5th edition* (p. Chapter 17). New York: WH Freeman. Retrieved from <https://www.ncbi.nlm.nih.gov/books/NBK21163/>
- Bonora, M., & Pinton, P. (2014). The mitochondrial permeability transition pore and cancer: molecular mechanisms involved in cell death. *Front Oncol*, 4, 302. doi:10.3389/fonc.2014.00302
- Boutbir, J., Alshikhali, A., Panajatovic, M. V., Abegg, V. F., Paech, F., & Krahenbuehli, S. (2019). Mitochondrial oxidative stress plays a critical role in the cardiotoxicity of sunitinib. *Toxicology*. doi:10.1016/j.tox.2019.152281
- Brand, M. D. (2010). The sites and topology of mitochondrial superoxide production. *Exp Gerontol*, 45(7-8), 466-72.
- Brand, M. D. (2016). Mitochondrial generation of superoxide and hydrogen peroxide as the source of mitochondrial redox signaling. *Free Radic Biol Med*, 100, 14-31. doi:10.1016/j.freeradbiomed.2016.04.001
- Brisson, L., Chadet, S., Lopez-Charcas, O., Jelassi, B., Ternant, D., Chamouton, J., . . . Jiang, L.-H. (2020). P2X7 Receptor Promotes Mouse Mammary Cancer Cell Invasiveness and Tumour Progression,

- and Is a Target for Anticancer Treatment. *Cancers (Basel)*, *12*(9), 2342. doi:10.3390/cancers12092342
- Brookes, P. S., Yoon, Y., Robotham, J. L., Anders, M. W., & Sheu, S.-S. (2004). Calcium, ATP, and ROS: a mitochondrial love-hate triangle. *Am J Physiol Cell Physiol*, *287*, C817–C833. doi:10.1152/ajpcell.00139.2004
- Burton L Shapiro, R. J.-H. (1979). Mitochondrial NADH Dehydrogenase in Cystic Fibrosis. *Proc. Natl. Acad. Sci. USA*, *76*(6), 2979-2983.
- Cadenas, E., & Davies, K. J. (2000). Mitochondrial free radical generation, oxidative stress, and aging. *Free Radic Biol Med*, *29*(3-4), 222-230. doi:10.1016/s0891-5849(00)00317-8.
- Camara¹, A. K., Zhou, Y. F., Wen, P.-C., Tajkhorshid, E., & Kwok, W.-M. (2017). Mitochondrial VDAC1: A Key Gatekeeper as Potential Therapeutic Target. *Frontiers in Physiology*, *8*, 460. doi:10.3389/fphys.2017.00460
- Cankurtaran-Sayar, S., Sayar, K., & Ugur, M. (2009). P2X7 receptor activates multiple selective dye-permeation pathways in RAW 264.7 and human embryonic kidney 293 cells. *Molecular Pharmacology*, *76*(6), 1323-32. doi:10.1124/mol.109.059923
- Cantu, J. C., Tarango, M., Beier, H. T., & Ibey, B. L. (2016). The biological response of cells to nanosecond pulsed electric fields is dependent on plasma membrane cholesterol. *Biochimica et Biophysica Acta (BBA) - Biomembranes*, *1858*(11), 2636-2646. doi:10.1016/j.bbamem.2016.07.006
- Carr, L., Bardet, S. M., Curke, R., Arnaud-Cormos, D., Leveque, P., & O'Connor, R. P. (2017). Calcium-independent disruption of microtubule dynamics by nanosecond pulsed electric fields in U87 human glioblastoma cells. *Scientific Reports*, *7*, 41267. doi:10.1038/srep41267
- Chang, D. C. (2006). Electroporation and Electrofusion. *Reviews in Cell Biology and Molecular Medicine*. doi:10.1002/3527600906.mcb.200300026
- Chen, M.-T., Jiang, C., Vernier, P. T., Wu, Y.-H., & Gundersen, M. A. (2009). Two-dimensional nanosecond electric field mapping based on cell electropermeabilization. *PMC Biophysics*, *2*, 9. doi:10.1186/1757-5036-2-9
- Chen, R., Chen, X., & Beebe, S. J. (2013). https://digitalcommons.odu.edu/bioelectrics_pubs/83/. *Surgery: Current Research*, *12*, 1-9. doi:10.4172/2161-1076.S12-005
- Chen, X., Li, H., Wang, K., Liang, X., Wang, W., Hu, X., . . . Wang, Y. (2019). Aerobic Exercise Ameliorates Myocardial Inflammation, Fibrosis and Apoptosis in High-Fat-Diet Rats by Inhibiting P2X7 Purinergic Receptors. *Frontiers in Physiology*, *10*, 1286. doi:10.3389/fphys.2019.01286
- Chen, X.-H., Beebe, S. J., & Zheng, S.-S. (2012). Tumor ablation with nanosecond pulsed electric fields. *Hepatobiliary Pancreat Dis Int*, *11*(2), 112-114. doi:10.1016/S1499-3872(12)60135-0
- Cheng, X., Zhang, X., Yu, L., & Xu, H. (2015). Calcium signaling in membrane repair. *Semin Cell Dev Biol.*, *45*, 24-31. doi:10.1016/j.semcdb.2015.10.031
- Chernets, N., Kurpad, D. S., Alexeev, V., Rodrigues, D. B., & Freeman, T. A. (2015). Reaction Chemistry Generated by Nanosecond Pulsed Dielectric Barrier Discharge Treatment is Responsible for the

- Tumor Eradication in the B16 Melanoma Mouse Model. *Plasma Processes and Polymers*, 12(12), 1400-1409. doi:10.1002/ppap.201500140
- Chicco, A. J. (2007). Role of cardiolipin alterations in mitochondrial dysfunction and disease. *Cell Physiology*, 292(1), C33-C44. doi:10.1152/ajpcell.00243.2006
- Claypool, S. M., Oktay, Y., Boontheung, P., Loo, J. A., & Koehler, C. M. (2008). Cardiolipin defines the interactome of the major ADP/ATP carrier protein of the mitochondrial inner membrane. *Journal of Cell Biology*, 182(5), 937-950. doi:10.1083/jcb.200801152
- Collins, Y., Chouchani, E. T., James, A. M., Menger, K. E., Cocheme, H. M., & Murphy, M. P. (2012). Mitochondrial redox signalling at a glance. *Journal of Cell Science*, 125(4), 801-806. doi:10.1242/jcs.098475
- Cooper, S. T., & McNeil, P. L. (2015). Membrane Repair: Mechanisms and Pathophysiology. *Physiological Reviews*, 95(4), 1205-1240. doi:10.1152/physrev.00037.2014
- Corning. (2021, June 28). *Corning® 100 mL Trypsin 1X, 0.25% Trypsin in HBSS [-] calcium, magnesium, Porcine Parvovirus tested*. (Corning) Retrieved June 28, 2021, from <https://ecatalog.corning.com/life-sciences/b2c/US/en/Media,-Sera,-and-Reagents/Cell-Culture-Reagents/Enzymatic-Cell-Dissociation-Reagents/Corning%C2%AE-100-mL-Trypsin-1X,-0-25%25-Trypsin-in-HBSS-%5B-%5D-calcium,-magnesium,-Porcine-Parvovirus-tested/p/25-0>
- Cosentino, K., & García-Sáez, A. J. (2014). Mitochondrial alterations in apoptosis. *Chemistry and Physics of Lipids*, 181, 62-75. doi:10.1016/j.chemphyslip.2014.04.001
- Cossarizza, A., & Salvio, S. (2001). Analysis of mitochondria during cell death. *Methods Cell Biol.*, 63, 467-86. doi:10.1016/s0091-679x(01)63025-5
- Craviso, G. L., Choe, S., Chatterjee, P., Chatterjee, I., & Vernier, P. T. (2010). Nanosecond Electric Pulses: A Novel Stimulus for Triggering Ca²⁺ Influx into Chromaffin Cells Via Voltage-Gated Ca²⁺ Channels. *Cellular and Molecular Neurobiology*, 30, 1259-1265. doi:10.1007/s10571-010-9573-1
- Crofts, A., Hollam, J., Victoria, D., Kolling, D., Dikanov, S., Gilbreth, R., . . . Kuras, R. (2008). The Q-Cycle Reviewed: How well does a monomeric mechanism of the bc1 complex account for the function of a dimeric complex? *Biochimica et Biophysica Acta*, 1777, 1001-1019.
- Dai, W., Wang, G., Chwa, J., Oh, M. E., Abeywardana, T., Yang, Y., . . . Jiang, L. (2020). Mitochondrial division inhibitor (mdivi-1) decreases oxidative metabolism in cancer. *British Journal of Cancer*, 122, 1288-1297. doi:10.1038/s41416-020-0778-x
- DeBerardinis, R. J., & Chandel, N. S. (2020). We need to talk about the Warburg effect. *Nature Metabolism*, 2, 127-129. doi:10.1038/s42255-020-0172-2
- Deng, J., Schoenbach, K., Buescher, E., Hair, P., Fox, P., & Beebe, S. (2003). The Effects of submicrosecond electrical pulses on cells. *Biophys J.*, 84(4), 2709-14.
- Ding, M., Liu, C., Shi, R., Yu, M., Zheng, K., Kang, J., . . . Mi, M. (2020). Mitochondrial fusion promoter restores mitochondrial dynamics balance and ameliorates diabetic cardiomyopathy in an optic atrophy 1-dependent way. *Acta Physiol (Oxf.)*, 229(1), e13428. doi:10.1111/apha.13428

- Djafarzadeh, S., & Jakob, S. M. (2017). High-resolution Respirometry to Assess Mitochondrial Function in Permeabilized and Intact Cells. *JOVE*, *120*, 54985. doi:10.3791/54985
- Dmitry B. Zorov, M. J. (2014). Mitochondrial Reactive Oxygen Species (ROS) and ROS-Induced ROS Release. *Physiological Reviews*, *94*(3), 909-950. doi:10.1152/physrev.00026.2013
- Dojindo Molecular Technologies. (2021, June 23). *Cell Counting Kit-8*. (Dojindo Molecular Technologies) Retrieved June 23, 2021, from <https://dojindo.com/product/cell-counting-kit-8/>
- Dong, B., Ding, Y., Huang, Q., & Guan, A. (2019). Different Triple-Negative Breast Cancer Tumor Cell Lysates (TCLs) Induce Discrepant Anti-Tumor Immunity by PD1/PDL-1 Interaction. *Medical Science Monitor*, *25*, 500-515. doi:10.12659/MSM.911689
- Doran, E., & Halestrap, A. P. (2000). Cytochrome c release from isolated rat liver mitochondria can occur independently of outer-membrane rupture: possible role of contact sites. *Biochem J*, *348*(2), 343-350. doi:10.1042/bj3480343
- Drago, L. C., Zampese, E., & Pozzan, T. (2010). Mitochondria: The Calcium Connection. *Biochimica et Biophysica Acta*, *1797*, 607-618.
- Drose, S., & Brandt, U. (2008). The Mechanism of Mitochondrial Superoxide Production by the Cytochrome bc1 Complex. *Journal of Biological Chemistry*, *283*(31), 21649-21654. doi:10.1074/jbc.M803236200
- Dudek, J. (2017). Role of Cardiolipin in Mitochondrial Signaling Pathways. *Front. Cell Dev. Biol.*, *29*. doi:10.3389/fcell.2017.00090
- DuPre, S. A., Redelman, D., & Kenneth W Hunter, J. (2007). The mouse mammary carcinoma 4T1: characterization of the cellular landscape of primary tumours and metastatic tumour foci. *International Journal of Experimental Pathology*, *88*(5), 351-360. doi:10.1111/j.1365-2613.2007.00539.x
- Eleanor C Kennett, P. W. (2003). Redox Reactions and Electron Transfer Across the Red Cell Membrane. *IUBMB Life*, *55*(7), 375-385. doi:10.1080/15216540310001592843
- Esser, A. T., Smith, K. C., Gowrishankar, T. R., Vasilkoski, Z., & Weaver, J. C. (2010). Mechanisms for the intracellular manipulation of organelles by conventional electroporation. *Biophys J*, *98*(11), 2506-14. doi:10.1016/j.bpj.2010.02.035.
- Esser, L., Quinn, B., Li, Y.-F., Zhang, M., Elberry, M., Yu, L., . . . Xia, D. (2004). Crystallographic Studies of Quinol Oxidation Site Inhibitors: A Modified Classification of Inhibitors for the Cytochrome bc1 Complex. *Journal of Molecular Biology*, *341*(1), 281-302. doi:10.1016/j.jmb.2004.05.065
- Estlack, L. E., Roth, C. C., Cerna, C. Z., Wilmlink, G. J., & Ibey, B. L. (2014). Investigation of a Direct Effect of Nanosecond Pulse Electric Fields on Mitochondria. *Optical Interactions with Tissue and Cells XXV; and Terahertz for Biomedical Applications*. San Francisco: SPIE. doi:10.1117/12.20419
- Feno, S., Butera, G., Reane, D. V., Rizzuto, R., & Raffaello, A. (2019). Crosstalk between Calcium and ROS in Pathophysiological Conditions. *Oxidative Medicine and Cellular Longevity*, *2019*, Article ID 9324018, 18 pages. doi:10.1155/2019/9324018

- Fernandez, M. L., Risk, M., Reigada, R., & Vernier, P. T. (2012). Size-controlled nanopores in lipid membranes with stabilizing electric fields. *Biochemical and Biophysical Research Communications*, *423*, 325-330. doi:10.1016/j.bbrc.2012.05.122
- FisherScientific. (2021, June 30). *Tetramethylhydroquinone 95.0+%, TCI America™*. (FisherScientific) Retrieved June 30, 2021, from <https://www.fishersci.com/shop/products/tetramethylhydroquinone-tci-america-2/T08221G>
- Fujisawa, S., Romin, Y., Barlas, A., Petrovic, L. M., Turkekul, M., Fan, N., . . . Sofocleouscorre, C. T. (2014). Evaluation of YO-PRO-1 as an early marker of apoptosis following radiofrequency ablation of colon cancer liver metastases. *Cytotechnology*, *66*(2), 259-273. doi:10.1007/s10616-013-9565-3
- Galluzzi, L., López-Soto, A., Kumar, S., & Kroemer, G. (2016). Caspases Connect Cell-Death Signaling to Organismal Homeostasis. *Immunity*, *44*(2), 221-231. doi:10.1016/j.immuni.2016.01.020
- Goncalves, R. L., Quinlan, C. L., Perevoshchikova, I. V., Hey-Mogensen, M., & Brand, M. D. (2015). Sites of Superoxide and Hydrogen Peroxide Production by Muscle Mitochondria Assessed ex Vivo under Conditions Mimicking Rest and Exercise. *Journal of Biological Chemistry*, *290*(1), 209-227. doi:10.1074/jbc.M114.619072
- Goncalves, R., Quinlan, C., Perevoshchikova, I., Hey-Mogensen, M., & Brand, M. (2015). Sites of superoxide and hydrogen peroxide production by muscle mitochondria assessed ex vivo under conditions mimicking rest and exercise. *J. Biol. Chem.*, *290*, 209-277. doi:10.1074/jbc.M114.619072
- Görlach, A., Bertram, K., Hudecova, S., & Krizanova, O. (2015). Calcium and ROS: A mutual interplay. *Redox Biology*, 260-271. doi:10.1016/j.redox.2015.08.010
- Görlach, A., Bertram, K., Hudecova, S., & Krizanova, O. (2015). Calcium and ROS: A mutual interplay. *Redox Biology*, *6*, 260-271. doi:10.1016/j.redox.2015.08.010
- Goswami, I., Perry, J. B., Allen, M. E., Brown, D. A., Spakovsky, M. R., & Verbridge, S. S. (2018). Influence of Pulsed Electric Fields and Mitochondria-Cytoskeleton Interactions on Cell Respiration. *Biophysical Journal*, *114*, 2951-2964. doi:10.1016/j.bpj.2018.04.047
- Gowrishankar, T. R., Esser, A. T., Vasilkoski, Z., Smith, K. C., & Weaver, J. C. (2006). Microdosimetry for conventional and supra-electroporation in cells with organelles. *Biochemical and Biophysical Research Communications*, *341*(4), 1266-1276. doi:10.1016/j.bbrc.2006.01.094
- Guo, H., Qian, H., Idris, N. M., & Zhang, Y. (2010). Singlet oxygen-induced apoptosis of cancer cells using upconversion fluorescent nanoparticles as a carrier of photosensitizer. *Nanomedicine: Nanotechnology, Biology and Medicine*, *6*(3), 486-495. doi:10.1016/j.nano.2009.11.004
- Halestrap, A. P. (2009). What is the mitochondrial permeability transition pore? *J Mol Cell Cardiol*, *46*(6), 821-831. doi:10.1016/j.yjmcc.2009.02.021
- Hansford, R. G., & Zorov, D. (1998). Role of mitochondrial calcium transport in the control of substrate oxidation. *Molecular and Cellular Biochemistry*, *184*, 359-369. doi:10.1023/A:1006893903113

- He, L., Xiao, D., Feng, J., Yao, C., & Tang, L. (2017). Induction of apoptosis of liver cancer cells by nanosecond pulsed electric fields (nsPEFs). *Med Oncol*, *34*(24). doi:10.1007/s12032-016-0882-1
- Heiden, M. G., Cantley, L. C., & Thompson, C. B. (2009). Understanding the Warburg Effect: The Metabolic Requirements of Cell Proliferation. *Science*, *324*(5930), 1029-1033. doi:10.1126/science.1160809
- Heinz, S., Freyberger, A., Lawrenz, B., Schladt, L., Schmuck, G., & Ellinger-Ziegelbauer, H. (2017). Mechanistic Investigations of the Mitochondrial Complex I Inhibitor Rotenone in the Context of Pharmacological and Safety Evaluation. *Scientific Reports*, *7*, 45465. doi:10.1038/srep45465
- Hernansanz-Agustín, P., Ramos, E., Navarro, E., Parada, E., Sánchez-López, N., Peláez-Aguado, L., . . . Martínez-Ruiz, A. (2017). Mitochondrial complex I deactivation is related to superoxide production in acute hypoxia. *Redox biology*, *12*, 1040–1051. doi:10.1016/j.redox.2017.04.025
- Hirst, J. (2013). Mitochondrial Complex I. *Annual Review of Biochemistry*, *82*, 551-575.
- Hoppel, C., Kerner, J., Turkaly, P., Minkler, P., & Tandler, B. (2002). Isolation of Hepatic Mitochondrial Contact Sites: Previously Unrecognized Inner Membrane Components. *Analytical Biochemistry*, *302*(1), 60-69.
- Hornef, J., Edelblute, C. M., Schoenbach, K. H., Heller, R., Guo, S., & Jiang, C. (2020). Thermal Analysis of Infrared Irradiation-Assisted Nanosecond-Pulsed Tumor Ablation. *Scientific Reports*, *10*, 5122. doi:10.1038/s41598-020-62017-8
- Horvath, S. E., & Daum, G. (2013). Lipids of mitochondria. *Progress in Lipid Research*, *52*(4), 590-614. doi:10.1016/j.plipres.2013.07.002
- Hughey, C. C., Hittel, D. S., Johnsen, V. L., & Shearer, J. (2011). Respirometric Oxidative Phosphorylation Assessment in Saponin-permeabilized. *Journal of Visualized Experiments*, *48*. doi:10.3791/2431
- Hummer, G., & Wikström, M. (2016). Molecular simulation and modeling of complex I. *Biochimica et Biophysica Acta (BBA) - Bioenergetics*, *1857*(7), 915-921.
- Hyo-Jung Choo, A. K. (2017). Inner Mitochondrial Membrane Disruption Links. (*Arterioscler Thromb Vasc Biol.*, *37*, 1503-1512. doi:10.1161/ATVBAHA.117.309473
- Ibey, B. L., Ullery, J. C., Pakhomov, O. N., Roth, C. C., Semenov, I., Beier, H. T., . . . Pakhomov, A. G. (2014). Bipolar nanosecond electric pulses are less efficient at electropermeabilization and killing cells than monopolar pulses. *Biochemical and Biophysical Research Communications*, *443*(2), 568-573.
- Ibey, B. L., Xiao, S., Schoenbach, K. H., Murphy, M. R., & Pakhomov, A. (2009). Plasma Membrane Permeabilization by 60- and 600-ns Pulses Is Determined by Absorbed Dose. *Bioelectromagnetics*, *30*, 92-99. doi:10.1002/bem.20451
- IEEE. (2011). IEEE Standard for Transitions, Pulses, and Related Waveforms. *IEEE Std 181-2011 (Revision of IEEE Std 181-2003)*, 1-72. doi:10.1109/IEEESTD.2011.6016198

- Jake Jacobson, M. R. (2002). Intracellular distribution of the fluorescent dye nonyl acridine orange responds to the mitochondrial membrane potential: implications for assays of cardiolipin and mitochondrial mass. *J Neurochem*, *82*(2), 224-33. doi:10.1046/j.1471-4159.2002.00945.x.
- Jardin, I., Lopez, J. J., Salido, G. M., & Rosado, J. A. (2018). Store-Operated Ca²⁺ Entry in Breast Cancer Cells: Remodeling and Functional Role. *International Journal of Molecular Sciences*, *19*(12), 4053. doi:10.3390/ijms19124053
- Jelassi, B., Anachelin, M., Chamouton, J., Cayuela, M. L., Clarysse, L., Li, J., . . . Roger, S. (2013). Anthraquinone emodin inhibits human cancer cell invasiveness by antagonizing P2X7 receptors. *Carcinogenesis*, *34*(7), 1487–1496. doi:10.1093/carcin/bgt099
- Jose, C., Bellance, N., & Rossignol, R. (2011). Choosing between glycolysis and oxidative phosphorylation: A tumor's dilemma? *Biochimica et Biophysica Acta*, *1807*, 552-561. doi:10.1016/j.bbabi.2010.10.012
- Joshi, R. (2021, September 22). Personal Correspondance. *Personal Correspondance - Modeling nsPEF Treatment Effect on Mitochondrial Membrane Voltage*. Lubbock, Texas, U.S.A: Ravi Joshi.
- Juvekar, A., Hu, H., Yadegarynia, S., Lyssiotis, C. A., Ullas, S., Lien, E. C., . . . Wulf, G. M. (2016). Phosphoinositide 3-kinase inhibitors induce DNA damage through nucleoside depletion. *PNAS*, *E4338–E4347*. doi:10.1073/pnas.1522
- Kaewsuya, P., Danielson, N. D., & Ekhterae, D. (2007). Fluorescent determination of cardiolipin using 10-N-nonyl acridine orange. *Anal Bioanal Chem*, *387*(8), 2775-82. doi:10.1007/s00216-007-1135-0.
- Kagan, V. E., Bayir, H. A., Belikova, N. A., Kapralov, O., Tyurina, Y. Y., Tyurin, V. A., . . . Borisenko, G. (2009). Cytochrome c/cardiolipin relations in mitochondria: a kiss of death. *Free Radic Biol Med.*, *46*(11), 1439-1453. doi:10.1016/j.freeradbiomed.2009.03.004
- Kamonwan Chamchoy, D. P. (2019). Application of WST-8 based colorimetric NAD(P)H detection for quantitative dehydrogenase assays. *BMC Biochemistry*, *20*(4). doi:10.1186/s12858-019-0108-1
- KB Nolop, C. R. (1987). Glucose utilization in vivo by human pulmonary neoplasms. *Cancer*, *60*(11), 2682-9. doi:10.1002/1097-0142(19871201)60:11<2682::aid-cnrcr2820601118>3.0.co;2-h.
- Kelly, S. C., Eccardt, A. M., & Fisher, J. S. (2018). Measuring Trans-Plasma Membrane Electron Transport by C2C12 Myotubes. *J Vis Exp*, *4*(135), 57565.
- Kim, J.-S., He, L., & Lemasters, J. J. (2003). Mitochondrial permeability transition: a common pathway to necrosis and apoptosis. *Biochem Biophys Res Commun*, *304*(3), 463-470. doi:10.1016/s0006-291x(03)00618-1.
- Kirby, D., Crawford, M., Cleary, M., Dahl, H., Dennett, X., & Thorburn, D. (1999). Respiratory chain complex I deficiency: an underdiagnosed energy generation disorder. *Neurology*, *52*, 1255-1264.
- Klenow, M. B., Heitmann, A. S., Nylandsted, J., & Simonsen, A. C. (2021). Timescale of hole closure during plasma membrane repair estimated by calcium imaging and numerical modeling. *Scientific Reports*, *11*, 4226.

- Krumschnabel, G., Makrecka-Kuka, M., Kumphune, S., Fontana-Ayoub, M., Fasching, M., & Gnaiger, E. (2014, January 1). *O2k-Fluorometry: HRR and simultaneous determination of H2O2 production with Amplex Red*. Retrieved June 28, 2021, from bioblast.at: https://bioblast.at/images/5/5d/MiPNet19.20_Amplex_Red_Data_Acquisition_and_Analysis.pdf
- Kuhlbrandt, W. (2015). Structure and function of mitochondrial membrane protein complexes. *BMC Biology*, *13*(89). doi:10.1186/s12915-015-0201-x
- Kuznetsov, A. V., Javadov, S., Sickinger, S., Frotschnig, S., & Grimm, M. (2015, Feb). H9c2 and HL-1 cells demonstrate distinct features of energy metabolism, mitochondrial function and sensitivity to hypoxia-reoxygenation. *Biochim Biophys Acta*, *1853*(2), 276–284. doi:10.1016/j.bbamcr.2014.11.015
- Lai, N., Kummitha, C. M., Rosca, M. G., Fujioka, H., Tandler, B., & Hoppel, C. L. (2018). Isolation of mitochondrial subpopulations from skeletal muscle: Optimizing recovery and preserving integrity. *Acta Physiologica*, *225*(2), e13182. doi:10.1111/apha.13182
- Lemasters, J. J. (2007). Modulation of mitochondrial membrane permeability in pathogenesis, autophagy and control of metabolism. *J Gastroenterol Hepatol*, *22 Suppl 1*, S31-7. doi:10.1111/j.1440-1746.2006.04643.x
- Lenaz, G., Fato, R., Genova, M. L., Bergamini, C., Bianchi, C., & Biondi, A. (2006). Mitochondrial Complex I: Structural and functional aspects. *1757*(9-10), 1406-1420. doi:10.1016/j.bbabi.2006.05.007
- Leskova, G. F. (2017). Phospholipids in mitochondrial dysfunction during hemorrhagic shock. *Journal of Bioenergetics and Biomembranes*, *49*, 121-129.
- Li Yu, X. C. (2017). The Glycolytic Switch in Tumors: How Many Players Are Involved? *Journal of Cancer*, *8*(17), 3430-3440. doi:10.7150/jca.21125
- Li, X., Fang, P., Mai, J., Choi, E. T., Wang, H., & Yang, X.-f. (2013). Targeting mitochondrial reactive oxygen species as novel therapy for inflammatory diseases and cancers. *J Hematol Oncol*, *6*(19). doi:10.1186/1756-8722-6-19
- Li, X., Fang, P., Yang, W. Y., Chan, K., Lavalley, M., Xu, K., . . . Yang, X. (2017). Endothelial mitochondrial ROS, un-coupled from ATP synthesis, determine both physiological endothelial activation for recruitment of patrolling cells, and pathological recruitment of inflammatory cells. *Can J Physiol Pharmacol.*, *95*(3), 247–252. doi:10.1139/cjpp-2016-0515
- Liberti, M. V., & Locasale, J. W. (2016). The Warburg Effect: How Does it Benefit Cancer Cells? *Trends Biochem Sci*, *41*(3), 211-218. doi:10.1016/j.tibs.2015.12.001
- Liu, Y. J., McIntyre, R. L., Janssens, G. E., & Houtkooper, R. H. (2020). Mitochondrial fission and fusion: A dynamic role in aging and potential target for age-related disease. *Mechanisms of Ageing and Development*, *186*, 111212. doi:10.1016/j.mad.2020.111212
- Long, Q., Huang, L., Huang, K., & Yang, Q. (2019). Assessing Mitochondrial Bioenergetics in Isolated Mitochondria from Mouse Heart Tissues Using Oroboros 2k-Oxygraph. *Methods Mol Biol.*, *1966*, 237-246. doi:10.1007/978-1-4939-9195-2_19

- Long, Q., Yang, K., & Yang, Q. (2015). Regulation of mitochondrial ATP synthase in cardiac pathophysiology. *Am J Cardiovasc Dis.*, 5(1), 19-32.
- Love, M. R., Palee, S., Chattipakorn, S. C., & Chattipakorn, N. (2017). Effects of electrical stimulation on cell proliferation and apoptosis. *Journal of Cellular Physiology*, 233(3), 1860-1876. doi:10.1002/jcp.25975
- Lu, C., & Armstrong, J. S. (2007). Role of calcium and cyclophilin D in the regulation of mitochondrial permeabilization induced by glutathione depletion. *Biochemical and Biophysical Research Communications*, 363, 572-577. doi:10.1016/j.bbrc.2007.08.196
- Madesh, M., & Hajnóczky, G. (2001). VDAC-dependent permeabilization of the outer mitochondrial membrane by superoxide induces rapid and massive cytochrome c release. *Journal of Cell Biology*, 155(6), 1003-1016. doi:10.1083/jcb.200105057
- Martin Ott, J. D. (2002). Cytochrome c release from mitochondria proceeds by a two-step process. *Proc Natl Acad Sci U S A.*, 99(3), 1259–1263. doi:10.1073/pnas.241655498
- Mekahli, D., Bultynck, G., Parys, J. B., Smedt, H. D., & Missiaen, L. (2011). Endoplasmic-Reticulum Calcium Depletion and Disease. *Cold Spring Harbor Perspectives in Biology*, 3(6), a004317. doi:10.1101/cshperspect.a004317
- Merla, C., Pakhomov, A. G., Semenov, I., & Vernier, P. T. (2017). Frequency spectrum of induced transmembrane potential and permeabilization efficacy of bipolar electric pulses. *Biochimica et Biophysica Acta (BBA) - Biomembranes*, 1859(7), 1282-1290. doi:10.1016/j.bbamem.2017.04.014
- Miao, X., Yin, S., Shao, Z., Zhang, Y., & Chen, X. (2014). Nanosecond pulsed electric field inhibits proliferation and induces apoptosis in human osteosarcoma. *Journal of Orthopaedic Surgery and Research*, 10, 104. doi:10.1186/s13018-015-0247-z
- Michel, A. D., Kaur, R., Chessell, I. P., & Humphrey, P. P. (2009). Antagonist effects on human P2X7 receptor-mediated cellular accumulation of YO-PRO-1. *British Journal of Pharmacology*, 130(3), 513-520. doi:10.1038/sj.bjp.0703368
- Mileykovskaya, E., & Dowhan, W. (2020). Visualization of Phospholipid Domains in Escherichia coli by Using the Cardiolipin-Specific Fluorescent Dye 10-N-Nonyl Acridine Orange. *Journal of Bacteriology*, 182(4). doi:10.1128/JB.182.4.1172-1175.2000
- Mileykovskaya, E., Dowhan, W., Birke, R. L., Zheng, D., Lutterodt, L., & Haines, T. H. (2001). Cardiolipin binds nonyl acridine orange by aggregating the dye at exposed hydrophobic domains on bilayer surfaces. *FEBS Letters*, 507(2), 187-190. doi:10.1016/S0014-5793(01)02948-9
- Miltenyl Biotec. (2021, June 28). *MACSQuant Analyzer 10 Flow Cytometer*. Retrieved June 28, 2021, from miltenyibiotec.com: <https://www.miltenyibiotec.com/US-en/products/macsqunt-analyzer-10.html>
- Mimaki, M., Wang, X., McKenzie, M., Thorburn, D. R., & Ryan, M. T. (2012). Understanding mitochondrial complex I assembly in health and disease. *Biochimica et Biophysica Acta (BBA) - Bioenergetics*, 1817(6), 851-862. doi:10.1016/j.bbabi.2011.08.010

- Mironov, S. L., Ivannikov, M. V., & Johansson, M. (2005). [Ca²⁺]_i signaling between mitochondria and endoplasmic reticulum in neurons is regulated by microtubules. From mitochondrial permeability transition pore to Ca²⁺-induced Ca²⁺ release. *J Biol Chem*, *280*(1), 715-21. doi:10.1074/jbc.M409819200.
- Moe, A., Golding, A. E., & Bement, W. M. (2015). Cell healing: calcium, repair and regeneration. *Semin Cell Dev Biol.*, *45*, 18-23. doi:10.1016/j.semcdb.2015.09.026
- Mohsin, A. A., Thompson, J., Hu, Y., Hollander, J., Lesnefsky, E. J., & Chen, Q. (2020). Endoplasmic reticulum stress-induced complex I defect: Central role of calcium overload. *Arc Biochem Biophys*. doi:10.1016/j.abb.2020.108299
- Molecular Devices. (2013, October 1). *SpectraMax i3 Multi-Mode Platform* . Retrieved June 28, 2021, from moleculardevices.com: <https://www.moleculardevices.com/sites/default/files/en/assets/brochures/br/spectramax-i3-multi-mode-platform.pdf>
- Morotomi-Yano, K., Akiyama, H., & Yano, K.-i. (2014). Different involvement of extracellular calcium in two modes of cell death induced by nanosecond pulsed electric fields. *Archives of Biochemistry and Biophysics*, *555-556*, 47-54. doi:10.1016/j.abb.2014.05.020
- Motiani, R. K., Abdullaev, I. F., & Trebak, M. (2010). A Novel Native Store-operated Calcium Channel Encoded by Orai3. *Journal of Biological Chemistry*, *285*(25), 19173-19183. doi:10.1074/jbc.M110.102582
- Mukhopadhyay, P., Rajesh, M., Yoshihiro, K., Haskó, G., & Pacher, P. (2007). Simple quantitative detection of mitochondrial superoxide production in live cells. *Biochemical and Biophysical Research Communications*, *358*(1), 203-208. doi:10.1016/j.bbrc.2007.04.106
- Muratori, C., Silkuniene, G., Mollica, P. A., Pakhomov, A. G., & Pakhomova, O. N. (2021). The role of ESCRT-III and Annexin V in the repair of cell membrane permeabilization by the nanosecond pulsed electric field. *Bioelectrochemistry*, *140*, 107837. doi:10.1016/j.bioelechem.2021.107837
- Murphy, M. P. (2008). How mitochondria produce reactive oxygen species. *Biochemical Journal*, *417*(1), 1-13. doi:10.1042/BJ20081386
- Nagata, S., Suzuki, J., Segawa, K., & Fujii, T. (2016). Exposure of phosphatidylserine on the cell surface. *Cell Death and Differentiation*, *23*(6), 952-961. doi:10.1038/cdd.2016.7
- Nászai, A., Terhes, E., Kaszaki, J., Boros, M., & Juhász, L. (2019). Ca(2+)N It Be Measured? Detection of Extramitochondrial Calcium Movement With High-Resolution FluoRespirometry. *Scientific Reports*, *9*, 19229. doi:10.1038/s41598-019-55618-5
- Nexcelom Bioscience. (2021, July 14). *Viability using Acridine Orange/Propidium Iodide*. (Nexcelcom Bioscience) Retrieved July 14, 2021, from <https://www.nexcelom.com/applications/cellometer/viability/viability-using-ao-pi/>
- North, R. A. (2002). Molecular Physiology of P2X Receptors. *Physiological Reviews*, *82*(4), 1013-1067. doi:10.1152/physrev.00015.2002

- Nuccitelli, R., Chen, X., Pakhomov, A. G., Baldwin, W. H., Sheikh, S., Pomicter, J. L., . . . Schoenbach, K. H. (2009). A new pulsed electric field therapy for melanoma disrupts the tumor's blood supply and causes complete remission without recurrence. *Int J Cancer*, *125*(2), 438–445. doi:10.1002/ijc.24345
- Nuccitelli, R., Lui, K., Kreis, M., Athos, B., & Nuccitelli, P. (2013). Nanosecond Pulsed Electric Field Stimulation of Reactive Oxygen Species in Human Pancreatic Cancer Cells is Ca²⁺-Dependent. *Biochem Biophys Res Commun.*, *435*(4), 580-585. doi:10.1016/j.bbrc.2013.05.014
- Nuccitelli, R., Pliquett, U., Chen, X., Ford, W., Swanson, R. J., Beebe, S. J., . . . Schoenbach, K. H. (2006). Nanosecond pulsed electric fields cause melanomas to self-destruct. *Biochem Biophys Res Commun*, *343*(2), 351–360. doi:10.1016/j.bbrc.2006.02.181
- Oroboros. (2019). MiR05-Kit Instruction Sheet. *Mitochondrial Physiology Network*, *22*(10), 1-2. Retrieved from https://wiki.oroboros.at/images/c/c8/MiPNet22.10_MiR05-Kit.pdf
- Oroboros Ecosystem. (2020, Dec 7). *MitoPedia: O2k hardware*. (Oroboros) Retrieved July 2021, 14, from https://wiki.oroboros.at/index.php/MitoPedia:_O2k_hardware
- Oroboros Ecosystem. (2021, July 8). *MitoPedia: DatLab*. (Oroboros) Retrieved July 14, 2021, from https://wiki.oroboros.at/index.php/MitoPedia:_DatLab
- Pakhomov, A. G., Gianulis, E., Vernier, P. T., Semenov, I., Xiao, S., & Pakhomova, O. N. (2015). Multiple nanosecond electric pulses increase the number but not the size of long-lived nanopores in the cell membrane. *Biochimica et Biophysica Acta (BBA) - Biomembranes*, *1848*(4), 958-966. doi:10.1016/j.bbamem.2014.12.026
- Pakhomov, A. G., Gudvangen, E., Xiao, S., & Semenov, I. (2021). Interference targeting of bipolar nanosecond electric pulses for spatially focused electroporation, electrostimulation, and tissue ablation. *Bioelectrochemistry*, *141*, 107876. doi:10.1016/j.bioelechem.2021.107876
- Pakhomov, A. G., Kolb, J. F., White, J. A., Joshi, R. P., Xiao, S., & Schoenbach, K. H. (2007). Long-lasting plasma membrane permeabilization in mammalian cells by nanosecond pulsed electric field (nsPEF). *BioElectroMagnetics*, *28*(8), 655-663. doi:10.1002/bem.20354
- Pakhomov, A. G., Shevin, R., White, J. A., Kolb, J. F., Pakhomova, O. N., Joshi, R. P., & Schoenbach, K. H. (2007). Membrane permeabilization and cell damage by ultrashort electric field shocks. *Archives of Biochemistry and Biophysics*, *465*(1), 109-118. doi:10.1016/j.abb.2007.05.003
- Pakhomova, O. N., Gregory, B. W., Semenov, I., & Pakhomov, A. G. (2013). Two Modes of Cell Death Caused by Exposure to Nanosecond Pulsed Electric Field. *PLOS ONE*, *8*(7). doi:10.1371/journal.pone.0070278
- Pakhomova, O. N., Gregory, B., Semenov, I., & Pakhomov, A. G. (2014). Calcium-mediated pore expansion and cell death following nanoelectroporation. *Biochimica et Biophysica Acta (BBA) - Biomembranes*, *1838*(10), 2547-2554. doi:10.1016/j.bbamem.2014.06.015
- Pakhomova, O. N., Khorokhorina, V. A., Bowman, A. M., Rodaitė-Riševičienė, R., Saulis, G., Xiao, S., & Pakhomov, A. G. (2012). Oxidative effects of nanosecond pulsed electric field exposure in cells

- and cell-free media. *Archives of Biochemistry and Biophysics*, 527(1), 55-64.
doi:10.1016/j.abb.2012.08.004
- Palmer, G., Horgan, D. J., Tisdale, H., Singer, T. P., & Beinert, H. (1968). Studies on the respiratory chain-linked reduced nicotinamide adenine dinucleotide dehydrogenase. XIV. Location of the sites of inhibition of rotenone, barbiturates, and piericidin by means of electron paramagnetic resonance spectroscopy. *J Biol Chem*, 243, 844-847.
- Panov, A., & Scaduto, R. (1995). Influence of Calcium on NADH and Succinate Oxidation by Rat Heart Submitochondrial Particles. *Archives of Biochemistry and Biophysics*, 316(2), 815-820.
doi:10.1006/abbi.1995.1109
- Paradies, G., Paradies, V., Benedictis, V. D., Ruggiero, F. M., & Petrosillo, G. (2014). Functional role of cardiolipin in mitochondrial bioenergetics. *Biochimica et Biophysica Acta (BBA) - Bioenergetics*, 1837(4), 408-417. doi:10.1016/j.bbabi.2013.10.006
- Patrice X. Petit, M. G. (1998). Disruption of the outer mitochondrial membrane as a result of large amplitude swelling: the impact of irreversible permeability transition. *FEBS Letters*, 426, 111-116.
- Patries M Herst, M. V. (2007). Cell Surface Oxygen Consumption: A major contributor to cellular oxygen consumption in glycolytic cancer cell lines. *Biochimica et Biophysica Acta*, 1767, 170-177.
doi:10.1016/j.bbabi.2006.11.018
- Patrushev, M., Kasymov, V., Patrusheva, V., Ushakova, T., Gogvadze, V., & Gaziev, A. (2004). Mitochondrial permeability transition triggers the release of mtDNA fragments. *Cellular and Molecular Life Sciences*, 61, 3100-3103. doi:10.1007/s00018-004-4424-1
- Pereverzev, M., Vygodina, T., Konstantinov, A., & Skulachev, V. (2003). Cytochrome c, an ideal antioxidant. *Biochem. Soc. Trans.*, 31, 1312-1315.
- Petrella, R. A., Mollica, P. A., Zamponi, M., Reid, J. A., Xiao, S., Bruno, R. D., & Sachs, P. C. (2018). 3D bioprinter applied picosecond pulsed electric fields for targeted manipulation of proliferation and lineage specific gene expression in neural stem cells. *J Neural Eng*, 15(5). doi:10.1088/1741-2552/aac8ec
- Petrella, R. A., Schoenbach, K. H., & Xiao, S. (2016). A dielectric rod antenna for picosecond pulse stimulation of neurological tissue. *IEEE Transactions on Plasma Science*, 44(4), 708-714.
doi:10.1109/tps.2016.253721
- Pfeiffer, K., Gohil, V., Stuart, R. A., Hunte, C., Brandt, U., Greenberg, M. L., & Schagger, H. (2003). Cardiolipin Stabilizes Respiratory Chain Supercomplexes. *Journal of Biological Chemistry*, 278(52), P52873-52880.
- Piotr Witek, A. K. (2016). The effect of a number of H9C2 rat cardiomyocytes passage on repeatability of cytotoxicity study results. *Cytotechnology*, 68(6), 2407-2415. doi:10.1007/s10616-016-9957-2
- Potter, M., Newport, E., & Morten, K. (2016). The Warburg effect: 80 years on. *Biochem Soc Trans*, 44(5), 1499-1505. doi:10.1042/BST20160094

- Presley, A. D., Fuller, K. M., & Arriaga, E. A. (2003). MitoTracker Green labeling of mitochondrial proteins and their subsequent analysis by capillary electrophoresis with laser-induced fluorescence detection. *J Chromatogr B Analyt Technol Biomed Life Sci*, 793(1), 141-50. doi:10.1016/s1570-0232(03)00371-4.
- ProMega. (2021, Aug 20). *Caspase-Glo® 3/7 Assay Technical Bulletin*. Retrieved from ProMega.com: <https://www.promega.com/resources/protocols/technical-bulletins/101/caspase-glo-37-assay-protocol/>
- Puleston, D. (2015). Detection of Mitochondrial Mass, Damage, and Reactive Oxygen Species by Flow Cytometry. *Cold Spring Harbor Protocols*. doi:doi:10.1101/pdb.prot086298
- Rachana Pattani Ramachandran, C. S.-B.-R. (2020). Mitochondrial Targeting of the Enteropathogenic Escherichia coli Map Triggers Calcium Mobilization, ADAM10-MAP Kinase Signaling, and Host Cell Apoptosis. *mBio*, 11(5), e01397-20. doi:10.1128/mBio.01397-20
- Rat, P., Olivier, E., Tanter, C., Wakx, A., & Dutot, M. (2017). A fast and reproducible cell- and 96-well plate-based method for the evaluation of P2X7 receptor activation using YO-PRO-1 fluorescent dye. *Journal of Biological Methods*, 4(1), e64. doi:10.14440/jbm.2017.136
- Rebeca Acin-Perez, E. S. (2009). Cyclic AMP produced inside Mitochondria Regulates Oxidative Phosphorylation. *Cell Metabolism*, 9, 265-276. doi:10.1016/j.cmet.2009.01.012
- Ren, M., Phoon, C. K., & Schlame, M. (2014). Metabolism and function of mitochondrial cardiolipin. *Progress in Lipid Research*, 55, 1-16. doi:10.1016/j.plipres.2014.04.001
- Ren, W., & Beebe, S. J. (2011). An apoptosis targeted stimulus with nanosecond pulsed electric fields (nsPEFs) in E4 squamous cell carcinoma. *Apoptosis*, 16, 382-393. doi:10.1007/s10495-010-0572-y
- Ren, W., Sain, N. M., & Beebe, S. J. (2012). Nanosecond pulsed electric fields (nsPEFs) activate intrinsic caspase-dependent and caspase-independent cell death in Jurkat cells. *Biochemical and Biophysical Research Communications*, 421(4), 808-812. doi:10.1016/j.bbrc.2012.04.094
- Reszka, K. J., Wagner, B. A., Burns, C. P., & Britigan, B. E. (2005). Effects of peroxidase substrates on the Amplex re/peroxidase assay: Antioxidant properties of anthracyclines. *Analytical Biochemistry*, 342, 327-337. doi:10.1016/j.ab.2005/04/017
- Richter, C., Gogvadze, V., Laffranchi, R., Schlapbach, R., Schweizer, M., Suter, M., . . . Yaffee, M. (1995). Oxidants in mitochondria: from physiology to diseases. *Biochim Biophys Acta*, 1271(1), 67-74. doi:10.1016/0925-4439(95)00012-s.
- Robb, E. L., Hall, A. R., Prime, T. A., Eaton, S., Szibor, M., Viscomi, C., . . . Murphy, M. P. (2018). Control of mitochondrial superoxide production by reverse electron transport at complex I. *Journal of Biological Chemistry*, 293(25), 9869–9879. doi:10.1074/jbc.RA118.003647
- Robb, E. L., Hall, A. R., Prime, T. A., Eaton, S., Szibor, M., Viscomi, C., . . . Murphy, M. P. (2018). Control of mitochondrial superoxide production by reverse electron transport at complex I: Complex I reverse electron transport. *Journal of Biological Chemistry*, 293(25), 9869-9879. doi:10.1074/jbc.RA118.003647

- Rogers, T. B., Inesi, G., Wade, R., & Lederer, W. J. (1995). Use of thapsigargin to study Ca²⁺ homeostasis in cardiac cells. *Biosci Rep*, *155*, 341-9. doi:10.1007/BF01788366
- Romeo, S., Wu, Y.-H., Levine, Z. A., Gundersen, M. A., & Vernier, P. T. (2013). Water influx and cell swelling after nanosecond electropermeabilization. *Biochimica et Biophysica Acta (BBA) - Biomembranes*, *1828*(8), 1715-1722. doi:10.1016/j.bbamem.2013.03.007
- Rosenheck, E., & Neumann, K. (1973). Permeability changes induced by electric impulses in vesicular membranes. *J. Membrane Biol.*, *10*, 194-196.
- Rossi, A., Pakhomova, O. N., Mollica, P. A., Casciola, M., Mangalanthan, U., Pakhomov, A. G., & Muratori, C. (2019). Nanosecond Pulsed Electric Fields Induce Endoplasmic Reticulum Stress Accompanied by Immunogenic Cell Death in Murine Models of Lymphoma and Colorectal Cancer. *Cancers*, *11*(12), 2034. doi:10.3390/cancers11122034
- Rossi, A., Pakhomova, O. N., Pakhomov, A. G., Weygand, S., A. A., Murray, L. E., . . . Muratori, C. (2019). Mechanisms and immunogenicity of nsPEF-induced cell death in B16F10 melanoma tumors. *Scientific Reports*, *9*, 431. doi:10.1038/s41598-018-36527-5
- Rostovtseva, T. K., Hoogerheide, D. P., Rovini, A., & Bezrukov, S. M. (2017). Lipids in Regulation of the Mitochondrial Outer Membrane Permeability, Bioenergetics and Metabolism. In T. K. (Editor), *Molecular Basis for Mitochondrial Signaling* (pp. 185-215). Cham, Switzerland: Springer.
- Rowland, A. A., & Voeltz, G. K. (2012). Endoplasmic reticulum–mitochondria contacts: function of the junction. *Nature Reviews Molecular Cell Biology*, *13*, 607-615. doi:10.1038/nrm3440
- S. C. Lopes, G. I. (2018). Revealing cardiolipins influence in the construction of a significant mitochondrial membrane model. *Biomembranes*, *1860*(11), 2465-2477. doi:10.1016/j.bbamem.2018.07.006
- Sabharwal, S. S., & Schumacker, P. T. (2014). Mitochondrial ROS in cancer: initiators, amplifiers or an Achilles' heel? *Nat Rev Cancer*, *14*(11), 709-21. doi:10.1038/nrc3803.
- Sanders, J. M., Kuthi, A., Wu, Y., Vernier, P. T., & Gundersen, M. A. (2009). A linear, single-stage, nanosecond pulse generator for delivering intense electric fields to biological loads. *IEEE Transactions on Dielectrics and Electrical Insulation*, *16*(4), 1048-1054. doi:10.1109/TDEI.2009.5211853
- Schapira, A. (2010). Complex I: Inhibitors, inhibition and neurodegeneration. *Experimental Neurology*, *224*(2), 331-335. doi:10.1016/j.expneurol.2010.03.028
- Schenkel, L. C., & Bakovic, M. (2014). Formation and Regulation of Mitochondrial Membranes. *International Journal of Cell Biology*, Article ID 709828, 13 pages. doi:10.1155/2014/709828
- Schlame, M. (2019). Mitochondrial cristae as insulated transformers of metabolic energy. *EMBO J*, *38*(22), e103472. doi:10.15252/embj.2019103472
- Schoenbach, K. H., Beebe, S. J., & Buescher, E. S. (2001). Intracellular Effect of Ultrashort Electrical Pulses. *Bioelectromagnetics*, *22*, 440-448.

- Schoenbach, K. H., Pakhomov, A. G., Semenov, I., Xiao, S., Pakhomova, O. N., & Ibey, B. L. (2015). Ion transport into cells exposed to monopolar and bipolar nanosecond pulses. *Bioelectrochemistry*, *103*, 44-51. doi:10.1016/j.bioelechem.2014.08.015
- Schoenbach, K. H., Joshi, R. P., Beebe, S. J., & Baum, C. E. (2009). A Scaling Law for Membrane Permeabilization with Nanopulses. *IEEE Transactions on Dielectrics and Electrical Insulation*, *16*(5).
- Schrörs, B., Boegel, S., Albrecht, C., Bukur, T., Bukur, V., Holtsträter, C., . . . Löwer, M. (2020). Multi-Omics Characterization of the 4T1 Murine Mammary Gland Tumor Model. *Frontiers in Oncology*, *10*(1195). doi:10.3389/fonc.2020.01195
- Scialò, F., Fernández-Ayala, D. J., & Sanz, A. (2017). Role of Mitochondrial Reverse Electron Transport in ROS Signaling: Potential Roles in Health and Disease. *Frontiers in Physiology*, *8*(428). doi:10.3389/fphys.2017.00428
- Scialò, F., Sriram, A., Fernández-Ayala, D., Gubina, N., Löhmus, M., Nelson, G., . . . Sanz, A. (2016). Mitochondrial ROS Produced via Reverse Electron Transport Extend Animal Lifespan. *Cell Metabolism*, *23*(4), 725-734. doi:10.1016/j.cmet.2016.03.009
- Selivanov, V. A., Votykova, T. V., Pivtoraiko, V. N., J, Z., Sukhomlin, T., & Trucco, M. (2011). Reactive Oxygen Species Production by Forward and Reverse Electron Fluxes in the Mitochondrial Respiratory Chain. *PLoS Comput Biol*, *7*(3), e1001115. doi:10.1371/journal.pcbi.1001115
- Shaikh, S. R., & Brown, D. A. (2013). Models of plasma membrane organization can be applied to mitochondrial membranes to target human health and disease with polyunsaturated fatty acids. *Fatty Acids*, *88*(1), 21-25. doi:10.1016/j.plefa.2012.03.004
- Shannon C Kelly, A. M. (2018). Measuring Trans-Plasma Membrane Electron Transport by C2C12 Myotubes. *Journal of Visualized Experiments*, *135*, e57656. doi:10.3791/57656
- Shoshan-Barmatz, V., Pinto, V., Zweckstetter, M., Raviv, Z., Keinan, N., & Arbel, N. (2010). VDAC, a multi-functional mitochondrial protein regulating cell life and death. *Molecular Aspects of Medicine*, *31*(3), 227-285. doi:10.1016/j.mam.2010.03.002
- Sigma-Aldrich. (2021, Aug 25). *Mitochondrial Division Inhibitor, mdivi-1 - CAS 338967-87-6 - Calbiochem*. Retrieved from sigmaaldrich.com: <https://www.sigmaaldrich.com/US/en/product/mm/475856?context=product>
- Sigma-Aldrich. (2021, August 25). *Mitochondrial Fusion Promoter M1*. Retrieved from sigmaaldrich.com: <https://www.sigmaaldrich.com/US/en/product/sigma/sml0629>
- Sílvia G. Estácio, S. S. (2015). Calcium binding to gatekeeper residues flanking aggregation-prone segments underlies non-fibrillar amyloid traits in superoxide dismutase 1 (SOD1). *Biochimica et Biophysica Acta (BBA) - Proteins and Proteomics*, *1854*(2), 118-126. doi:10.1016/j.bbapap.2014.11.005
- Simões, R. V., Serganova, I. S., Kruchevsky, N., Leftin, A., Shestov, A. A., Thaler, H. T., . . . Ackerstaff, E. (2015). Metabolic Plasticity of Metastatic Breast Cancer Cells: Adaptation to Changes in the Microenvironment. *Neoplasia*, *17*(8), 671-684.

- Skladal, D., Halliday, J., & Thorburn, D. (2003). Minimum birth prevalence of mitochondrial respiratory chain disorders in children. *Brain*, *126*, 1905-1912.
- Smith, K. C., & Weaver, J. C. (2008). Active mechanisms are needed to describe cell responses to submicrosecond, megavolt-per-meter pulses: cell models for ultrashort pulses. *Biophys J*, *94*(5), 1547-63. doi:10.1529/biophysj.107.121921
- Solaini, G., Sgarbi, G., & Baracca, A. (2011). Oxidative Phosphorylation in Cancer Cells. *Biochimica et Biophysica Acta*, *1807*, 534-542. doi:10.1016/j.bbabi.2010.09.003
- Sozer, E. B., & Vernier, P. T. (2019). Modulation of biological responses to 2 ns electrical stimuli by field reversal. *Biochimica et Biophysica Acta (BBA) - Biomembranes*, *1861*(6), 1228-1239. doi:10.1016/j.bbamem.2019.03.019
- Stefan, K. (2001). Mitochondria: Structure and Role in Respiration. *Nature Publishing Group*. Retrieved from https://web.archive.org/web/20121021071651/http://www.med.ufro.cl/clases_apuntes/cs_pre_clinicas/mg-fisica-medica/sub-modulo-1/Mitochondria.pdf
- Stefanyk, L. E., Coverdale, N., Roy, B. D., Peters, S. J., & LeBlanc, P. J. (2010). Skeletal Muscle Type Comparison of Subsarcolemmal Mitochondrial Membrane Phospholipid Fatty Acid Composition in Rat. *Journal of Membrane Biology*, *234*, 207-215. doi:10.1007/s00232-010-9247-4
- St-Pierre, J., Buckingham, J., Roebuck, S., & Brand, M. (2002). Topology of superoxide production from different sites in the mitochondrial electron transport chain. *J. Biol. Chem*, *277*, 44784-44790. doi:10.1074/jbc.M207217200
- Tektronix. (2006, October 6). *TDS3000B Series User Manual*. Retrieved June 28, 2021, from tek.com: <https://www.tek.com/oscilloscope/tds3014b-manual/tds3000b-series-user-manual>
- Tenorio, M. F., & Niggli, E. (2016). Real-time intra-store confocal Ca²⁺ imaging in isolated mouse cardiomyocytes. *Cell calcium*, *60*(5), 331-340. doi:10.1016/j.ceca.2016.07.002
- ThermoFisher. (2021, August 12). *AlamarBlue™ Cell Viability Reagent*. Retrieved from ThermoFisherScientific: <https://www.thermofisher.com/order/catalog/product/DAL1025#/DAL1025>
- ThermoFisher. (2021, June 23). *Carboxy-H2DCFDA (general oxidative stress indicator)*. (ThermoFisher) Retrieved June 23, 2021, from <https://www.thermofisher.com/order/catalog/product/C400#/C400>
- ThermoFisher. (2021, June 23). *DAPI (4',6-diamidino-2-phenylindole)*. (ThermoFisher) Retrieved June 23, 2021, from <https://www.thermofisher.com/us/en/home/life-science/cell-analysis/fluorophores/dapi-stain.html>
- ThermoFisher. (2021, June 23). *MitoSOX™ Red Mitochondrial Superoxide Indicator, for live-cell imaging*. (ThermoFisher) Retrieved June 23, 2021, from <https://www.thermofisher.com/order/catalog/product/M36008#/M36008>

- ThermoFisher. (2021, June 23). *MitoTracker™ Green FM*. (ThermoFisher) Retrieved June 23, 2021, from <https://www.thermofisher.com/order/catalog/product/M7514#/M7514>
- ThermoFisher. (2021, June 23). *Nonyl Acridine Orange (Acridine Orange 10-Nonyl Bromide)*. (ThermoFisher) Retrieved June 23, 2021, from <https://www.thermofisher.com/order/catalog/product/A1372#/A1372>
- ThermoFisher. (2021, June 30). *Rhod-2 AM, cell permeant*. (ThermoFisher) Retrieved June 30, 2021, from <https://www.thermofisher.com/order/catalog/product/R1244#/R1244>
- ThermoFisher. (2021, June 22). *TMRE*. Retrieved from ThermoFisher.com: <https://www.thermofisher.com/order/catalog/product/T669?SID=srch-hj-TMRE#/T669?SID=srch-hj-TMRE>
- ThermoFisher. (2021, June 23). *YO-PRO™-1 Iodide (491/509)*. (ThermoFisher) Retrieved June 23, 2021, from <https://www.thermofisher.com/order/catalog/product/Y3603#/Y3603>
- Thibaud T Renault, J. E. (2014). Death upon a Kiss: Mitochondrial Outer Membrane COmposition and Organelle Communication Govern Sensitivity to BAK/BAX-Dependent Apoptosis. *Chemistry and Biology Review*, 21, 114-123. doi:10.1016/j.chembiol.2013.10.009
- Tina Batista Napotnik, Y.-H. W. (2011). Nanosecond electric pulses cause mitochondrial membrane permeabilization in Jurkat cells. *Bioelectromagnetics*, 33(3), 257-264. doi:10.1002/bem.20707
- Trewin, A. J., Bahr, L. L., Almast, A., Berry, B. J., Wei, A. Y., Foster, T. H., & Wojtovich, A. P. (2019). Mitochondrial Reactive Oxygen Species Generated at the Complex-II Matrix or Intermembrane Space Microdomain Have Distinct Effects on Redox Signaling and Stress Sensitivity in *Caenorhabditis elegans*. *Antioxid Redox Signal.*, 31(9), 594–607. doi:10.1089/ars.2018.7681
- Triepels, R., Heuvel, L. V., Trijbels, J., & Smeitink, J. (2001). Respiratory chain complex I deficiency. *Am. J. Med. Genet.*, 106, 37-45.
- Turrens, J. F. (2003). Mitochondrial formation of reactive oxygen species. *J Physiol*, 552(2), 335-344. doi:10.1113/jphysiol.2003.049478.
- Turrens, J., Alexandre, A., & Lehninger, A. (1985). Ubisemiquinone is the electron donor for superoxide formation by complex III of heart mitochondria. *Arch Biochem Biophys*, 237(2), 408-414. doi:10.1016/0003-9861(85)90293-0
- Ullery, J. C., Tarango, M., Roth, C. C., & Ibey, B. L. (2015). Activation of autophagy in response to nanosecond pulsed electric field exposure. *Biochemical and Biophysical Research Communications*, 458(2), 411-417. doi:10.1016/j.bbrc.2015.01.131
- V, S., T, M., R, S., R, P., H, K., & ME, L. (2013). Oxidative stress and cancer: an overview. *Ageing Res Rev*, 12(1), 376-90. doi:10.1016/j.arr.2012.10.004
- Velarde, M. C., Flynn, J. M., Day, N. U., Melov, S., & Campisi, J. (2012). Mitochondrial oxidative stress caused by Sod2 deficiency promotes cellular senescence and aging phenotypes in the skin. *Aging (Albany NY)*, 4(1), 3-12. doi:10.18632/aging.100423

- Vernier, P. T. (2011). Mitochondrial membrane permeabilization with nanosecond electric pulses. *Annual International Conference of the IEEE Engineering in Medicine and Biology Society (EMBC)*, (pp. 743-745). doi:10.1109/IEMBS.2011.6090169.
- Vernier, P. T., Sun, Y., & Gundersen, M. A. (2006). Nanoelectropulse-driven membrane perturbation and small molecule permeabilization. *BMC Cell Biology*, 7, 37. doi:10.1186/1471-2121-7-37
- Vernier, P. T., Sun, Y., Chen, M.-T., Gundersen, M. A., & Craviso, G. L. (2008). Nanosecond electric pulse-induced calcium entry into chromaffin cells. *Bioelectrochemistry*, 73(1), 1-4. doi:10.1016/j.bioelechem.2008.02.003
- Vernier, P. T., Sun, Y., Marcu, L., Craft, C. M., & Gundersen, M. A. (2004). Nanoelectropulse-Induced Phosphatidylserine Translocation. *Biophysical Journal*, 86(6), 4040-4048. doi:10.1529/biophysj.103.037945
- Vernier, P. T., Sun, Y., Marcu, L., Salemi, S., Craft, C. M., & Gundersen, M. A. (2003). Calcium bursts induced by nanosecond electric pulses. *Biochemical and Biophysical Research Communications*, 310(2), 286-295. doi:10.1016/j.bbrc.2003.08.140
- Vernier, P. T., Ziegler, M. J., Sun, Y., Chang, W. V., Gundersen, M. A., & Tieleman, D. P. (2006). Nanopore Formation and Phosphatidylserine Externalization in a Phospholipid Bilayer at High Transmembrane Potential. *J Am Chem Soc*, 128(19), 6288-6289. doi:10.1021/ja0588306
- Vernier, P. T., Ziegler, M. J., Sun, Y., Gundersen, M. A., & Tieleman, D. P. (2006). Nanopore-facilitated, voltage-driven phosphatidylserine translocation in lipid bilayers—in cells and in silico. *3(233)*. doi:10.1088/1478-3975/3/4/001
- Vernier, P., Li, A., Marcu, L., Craft, C., & Gundersen, M. (2003). Ultrashort pulsed electric fields induce membrane phospholipid translocation and caspase activation: differential sensitivities of Jurkat T lymphoblasts and rat glioma C6 cells. *IEEE Transactions on Dielectrics and Electrical Insulation*, 10(5), 795-809. doi:10.1109/TDEI.2003.1237329
- Vernier, P., Y., S., Marcu, L., Salemi, S., Craft, C., & Gundersen, M. (2003). Calcium bursts induced by nanosecond electric pulses. *Biochem Biophys Res Commun*, 310(2), 286-95.
- Victorino, V. J., Barroso, W. A., Assunção, A. K., Cury, V., Jeremias, I. C., Petroni, R., . . . Souza, H. P. (2016). PGC-1 β regulates HER2-overexpressing breast cancer cells proliferation by metabolic and redox pathways. *Tumor Biology*, 37, 6035–6044. doi:10.1007/s13277-015-4449-0
- Virginio, C., Church, D., North, R. A., & Surprenant, A. (1997). Effects of divalent cations, protons and calmidazolium at the rat P2X7 receptor. *Neuropharmacology*, 36(9), 1285-94. doi:10.1016/s0028-3908(97)00141-x
- Virginio, C., Church, D., North, R. A., & Surprenant, A. (1997). Effects of divalent cations, protons and calmidazolium at the rat P2X7 receptor. *Neuropharmacology*, 36(9), 1285-1294. doi:10.1016/S0028-3908(97)00141-X
- Wagenblast, E., Soto, M., Gutiérrez-Ángel, S., Hartl, C. A., Gable, A. L., Maceli, A. R., . . . Wilkinson, J. E. (2015). A model of breast cancer heterogeneity reveals vascular mimicry as a driver of metastasis. *Nature*, 520(7547), 358-362. doi:10.1038/nature14403

- Wang, S., Chen, J., Chen, M.-T., Vernier, P. T., Gundersen, M. A., & Valderrábano, M. (2009). Cardiac Myocyte Excitation by Ultrashort High-Field Pulses. *Biophysical Journal*, *96*(4), 1640-1648. doi:10.1016/j.bpj.2008.11.011
- Warburg, O., Wind, F., & Negelein, E. (1927). The Metabolism of Tumors in the Body. *Journal of General Physiology*, *8*(7), 519-30. doi:10.1085/jgp.8.6.519
- Weaver, J. (1990). Electroporation: A New Phenomenon to Consider in Medical Technology. In B. R. O'Connor M.E., *Emerging Electromagnetic Medicine* (pp. 81-101). New York, NY.: Springer. doi:10.1007/978-1-4612-3386-2_6
- Weaver, J. (1995). *The Biomedical Engineering Handbook*. (J. Bronzino, Ed.) Boca Raton, Florida: CRC Press and IEEE Press.
- Weaver, J. C., Smith, K. C., Esser, A. T., Son, R. S., & Gowrishankar, T. R. (2012). A brief overview of electroporation pulse strength-duration space: A region where additional intracellular effects are expected. *Bioelectrochemistry*, *87*, 236–243. doi:10.1016/j.bioelechem.2012.02.007
- West, A. P., Shadel, G. S., & Ghosh, S. (2011). Mitochondria in innate immune responses. *Nature Reviews Immunology*, *11*, 389-402.
- White, J. A., Blackmore, P. F., Schoenbach, K. H., & S. J. (2004, May). Stimulation of Capacitative Calcium Entry in HL-60 Cells by Nanosecond Pulsed Electric Fields. *Journal of Biological Chemistry*, *279*(22), P22964-22972. doi:10.1074/jbc.M311135200
- White, J. A., Pliquett, U., Blackmore, P. F., Joshi, R. P., Schoenbach, K. H., & Kolb, J. F. (2011). Plasma membrane charging of Jurkat cells by nanosecond pulsed electric fields. *Eur Biophys J*, *40*, 947–957. doi:10.1007/s00249-011-0710-7
- White, J., Blackmore, P., Schoenbach, K., & Beebe, S. (2004). Stimulation of capacitative calcium entry in HL-60 cells by nanosecond pulsed electric fields. *J Biol Chem*, *279*(22), 22964-72.
- Wikstrom, M., Sharma, V., Kaila, V. R., Hosler, J. P., & Hummer, G. (2015). New Perspectives on Proton Pumping in Cellular Respiration. *Chemical Reviews*, *115*, 2196-2221. doi:10.1021/cr500448t
- Williams, G. S., Boyman, L., Chikando, A. C., Kahirallah, R. J., & Lederer, W. (2013). Mitochondrial Calcium Uptake. *PNAS*, *110*(26), 10479-10486.
- Wirth, C., Brandt, U., Hunte, C., & Zickermann, V. (2016). Structure and function of mitochondrial complex I. *Biochim Biophys Acta*, *1857*(7), 902-14. doi:10.1016/j.bbabi.2016.02.013
- Wolf, D. M., Segawa, M., Kondadi, A. K., Anand, R., Bailey, S. T., Reichert, A. S., . . . Shrihai, O. S. (2019). Individual cristae within the same mitochondrion display different membrane potentials and are functionally independent. *EMBO Journal*, *38*(22), e101056. doi:10.15252/embj.2018101056
- Wong, H., Dighe, P., Mezera, V., Monternier, P., & Brand, M. (2017). Production of superoxide and hydrogen peroxide from specific mitochondrial sites under different bioenergetic conditions. *J. Biol. Chem*, *292*, 16804-16809. doi:10.1074/jbc.R117.789271
- Xiao, S. (2021). Chapter 15: Pulsed Power Generators. In R. J. S. J. Beebe, *Ultrashort Electric Pulse Effects in Biology and Medicine* (pp. 339-370). Springer.

- Ye, F., & Hoppel, C. L. (2013). Measuring oxidative phosphorylation in human skin fibroblasts. *Analytical Biochemistry*, 437, 52-58. doi:10.1016/j.ab.2013.02.010
- Yin, S., Chen, X., Hu, C., Zhang, X., Hu, Z., Yu, J., . . . Zheng, S. (2014). Nanosecond pulsed electric field (nsPEF) treatment for hepatocellular carcinoma: A novel locoregional ablation decreasing lung metastasis. *Cancer Letters*, 346(2), 285-291. doi:10.1016/j.canlet.2014.01.009
- Yin, S., Chen, X., Xie, H., Zhou, L., Guo, D., Xu, Y., . . . Zheng, S. (2016). Nanosecond pulsed electric field (nsPEF) enhance cytotoxicity of cisplatin to hepatocellular cells by microdomain disruption on plasma membrane. *Experimental Cell Research*, 346(2), 233-240. doi:10.1016/j.yexcr.2016.06.018
- Yong-Lin P Ow, D. R. (2008). Cytochrome c: functions beyond respiration. *Nat Rev Mol Cell Biol.*, 9(7), 532-42. doi:10.1038/nrm2434
- Zhang, K., Guo, J., Ge, Z., & Zhang, J. (2014). Nanosecond Pulsed Electric Fields (nsPEFs) Regulate Phenotypes of Chondrocytes through Wnt/ β -catenin Signaling Pathway. *Scientific Reports*, 4, 5836. doi:10.1038/srep05836
- Zhang, Y., Dong, F., Liu, Z., Guo, J., Zhang, J., & Fang, J. (2018). Nanosecond pulsed electric fields promoting the proliferation of porcine iliac endothelial cells: An in vitro study. *PLOS One*. doi:10.1371/journal.pone.0196688
- Zhao, B., Summers, F. A., & Mason, R. P. (2012). Photooxidation of Amplex red to resorufin: Implications of exposing the Amplex red assay to light. *Free Radical Biology and Medicine*, 53, 1080-1087. doi:10.1016/j.freeradbiomed.2012.06.034
- Zharkova, L. P., Romanchenko, I. V., Buldakov, M. A., Pripitnev, P. V., Bolshakov, M. A., & Rostov, V. V. (2018). Mitochondrial Membrane Permeability After Nanosecond Electromagnetic Pulsed Exposure. *20th International Symposium on High-Current Electronics (ISHCE)*, (pp. 158-161). doi:10.1109/ISHCE.2018.8521236.
- Zhou, R.-Z., Jiang, S., Zhang, L., & Yu, Z.-B. (2019). Mitochondrial Electron Transport Chain, ROS Generation and Uncoupling (Review). *Int J Mol Med*, 44(1), 3-15. doi:10.3892/ijmm.2019.4188
- Ziegler, M. J., & Vernier, P. T. (2008). Interface Water Dynamics and Porating Electric Fields for Phospholipid Bilayers. *J Phys Chem*, 112(43), 13588-13596. doi:10.1021/jp802772
- Zordoky, B. N., & El-Kadi, A. O. (2007). H9c2 cell line is a valuable in vitro model to study the drug metabolizing enzymes in the heart. *J Pharmacol Toxicol Methods*, 56(3), 317-22. doi:10.1016/j.vascn.2007.06.001

APPENDICES

Appendix A: Cell Growth / Culture media

The following lists the components of the growth media that was used for incubation and preparation of the cell lines used in this work. The first component in each is the 500mL container of primary media, and subsequent entries in the list are the additional components (such as serum, antibiotics, et cetera).

H9C2

- 1) DMEM with 4500 mg glucose – Corning
- 2) 10% Fetal Bovine Serum – Hyclone
- 3) 1% Pen/Strep – Gibco

4T1

- 1) RPPMI-1640 – Corning
- 2) 10% Fetal Bovine Serum - ATL Biological

MCF10A

- 1) DMEM – Corning
- 2) 5% Horse Serum – Gibco
- 3) 20ng/mL EGF
- 4) 0.5ug/mL Hydrocortisone
- 5) 100ng/mL Cholera Toxin
- 6) 10ug/mL Insulin

7) 1% Pen/Strep – Gibco

HCC1937

1) RPMI-1640 – ATCC

2) 10% Fetal Bovine Serum – Hyclone

Appendix B: Electrode Media

To prepare Gemish Electrode Media, follow the below steps.

- 1) Suspend 14.9g/L KCl (0.199M) and 20.9g/L MOPS (3-(*N*-morpholino)propanesulfonic acid, 0.099M) in at least 50mL. pH balance with KOH to 7.4pH. This solution is referred to as 2XKM.
- 2) To 50mL of 2XKM, add
 - a. 5mL of 0.1M Phosphate buffer (pH 7.4)
 - b. 2mL of 5% defatted BSA (Bovine Serum Albumin)
 - c. 1mL of 0.1M EGTA
- 3) Bring solution up to 100mL with H₂O

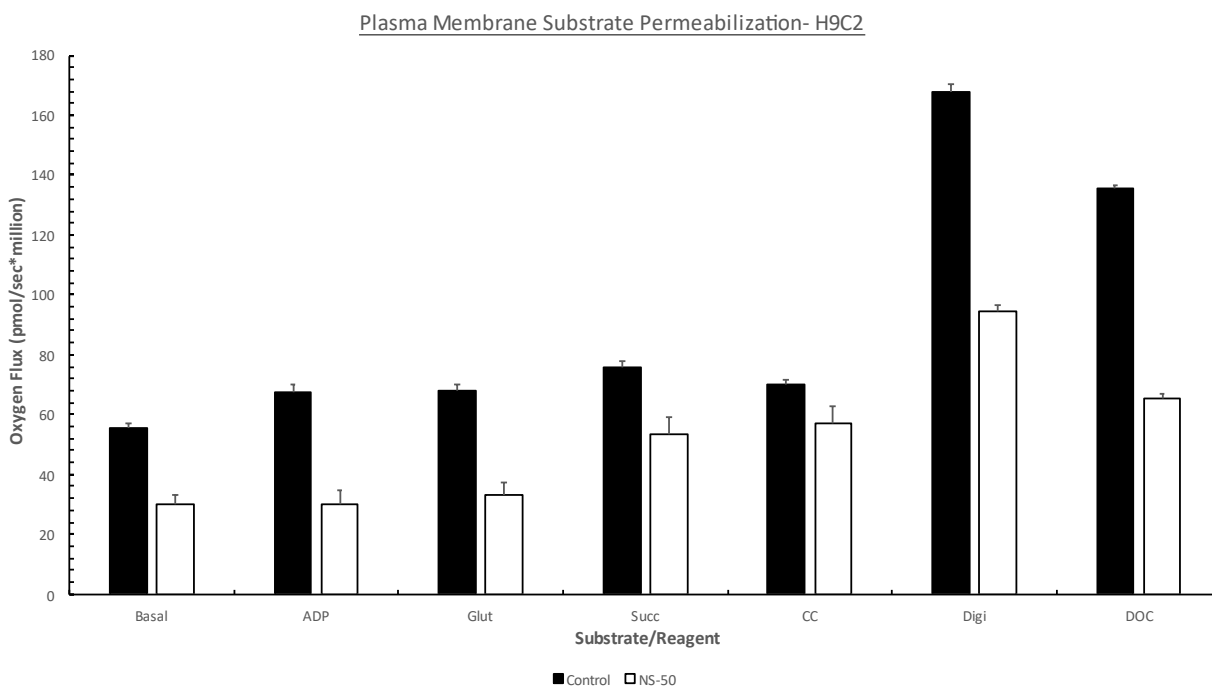
Final Concentrations are therefore: 1M KCl, 50mM MOPS, 5mM Phosphate Buffer, X defatted BSA, and 1mM EGTA.

Mir05 (Oroboros, 2019)

- 1) EGTA – 0.5mM
- 2) MgCl₂ – 3mM
- 3) Lactobionic Acid – 60mM
- 4) Taurine – 20mM
- 5) KH₂PO₄ – 10mM
- 6) HEPES – 20mM
- 7) D-Sucrose – 110mM
- 8) BSA Fatty Acid Free – 1g/L (Final Concentration 15mM)

Appendix C: Substrate Permeabilization

Once the technical parameters of plasma membrane permeabilization were found, the functional changes in the plasma membrane were delineated by adding substrates to control and cells pulsed 50 times. Once substrates were added, their respiration rates were tracked in the O2K as in previous experiments.

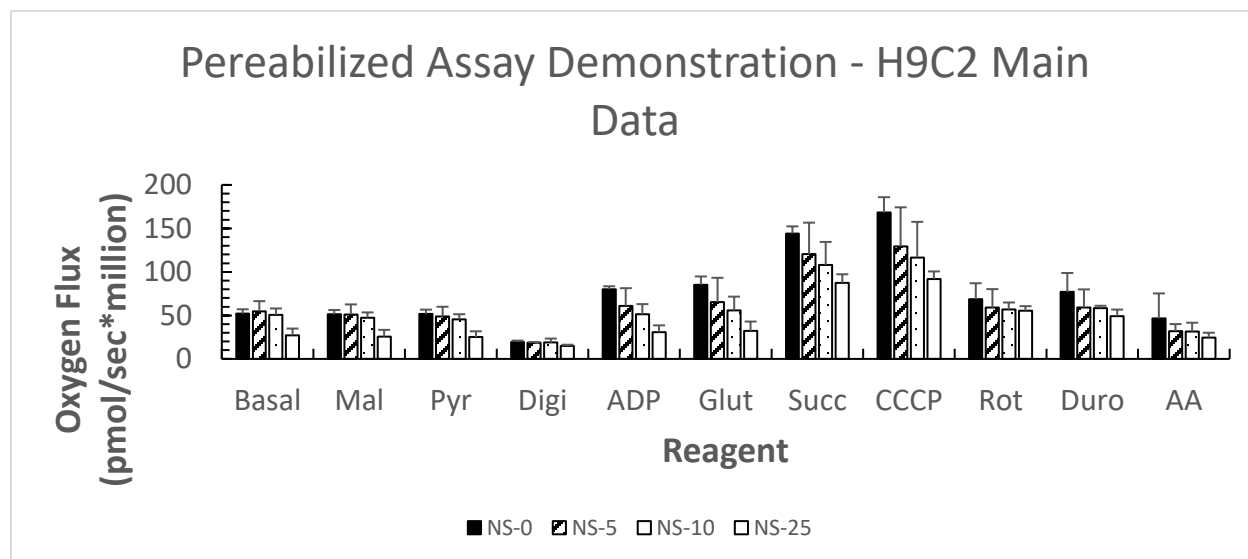


Graph 44: After nsPEF treatment, succinate may infiltrate past the plasma membrane. H9C2 cells were suspended in growth media. The samples were then either exposed to no nsPEF treatment (Control) or pulsed 50 times with 60ns, 40kv/cm, 15ns rise-time pulses. Cells were then suspended in Mir05 electrode media and sequentially exposed to ADP, Glutamate, Succinate, CytC, and then permeabilized with digitonin and DOC. Back bars represent control cells, which have a higher oxygen flux value than treated cells – however their respiration does not change meaningfully until digitonin is administered. Treated cell have a lower oxygen flux than control cell generally, but their oxygen flux values rise dramatically after the addition of succinate, which is not seen in treated cells. Error bars represent 1 standard deviation. (* = significance with $\alpha= 0.05$, Student's T Test). (n=2, no statistically significant results were found, even though the control condition (digitonin) is obviously different).

In this experiment, substrates were added to cell samples, and the change in oxygen flux was quantified. Cells that were pulsed 50 times show a significant increase in oxygen flux after the addition of the substrate succinate. The control cells showed no significant change in oxygen flux until the forced control condition – where digitonin was added to the cell samples and the plasma membrane chemically permeabilized. Digitonin injection caused both cell types to increase in oxygen flux – presumably because the substrates could then infiltrate to the mitochondria.

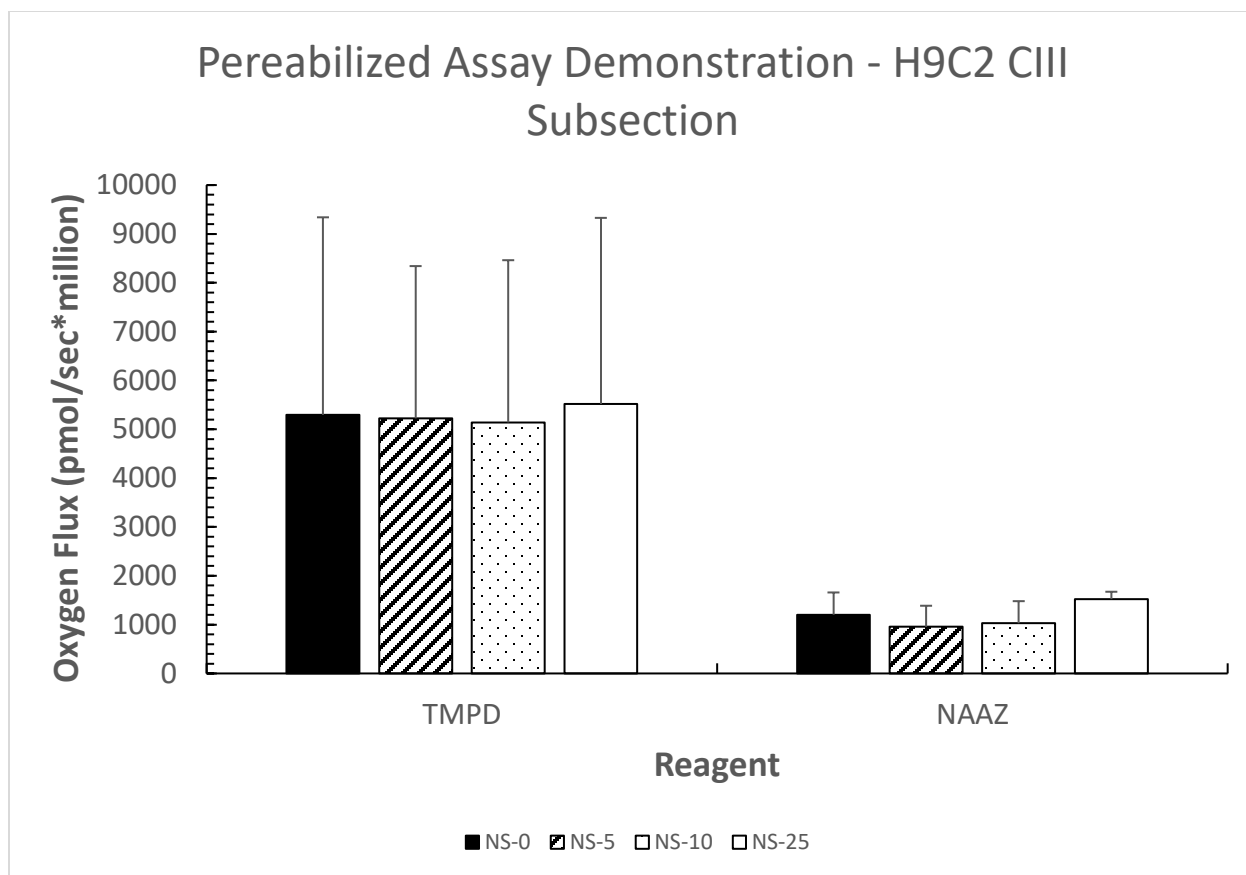
Appendix D: Full Permeabilized Protocol

The two below graphs (48 and 49) are provided as an example – the results from the permeabilized data are extracted from this data. However, it is not as important to the discussion above as the oxygen fluxes that are related to the ETC complexes. For experimental methods, refer to the methods section for permeabilized cell samples.



Graph 45: Example of Permeabilized analysis - CI and indirect CIII - unprocessed data. Here is an example of the permeabilized protocol with H9C2 cells. Note especially that after the cells were permeabilized with digitonin, the oxygen flux reaches exceptionally low values. This is likely due to the substrates that were localized within the confines of the plasma membrane becoming distributed homogenously within the O₂K chamber. Once that occurs, exogenous substrates must be added in order to see respiration again – and it occurs dramatically in H9C2 cells, ADP alone causing a nearly 4-fold difference in oxygen flux values. Note also that even before uncoupling of mitochondrial function, a clear difference can be seen in respiration levels. The assay for CIV activity was given at the end of this protocol, but due to the disparity of oxygen flux values, those values are in the next graph.

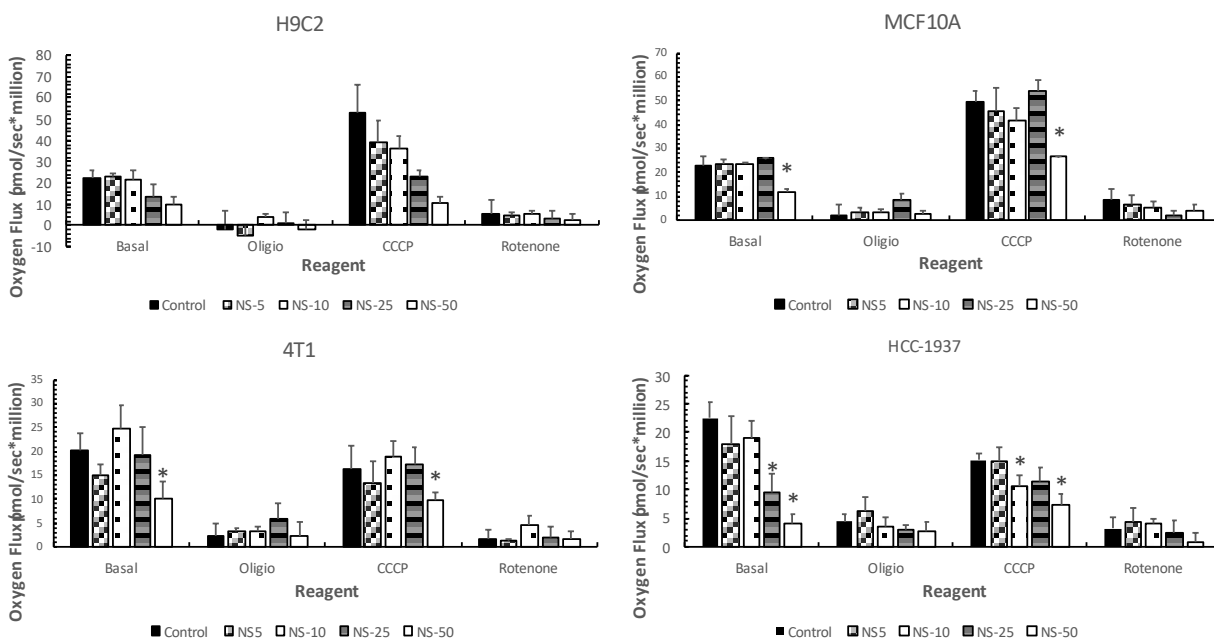
Significance was not calculated for changes directly due to additions of substrates – though there is a clear difference from the maximal nsPEF dose to the control samples in terms of oxygen flux.



Graph 46: Example of Permeabilized analysis - CIV - unprocessed data

Appendix E: Intact Oxygen Flux (O2K) Residual Oxygen Flux Correction

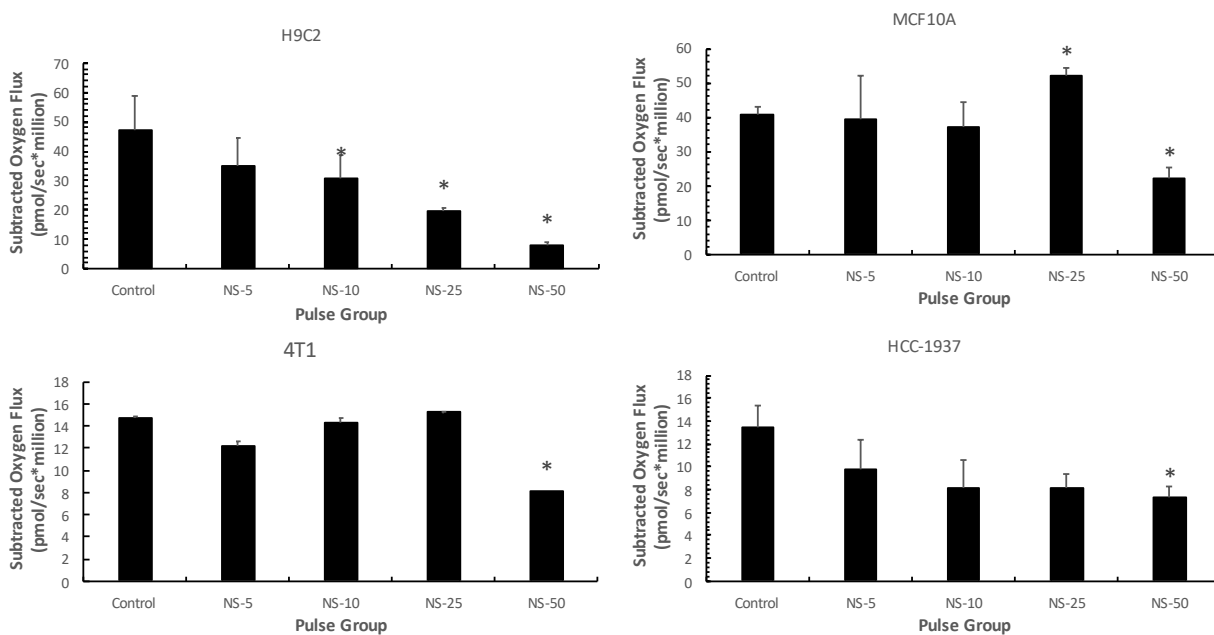
After the preliminary values for oxygen flux were found (see Section 3: Results - Mitochondrial ETC Complex Changes) there were some concerns that the flux after Antimycin A was added was higher than could be reasonably explained. The data from these experiments was taken and the flux that remained after the administration of AA was subtracted from every subgroup. Then the same analysis to determine the amount of oxygen flux due to CI was repeated. No statistical significance calculations changed, but the data is represented here for clear diligence.



Graph 47: Subtraction of residual oxygen flux does not change any significant analysis.

Oxygen flux post-Antimycin A addition shows no significant change in CI activity. The elevated levels of activity after the addition of AA (as seen in Graph 14) were a cause of contention.

So the oxygen flux after the addition of AA was subtracted from all groups and the CI oxygen flux and statistical analysis were redone (See Graph 48).



Graph 48: CI activity with AA correction shows no changes in statistical significance.

Appendix F: Liver Mitochondria Extraction

Protocol for rat and mouse liver mitochondria isolation

Minimum personal protective equipment for this procedure includes appropriate eye protection, a buttoned lab coat, and appropriate gloves. Harvest tissue and prepare washed rat liver mitochondria (≈ 15 mg mitochondrial protein per g liver)

_____ Body weight: _____ grams; Sex: _____;

_____ Age: _____ months other data: _____;

_____ Prepare cylinder with ice and water for homogenizer;

_____ Place liver in MSM;

_____ Rinse liver out with MSM until blood is not visible in the MSM solution: a) Dip liver in fresh MSM solution of a beaker using steel tweezers. Repeat this step in two different beakers with fresh MSM solution;

_____ Blot dry liver with #2 filter paper;

_____ Weigh tissue: _____ grams and put in a beaker in cold temperature (ice);

_____ Mince with clean scissors in clean, dry beaker (300-350 cuts) in cold temperature (ice);

_____ Wash with MSM, pour off rinsate and repeat until rinsate looks clear (3 or 4 times). Add MSM to the minced liver, mix and wait a few seconds to separate rinsate from minced liver. During pouring, don't stop and pour again;

_____ Measure 10 mL of MSM-EDTA solution per gram liver: _____ mL MSM-EDTA. Prepare this solution before you start your experiment and place it in plastic tubes on ice;

_____ Use a portion of the MSM-EDTA solution to suspend minced liver and pour into homogenizer (tissue grinder);

_____ Insert homogenizer inside a cylinder with ice and water;

_____ Homogenize with 3 strokes of loose-fitting pestle at pre-determined speed. Hand must hold the homogenizer;

_____ Pour homogenate in one or more centrifuge tubes. Keep centrifuge tubes on ice;

_____ Use remaining MSM-EDTA to rinse homogenizer and pestle with one more stroke;

_____ Mix homogenate with that poured in the centrifuge tubes and distribute between centrifuge tubes;

_____ Centrifuge in RC-5 with SS-34 rotor, at 1,700 rpm for 10 minutes;

_____ Save supernatant by pouring into two new tubes and filtering using gauze. (don't pour junk);

_____ Centrifuge supernatant at 7,650 rpm for 10 min;

_____ Save pellet by pouring off supernatant ending with a flip of the wrist to dislodge cell debris;

_____ Clean tube wall with gauze and resuspend with small pestle (no grooves) the pellet of the first and second tube. Then add 1-2mL of MSM to the first tube and resuspend with pestle, repeat this step with all centrifuge tubes. Pour the content of the second tube on the first tube and resuspend with pestle using the rest of the MSM solution (5mL MSM/gr liver____mL MSM);

_____ Centrifuge at 7,650 rpm for 10 min;

_____ Save pellet by pouring off supernatant ending with a flip of the wrist to dislodge cell debris;

_____ Resuspend pellet with small pestle. Then dry pestle before put it back in the tube. 2.5mL MSM/gr liver: __mLMSM;

_____ Centrifuge at 7,650 rpm for 10 min;

_____ Save pellet by pouring off supernatant ending with a flip of the wrist to dislodge cell debris;

_____ Resuspend with small pestle in 0.2 mL MSM/gr liver and pour into calibrated tube;

_____ Final volume of resuspended mitochondria: _____ mL;

MATERIAL

- Cylinder for homogenizer;
- Four beakers with a volume of 30-40 mL (no large diameter);
- Scissor and Steel tweezers;
- Large vessel to collect waste product: Large diameter (15 cm);
- A graduated cylinder 100 mL or a prepared EDTA+MSM solution in 1 or 2 50mL tube;
- MSM solution in three 50 mL tube;
- Homogenizer and Teflon pestle with no smooth surface;
- Small Teflon pestle with smooth surface;
- 4 (mouse), 6 (rat) centrifuge tubes;

SOLUTIONS

MSM (prepare fresh each week)

- | | | | |
|-----|--|-------|---------------------|
| 1. | 40.08 g of mannitol | 220mM | Amounts for 500 mL: |
| | 20.04 g of mannitol | | |
| 2. | 23.96 g of sucrose | 70mM | 11.98 g |
| | of sucrose | | |
| 3. | 1.047 g of MOPS | 5mM | 0.5235 |
| | g of MOPS | | |
| 4. | mix substances in a beaker (1L, large diameter); | | |
| 5. | clean the plastic trays used for weighing with MQ water and pouring it in the same beaker of 1L; | | |
| 6. | use graduate cylinder to add 0.6L of MQ H ₂ O to the beaker and mix solution for 10 min using a magnetic stirrer; | | |
| 7. | bring up to 1.0 liter with MQ water using a graduate cylinder; | | |
| 8. | filter the solution of the graduated cylinder using a funnel and a 1L bottle with medium diameter; | | |
| 9. | mix solution for 5 min using a magnetic stirrer; | | |
| 10. | pH to 7.4 at standstill (without stirring); | | |

EDTA, 100 mM

2.92 grams of EDTA (disodium)

bring up to 100 mL with water

pH to 7.0 with 10 M KOH

1. Measure 2.92g of EDTA powder measured with microscale;
2. Transfer the EDTA powder into a 150mL beaker and wash out weighing dish with MilliQ water. Pour approximately 70-80mL of MilliQ water into the same beaker;
3. Stir vigorously the solution until all the particles of EDTA floating in water (the particles appears immiscible and the mixture seem creamy at this step);
4. Set up the pH meter and measure the pH of the EDTA mixture;
5. The pH of the mixture will be very low. Add 10M KOH in drops until the pH reaches up to 7 while stirring;
6. The pH fluctuates as EDTA powder is dissolved. As solution becomes clearer and clearer, slow down the rates of adding KOH;
7. When the pH reach a stable value of 7.2–7.3, stop the addition of KOH and stir for about 5 minutes. The solution at this step should be clear and completely transparent;
8. After 5 min when pH does not fluctuate, add less concentrated KOH (0.1M, 1M) to set pH of the solution to 7.4;
9. Pour the solution into the 100mL graduated cylinder and level the solution up to 100mL;
10. Transfer the solution into an appropriate container and store in the refrigerator;

MSM with EDTA MSM-EDTA Solution

50mL MSM

1.0mL 100 mM EDTA

Gemish: O₂ electrode mix:

25 mL 2X KM

2.5 mL 0.1 M KPi buffer, pH 7.4

1.0 mL 5% BSA with no Fatty Acid

0.5 mL 0.1 M EGTA

bring up to 50 mL with water in a graduated cylinder. Add the water to the wall of the cylinder to avoid foam.

Appendix G: Common Pulse number to Charging Effect Conversions

<u>Pulse Number (#)</u>	<u>Resulting Charging Effect (Volt*Sec/cm)</u>
0	0
1	0.0024
5	0.0054
10	0.0076
15	0.0093
25	0.0120
50	0.0170
100	0.0240
200	0.0339

VITA

Selected Professional Experience

Engineering Positions

December 2021 – Present / KBR Science and Space / Senior Technical Professional
 March 2019 – Present / BioSView / Lab Administrator
 December 2017-May 2023 / SAMPE (Systems Analysis of Metabolic Physiology) Lab /
 Graduate Research Assistant
 August 2020- May 2021 / ODU Department of Electrical and Computer Engineering (ECE) /
 Graduate Administrative Assistant
 May 2019-August 2019 / NASA Space Mission Analysis Branch (SMAB) Exploration Medical
 Capabilities (ExMC) / Graduate Intern
 September 2015-December 2021 / Human Factors and Ergonomics Society (HFES)
 May 2018-August 2018 / ODU Engineering Management and Systems Engineering (ODU
 EMSE) / Learning Management System UX Developer

Medical Positions

May 2019-September 2019 / HHS-FDA Ignite / HHS-FDA Ignite Accelerator Participant
 August 2016-Present / Engineers Without Borders-ODU / Member
 August 2016-Present / Norfolk Medical Reserve Corps / Volunteer

Educational Positions

August 2016-August 2018 / ODU Biomedical Engineering / Graduate Teaching Assistant

Selected Publications/ Presentations/Posters

Academic Publications

Meimei Lai, Shutong Song, Edwin Oshin, Lucas Potter, Nicola Lai, and Chunqi Jiang. The
 production of OH in a nanosecond pulsed helium plasma jet impinging on water, saline or
 pigskin. *Journal of Applied Physics*. 131 (17). epub 05-02-2022
 Xavier-Lewis Palmer, Lucas Potter, Saltuk Karahan. Covid-19 and Biocybersecurity's Increasing
 Role on Defending Forward. *International Journal of Cyber Warfare and Terrorism (IJCWT)*.
 Special Issue: Decision Making in Cybersecurity.
 Potter L, Krusienski D, Kennedy J, Hoppel, C., Lai N. (1-Feb-2020) Data acquisition,
 visualization and processing of polarographic systems for bioenergetics studies. *Analytical
 Biochemistry*. 590.

Conference/Proceedings Publications

Brandon Griffin, Keitavius Alexander, Xavier-Lewis Palmer, Lucas Potter. Social-Engineering,
 Bio-economies, and Nation-State Ontological Security: A Commentary. Vol. 18 No. 1
 (2023): Proceedings of the 18th International Conference on Cyber Warfare and Security.
 Issah Samori, Gbadebo Odularu, Lucas Potter, Xavier-Lewis Palmer. Biocybersecurity and
 Deterrence: Hypothetical Rwandan Considerations. Vol. 18 No. 1 (2023): Proceedings of the
 18th International Conference on Cyber Warfare and Security.
 Hilary Finch, Affia Amefon, Woosub Jung, Xavier-Lewis Palmer, Lucas Potter. Commentary on
 Healthcare and Disruptive Innovation. Vol. 18 No. 1 pp. 77-84 (2023): Proceedings of the
 18th International Conference on Cyber Warfare and Security
 Simone Stephen, Keitavius Alexander, Xavier-Lewis Palmer, Lucas Potter, Implications of
 Cyberbiosecurity in Advanced Agriculture. Vol. 18 No. 1 (2023): Proceedings of the 18th
 International Conference on Cyber Warfare and Security.